JAERI-Tech
2003-021

EXTENDED CALCULATIONS OF OECD/NEA PHASE Ⅱ-C BURNUP CREDIT CRITICALITY BENCHMARK PROBLEM FOR PWR SPENT FUEL TRANSPORT CASK BY USING MCNP-4B2 CODE AND JENDL-3.2 LIBRARY

March 2003

Takeshi KUROISHI, Anh Tuan HOANG, Yasushi NOMURA and Hiroshi OKUNO

日本原子力研究所
Japan Atomic Energy Research Institute

本レポートは、日本原子力研究所が不定期に公刊している研究報告書です。
入手の問合わせは、日本原子力研究所研究情報部研究情報課（〒319-1195　茨城県那珂郡東海村）あて、お申し越しください。なお、このほかに財団法人原子力弘済会資料センター（〒319-1195　茨城県那珂郡東海村日本原子力研究所内）で複写による実費頒布をおこなっております。

This report is issued irregularly.
Inquiries about availability of the reports should be addressed to Research Information Division, Department of Intellectual Resources, Japan Atomic Energy Research Institute, Tokai-mura, Naka-gun, Ibaraki-ken 319-1195, Japan.

編集兼発行　日本原子力研究所

Extended Calculations of OECD/NEA Phase II-C Burnup Credit Criticality Benchmark Problem for PWR Spent Fuel Transport Cask by Using MCNP-4B2 Code and JENDL-3.2 Library

Takeshi KUROISHI, Anh Tuan HOANG*, Yasushi NOMURA and Hiroshi OKUNO

Department of Fuel Cycle Safety Research

Nuclear Safety Research Center

Tokai Research Establishment

Japan Atomic Energy Research Institute

Tokai-mura, Naka-gun, Ibaraki-ken

(Received January 30, 2003)

The reactivity effect of the asymmetry of axial burnup profile in burnup credit criticality safety is studied for a realistic PWR spent fuel transport cask proposed in the current OECD/NEA Phase II-C benchmark problem. The axial burnup profiles are simulated in 21 material zones based on in-core flux measurements varying from strong asymmetry to more or less no asymmetry. Criticality calculations in a 3-D model have been performed using the continuous energy Monte Carlo code MCNP-4B2 and the nuclear data library JENDL-3.2.

Calculation conditions are determined with consideration of the axial fission source convergence. Calculations are carried out not only for cases proposed in the benchmark but also for additional cases assuming symmetric burnup profile. The actinide-only approach supposed for first domestic introduction of burnup credit into criticality evaluation is also considered in addition to the actinide plus fission product approach adopted in the benchmark. The calculated results show that k_{eff} and the end effect increase almost linearly with increasing burnup axial offset that is defined as one of typical parameters showing the intensity of axial burnup asymmetry. The end effect is more sensitive to the asymmetry of burnup profile for the higher burnup. For an axially distributed burnup, the axial fission source distribution becomes strongly asymmetric as its peak shifts toward the top end of the fuel's active zone where the local burnup is less than that of the bottom end. The peak of fission source distribution becomes higher with the increase of either the asymmetry of burnup profile or the assembly-averaged burnup. The conservatism of the assumption of uniform axial burnup based on the actinide-only approach is estimated quantitatively in comparison with the k_{eff} result calculated with experiment-based strongest asymmetric axial burnup profile with the actinide plus fission product approach.

Keywords: Criticality Safety, Spent Fuel, Transport Cask, Burnup Credit, Axial Burnup Profile, End Effect, Asymmetry, Burnup Axial Offset, MCNP-4B2, JENDL-3.2

---

* MEXT Nuclear Researchers Exchange Program (Vietnam Atomic Energy Commission)

PWR使用済み燃料輸送キャスクを対象としたOECD/NEA燃焼度クレジット臨界ベンチマーク問題II-CへのMCNP-4B2コード及びJENDL-3.2ライブラリーを用いた拡張計算

日本原子力研究所東海研究所安全性試験研究センター燃料サイクル安全工学部
黒石　武・黄　英俊*・野村　靖・奥野　浩

(2003年1月30日受理)

現在進行中のOECD/NEAベンチマーク問題II-Cにおいて提案された、現実的なPWR使用済み燃料輸送容器を対象とした、燃焼度クレジット臨界安全性における軸方向燃焼度分布の非対称性による反応度効果について研究した。炉内中性子束測定に基づいた強い非対称から、非対称が概ね消失するまでの変化を考慮すべく、軸方向燃焼度分布は21の組成領域により模擬されている。連続エネルギーモンテカルロコードMCNP-4B2と核データライブラリーJENDL-3.2を用いて、3次元モデルの臨界計算を実施した。

軸方向核分裂源分布の収束性を考慮して計算条件を決定した。ベンチマーク問題で指定されたケースに加えて、対称な軸方向燃焼度分布を仮定した場合の計算も実施した。また、ベンチマーク問題におけるアクチニドと核分裂生成物を考慮する手法に加え、燃焼度クレジットを国内の臨界評価に導入する第一段階として、アクチニドのみを考慮する手法についても採用した。計算の結果、軸方向燃焼度非対称性の強度を示す典型的なパラメータとして定義された燃焼度軸方向オフセットの増加に伴って、実効増倍率及び端部効果はほぼ直線的に増加することが示された。また、より高い燃焼度に対して、燃焼度分布非対称性の端部効果への感度はより高い。軸方向分布を持つ燃焼度に対して、軸方向核分裂源分布は、燃料領域下端部よりも局所的燃焼度が低い上端部に向かってピークがシフトするという強い非対称となった。燃焼度分布の非対称性のみならず平均燃焼度の増加にも伴って、核分裂源分布のピーク値はより高くなった。実測値から得られた最も非対称性の強い軸方向燃焼度分布を用いてアクチニドと核分裂生成物を考慮する手法と軸方向燃焼度の一様分布を仮定したアクチニドのみを考慮する手法の実効増倍率計算結果を比較することより、後者の保守性を定量的に評価することができる。

東海研究所：〒319-1195　茨城県那珂郡東海村白方白根2-4
* 文部科学省原子力交流制度研究員（ベトナム原子力委員会）

Contents

目次

1. Introduction

In the framework of the OECD/NEA burnup credit (BUC) criticality safety research activities, the effect of axial burnup profile on criticality of PWR spent fuel was studied for an infinite array of fuel rods with a finite axial height in the Phase II-A benchmark [1], and for a realistic spent fuel transport cask in the Phase II-B benchmark [2]. The end effect, which is defined as the reactivity difference between the neutron effective multiplication factor (k_{eff}) calculated with an explicit representation of the axial burnup profile, and k_{eff} calculated assuming a uniform axial burnup, was evaluated. It has been known from the Phases II-A and II-B as well as from other studies [3][4] that the end effect becomes positive for PWR spent fuel of an average burnup of more than about 30 MWd/kgU. This means that the assumption of uniform axial burnup is non-conservative for a high burnup, while it is conservative for a low burnup of below 30 MWd/kgU.

In the Phases II-A and II-B, the end effect was evaluated with an assumption of a symmetric axial burnup profile. In reality, however, the axial burnup profile of spent fuel is asymmetric due to asymmetry of the reactor's core configuration and operation history. In the late 2000, J. Ch. Neuber and Th. Lamprecht (Germany) have proposed the OECD/NEA Phase II-C burnup credit criticality benchmark for PWR spent fuels* loaded into the transport cask that is the same as in the Phase II-B benchmark in order to study the effect of the asymmetry of axial burnup profiles. The benchmark is based on a set of actual shapes of outstanding quality with the error in the nodal burnup being less than 5%. The axially asymmetric change with burnup is also taken into account. Thus, the OECD/NEA Phase II-C benchmark problem forms an experiment-based database for international studies of BUC criticality safety for PWR spent fuel of high burnup.

To study the effect of the asymmetry of axial burnup profiles proposed in the Phase II-C benchmark problem, we have performed three- dimensional criticality calculations by using the continuous energy Monte Carlo code MCNP-4B2 [5] and the nuclear data library JENDL-3.2 [6]. As additional cases to the benchmark problem, we propose symmetric burnup profiles of 32 MWd/kgU and 50 MWd/kgU in order to cover the range of burnup profile variation from pure symmetry to strong asymmetry [7]. Consequently, our calculations also include the cases of symmetric axial burnup profiles. Moreover, calculations based on the actinide-only approach for BUC criticality safety are also performed in addition to the actinide plus fission product approach. Such additional calculations are carried out as an extension of the original OECD/NEA Phase II-C benchmark problem. The obtained results contribute to the currently required international comparison in the OECD/NEA expert group on burnup credit and help to better understand the physics of PWR spent fuel criticality safety.

A description of the Phase II-C benchmark problem including the additional cases is presented

* Siemens Konvoi fuel assembly type FOCUS™: Specifications can be downloaded from the website; http://www.nea.fr/html/science/wpncs/buc/specifications/phase-2c/index.html

in Chap. 2. The calculation method and model are presented in Chap. 3. In order to determine the calculation conditions concerning Monte Carlo simulation, convergence not only for k_{eff} but also for fission distribution should be carefully achieved. Hence, prior examinations for calculation conditions and convergence checks are performed and described with calculated results in Chap. 4. At the end of the report, a sample input of MCNP-4B2 is provided in Appendix I to show the calculation model in detail, and the calculated results for the fission source distributions illustrated in the section 4.4.2. are listed in the Tables in Appendix II.

2. Description of the Benchmark Problem

2.1. Configuration

The transport cask configuration of Phase II-C benchmark is similar to the one already used in Phase II-B (cf. Ref.2) in structure and arrangement of fuel assemblies. According to Phase II-C specification downloaded from the website, some modifications have been made due to the fact that the fuel assembly of the Konvoi type for Phase II-C is somewhat bigger than the 17x17 fuel assembly type for Phase II-B. The configuration is summarized below as shown in Fig. 1 and Fig. 2.

Cask shell

Inner diameter:	146cm,	Inner cavity height:	496cm,
Outer diameter:	206cm,	Outside height:	556cm,

Material: Stainless Steel of 30cm thickness, the same as for the upper and lower lids

Cask interior

21 fuel assemblies are arranged in a 5x5 array without corner positions, separated by basket wall and positioned centrally within the basket regions. The cask is completely filled with water.

Assembly basket

Inner basket compartment dimensions: 23.5cm x 23.5cm x 496 cm per assembly position

Basket wall thickness: 1cm (only one basket wall between two adjacent assembly positions)

Material: Borated stainless steel (1wt% natural boron)

Fuel assembly (18x18-24 lattice)

Number of fuel rods: 300, Number of guide thimbles: 24, Rod pitch: 1.27cm

Spacer grid: to be ignored

Upper and lower hardware: 30.0 and 19.5cm high, respectively (width: 22.86cm), assumed as a smeared mixture of 50vol% water and 50vol% stainless steel.

Fuel rod

Pellet diameter:	0.822cm,	Cladding inner diameter:	0.822cm,
Cladding outer diameter:	0.95cm,	Cladding material:	Zircaloy,
Active fuel length:	390cm (fuel compositions will be described in the next section.),		
Full fuel length:	439.5cm,	Initial ^{235}U enrichment:	4.0 wt%,
Upper inactive zone:	17.1cm,	Lower inactive zone:	32.4cm

End plugs are ignored. The fuel pellet region is treated as void inside the inactive zone between top (or bottom) end of the active zone and upper (or lower) hardware, and the others inside the inactive zone are treated the same as the active zone.

Guide thimble

Inner diameter:	1.11cm,	Outer diameter:	1.232cm,
Material:	Zircaloy		

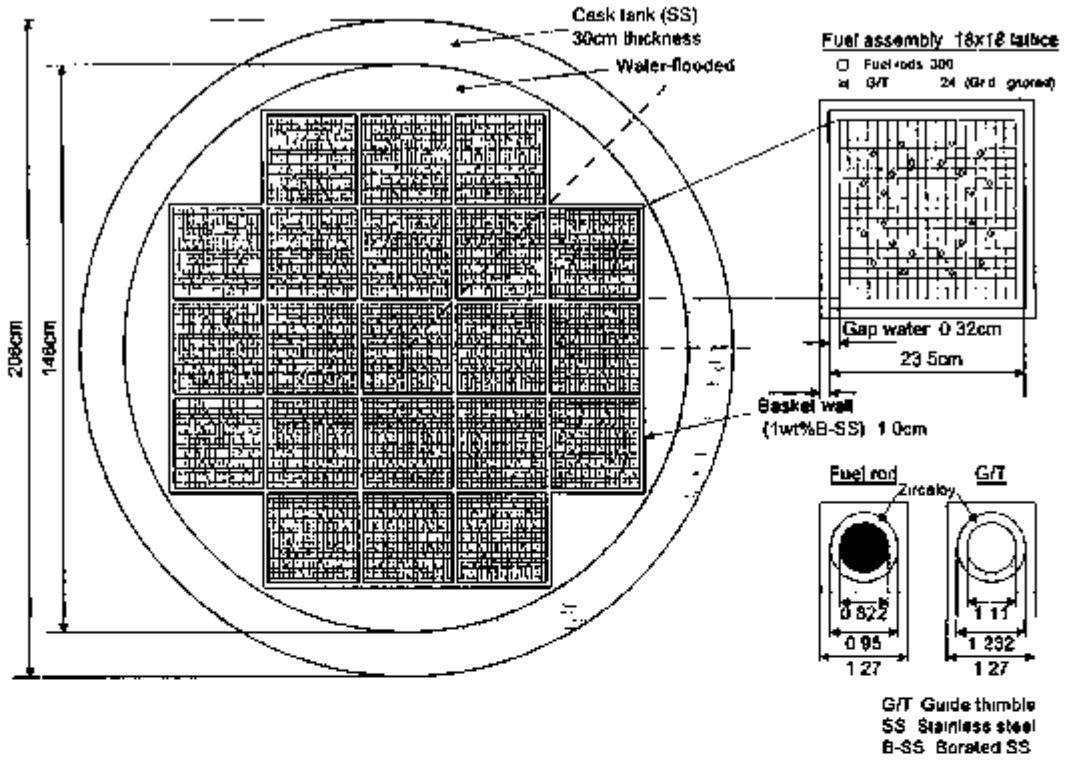

Fig 1 Configuration of transport cask for Phase II-C benchmark

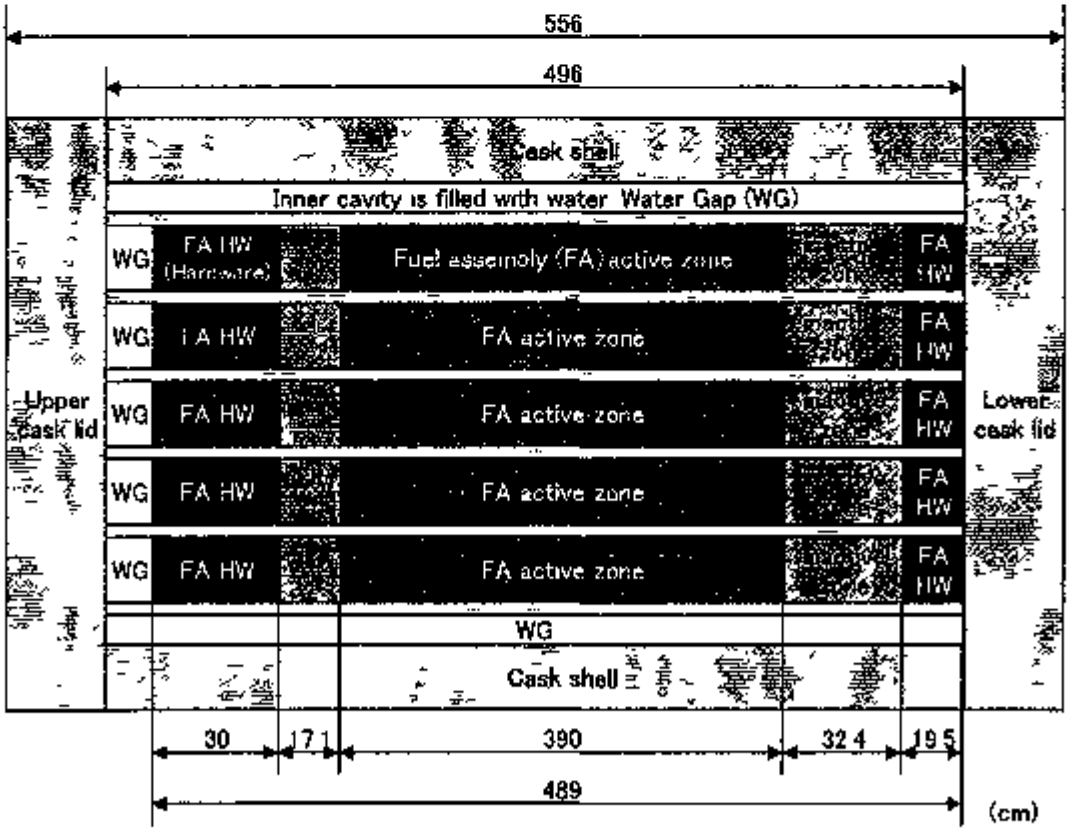

Fig 2 Vertical cross section of transport cask for Phase II-C benchmark

2.2. Axial Burnup Profiles for Benchmark

2.2.1. Proposed Cases in Phase II-C

For the benchmark, initial ^{235}U enrichment of 4.0wt% and two average burnups of the fuel assemblies of 32MWd/kgU and 50MWd/kgU, and cooling time of five years are assumed.

Axial burnup profiles for Phase II-C benchmark problem are based on evaluations of 850 axial burnup shapes in fuel assemblies derived from in-core 3D power density (flux) distribution measurements. According to Phase II-C specifications, axial burnup shapes are evaluated by 850 various assembly-wise averaged burnups $\hat{B}_j$ (as shown by B(average) in Fig. 3); here each

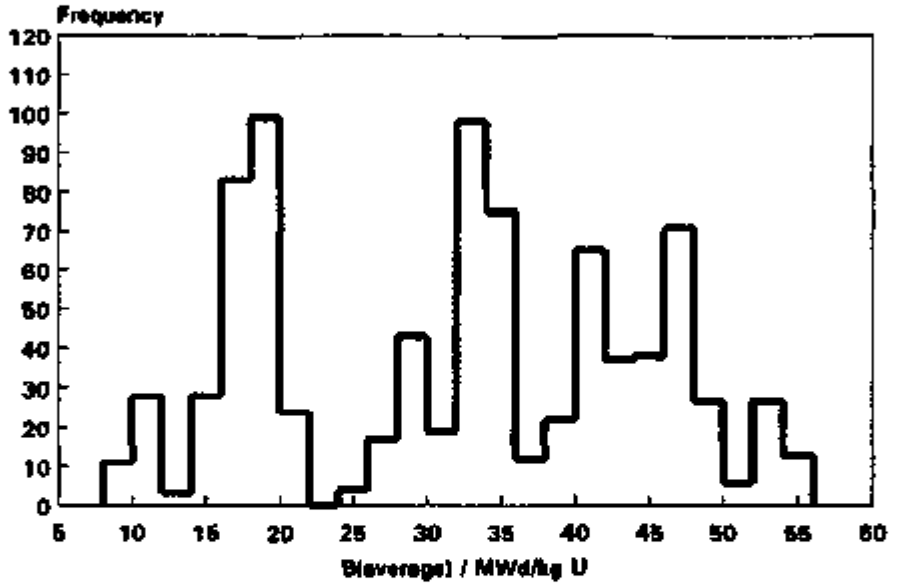

Fig. 3 Distribution of assembly-wise averaged burnups

assembly is referred to as j (j=1,850). $\hat{B}_j$ is given as the average of B_{ij} of 850 axial burnup data monitored at 32 equidistant axial nodes, here, i means axial nodes (i=1,32).

$$\hat{B}_j = \frac{1}{32}\sum_{i=1}^{32} B_{ij} \tag{1}$$

The analyses are carried out by means of the relative burnup distribution α_{ij} ($= B_{ij}/\hat{B}_j$). The sample mean $\hat{\alpha}_i$ of the ratio α_{ij} as shown by solid line in Fig. 4 is the basic case proposed in Phase II-C.

$$\hat{\alpha}_i = \frac{1}{N}\sum_{j=1}^{N}\alpha_{ij} = \sum_{j=1}^{N}\frac{B_{ij}}{\hat{B}_j}, \text{ (i=1,...,32, N=850)} \tag{2}$$

The dashed line on a log scale in Fig.4 shows the standard deviation of axial burnup data,

simultaneously. It is found that the variance is significantly greater at the top end of fuel zone than that at the others.

$$\hat{\sigma}_i = \sqrt{\frac{1}{N-1}\sum_{j=1}^{N}(\alpha_{ij} - \hat{\alpha}_i)^2}\ , \text{(i=1,...,32, N=850)} \tag{3}$$

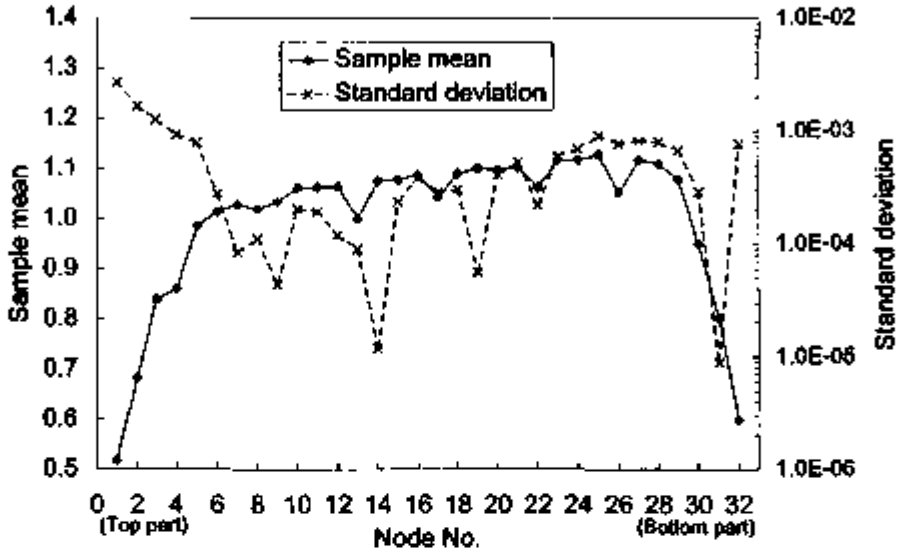

Fig. 4 Sample mean and standard deviation of axial burnup profiles

In consideration of the measured data whereby the decrease of the height of the burnup shape at the top nodes results in higher asymmetry of the shape and increase of the height of the shape at top nodes results in lower asymmetry, various burnup shapes are proposed in the benchmark by adding the mean values $\hat{\alpha}_i$ of the top six nodes by $\Delta\alpha_i$ (i=1,6). The variation of the top nodes is also counterbalanced by multiplying the mean values of the nodes m=18 through m=29 with f_m in order to preserve the sum of $\hat{\alpha}_i$ as described blow.

$$f_m = s\,(m-17)+1,\ (m=18,\ldots,29) \tag{4}$$

$$s = \frac{\sum_{i=1}^{6}\Delta\alpha_i}{\sum_{m=18}^{29}(m-17)\hat{\alpha}_m} \tag{5}$$

The variations $\Delta\alpha_i$ are bounded by the minimum and maximum values of the ratio α_{ij} observed in the sample of axial shapes under examination. It is taken into account that the minimum and maximum values depend on the average burnup. The observed minimum and maximum values are listed in Table 1.

Table 1 The observed minimum and maximum values of the rations α_{ij}

Node No. i	Average Burnup MWd/kgU	$\min_{j=1,\ldots,850}(\alpha_{ij})$	$\max_{j=1,\ldots,850}(\alpha_{ij})$
1	32	0.444	0.638
	50	0.492	0.665
2	32	0.621	0.778
	50	0.644	0.763
3	32	0.796	0.926
	50	0.818	0.917
4	32	0.808	0.936
	50	0.845	0.920
5	32	0.930	1.047
	50	0.978	1.036
6	32	0.977	1.062
	50	1.006	1.051

The cases proposed in the benchmark are given in Table 2. The cases with the serial numbers 2 through 7, 1, and 8 through 13 in this order represent the variation of the shape from strong asymmetry (case No.2) to more or less no asymmetry (case No.13). The cases No. 14 and 15 represent those often had when a fuel assembly is positioned at the edge of the core during its first

Table 2 Cases proposed by OECD/NEA BUC Phase II-C benchmark

Serial No.	Identification[*]	Node					
		1	2	3	4	5	6
1	Bbb Cyy A222222	Mean[***]	Mean	Mean	Mean	Mean	Mean
2	Bbb Cyy A111111	Min[***]	Min	Min	Min	Min	Min
3	Bbb Cyy A111112	Min	Min	Min	Min	Min	Mean
4	Bbb Cyy A111122	Min	Min	Min	Min	Mean	Mean
5	Bbb Cyy A111222	Min	Min	Min	Mean	Mean	Mean
6	Bbb Cyy A112222	Min	Min	Mean	Mean	Mean	Mean
7	Bbb Cyy A122222	Min	Mean	Mean	Mean	Mean	Mean
8	Bbb Cyy A222223	Mean	Mean	Mean	Mean	Mean	Max[***]
9	Bbb Cyy A222233	Mean	Mean	Mean	Mean	Max	Max
10	Bbb Cyy A222333	Mean	Mean	Mean	Max	Max	Max
11	Bbb Cyy A223333	Mean	Mean	Max	Max	Max	Max
12	Bbb Cyy A233333	Mean	Max	Max	Max	Max	Max
13	Bbb Cyy A333333	Max	Max	Max	Max	Max	Max
14	Bbb Cyy A122223	Min	Mean	Mean	Mean	Mean	Max
15	Bbb Cyy A112233	Min	Min	Mean	Mean	Max	Max
16	Bbb Cyy A322221	Max	Mean	Mean	Mean	Mean	Min
17	Bbb Cyy A332211	Max	Max	Mean	Mean	Min	Min

*: Bbb stands for the average burnup (B32: 32MWd/kgU, B50: 50MWd/kgU).

Cyy stands for the cooling time (C05: five years cooling time is just considered in Phase II-C).

Annnnnn is for the identification of the variation of the top six nodes (1: Min, 2: Mean, 3: Max).

**: Reference case (cf. Solid line in Fig. 4)

***: Mean stands for $\hat{\alpha}_i$ given by Eq. (2), Min and Max are given in Table 1.

cycle. In the cases No. 16 and 17, the difference of the averaged burnup of 6 top nodes from that of the lower half is almost conserved. All cases are well suited to study the impact of the axial shape on the local reactivity within the fuel zone.

All burnup shapes are divided into 21 axial zones. For each of the 21 axial zones, the benchmark provides the number densities of twenty-eight nuclides such as actinides and fission products. The division of the axial shapes is shown in Table 3.

Table 3 Division of the axial burnup shape in 21 zones

Axial Zone No.	Nodes collapsed	Length of the zone, cm	Height of the upper bound of the zone, cm (with respect to the bottom of the fuel zone)
1	32	12.19	12.19
2	31	12.19	24.38
3	30	12.18	36.56
4	29	12.19	48.75
5	27, 28	24.38	73.13
6	26	12.18	85.31
7	23,24,25	36.57	121.88
8	22	12.18	134.06
9	20,21	24.38	158.44
10	18,19	24.37	182.81
11	17	12.19	195.00
12	14,15,16	36.56	231.56
13	13	12.19	243.75
14	10,11,12	36.56	280.31
15	7,8,9	36.57	316.88
16	6	12.18	329.06
17	5	12.19	341.25
18	4	12.19	353.44
19	3	12.19	365.63
20	2	12.18	377.81
21	1	12.19	390.00

2.2.2. Additional Cases as an Extension of Phase II-C

The benchmark provides the axial burnup shapes varying from slight asymmetry to strong asymmetry. Naturally, one is interested in knowing the end effect for a symmetric axial burnup shape, although it is probably not a realistic one. We proposed symmetric shapes for two average burnups as additional cases to the benchmark problem in order to cover the range of burnup shape variation from a pure symmetry to a strong and realistic asymmetry.

The burnup shapes for symmetric cases, identified as BbbC05Symmetric, are assumed from those of the cases BbbC05A333333, which is the least asymmetric burnup shape, by averaging burnup data of two nodes that are located symmetrically about mid point in the axial direction. The

axial burnup shapes of BbbC05A333333 and BbbC05Symmetric for 32MWd/kgU and 50MWd/kgU are presented in Fig. 5 and Fig. 6, respectively. We can see that, the symmetric burnup shapes BbbC05Symmetric improve its symmetry compared with the least asymmetric burnup shapes BbbC05A333333.

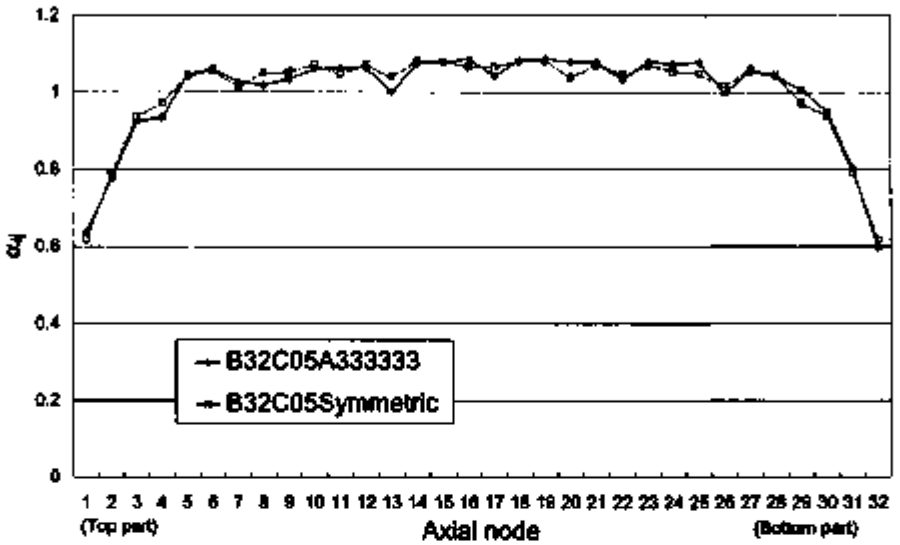

Fig. 5 Axial burnup shapes of B32C05A333333 and B32C05Symmetric

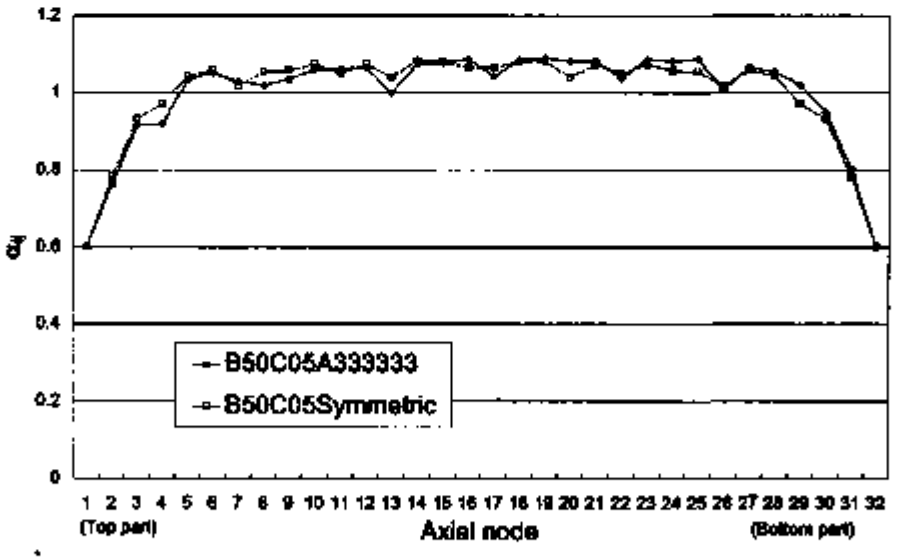

Fig. 6 Axial burnup shapes of B50C05A333333 and B50C05Symmetric

The number densities of each nuclide in the 32 equidistant nodes for BbbC05Symmetric are obtained by averaging the ones in the corresponding 32 equidistant nodes for BbbC05A333333 in the same manner as explained above for burnup shape.

The original OECD/NEA Phase II-C benchmark problem involves fifteen nuclides of fission product in the fuel composition. Here, the calculations for these cases are referred to as the actinide plus fission product (AC+FP) approach. In addition, we carried out calculations for the actinide-only (AC-only) approach, in which the fission products are neglected.

2.2.3. Introduction of Burnup Axial Offset

As a representative parameter of intensity of axial burnup asymmetry, we introduce burnup axial offset (burnup A. O.). The definition of the burnup A. O. is as follows. The values of burnup A. O. are listed in Table 4.

Burnup A. O. ≡ (average burnup of lower 16 nodes – that of upper 16 nodes) / that for all nodes

Table 4 Burnup A. O.

Case ID	Serial No.	Burnup A.O. (%)	Case ID	Serial No.	Burnup A.O. (%)
B32C05Symmetric	--	0.00	B50C05Symmetric	--	0.00
B32C05Uniform	--	0.00	B50C05Uniform	--	0.00
B32C05A222222	1	7.21	B50C05A222222	18	7.21
B32C05A111111	2	11.20	B50C05A111111	19	8.46
B32C05A111112	3	10.73	B50C05A111112	20	8.35
B32C05A111122	4	10.27	B50C05A111122	21	8.24
B32C05A111222	5	9.60	B50C05A111222	22	8.04
B32C05A112222	6	8.93	B50C05A112222	23	7.77
B32C05A122222	7	8.14	B50C05A122222	24	7.54
B32C05A222223	8	6.62	B50C05A222223	25	6.76
B32C05A222233	9	5.87	B50C05A222233	26	6.15
B32C05A222333	10	4.93	B50C05A222333	27	5.41
B32C05A223333	11	3.86	B50C05A223333	28	4.45
B32C05A233333	12	2.68	B50C05A233333	29	3.46
B32C05A333333	13	1.19	B50C05A333333	30	2.38
B32C05A122223	14	7.55	B50C05A122223	31	7.09
B32C05A112233	15	7.59	B50C05A112233	32	6.70
B32C05A322221	16	6.19	B50C05A322221	33	6.24
B32C05A332211	17	5.48	B50C05A332211	34	5.36

In Table 4, the uniform burnup case is identified by BbbC05Uniform.

Region-wise averaged burnup differences both between top 6 nodes and bottom 6 nodes, and between end part of 12 nodes and middle part of 20 nodes, increase linearly with increasing burnup A. O. as shown in Fig. 7. Consequently, the burnup A. O. shows the intensity of not only burnup profile asymmetry but also the neutron decoupling between upper and lower fuel parts.

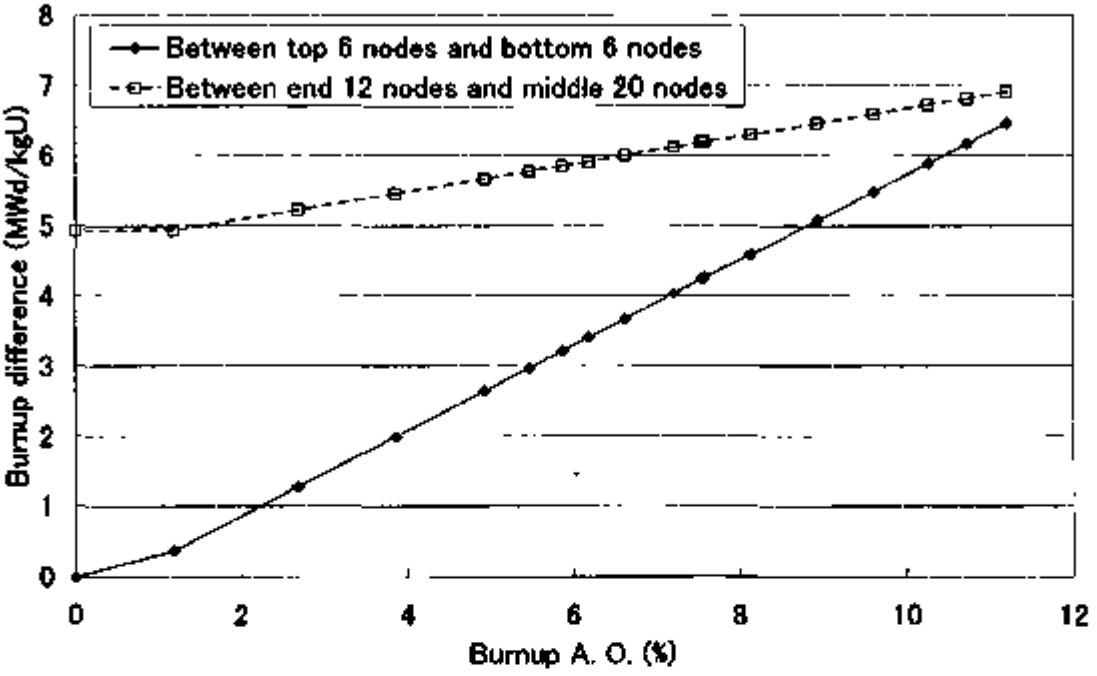

(a) 32 MWd/kgU

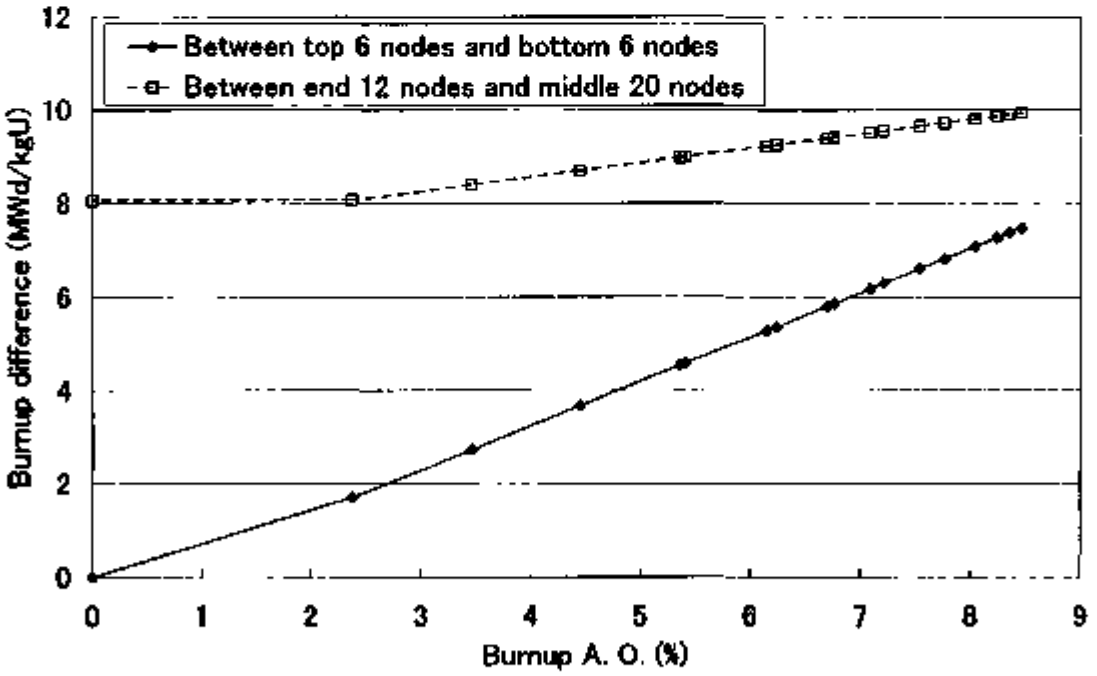

(b) 50 MWd/kgU

Fig. 7 Burnup differences vs. burnup A. O.

3. Calculation Method, Model and Conditions

3.1. Calculation Method

The calculation method is a combination of the continuous energy Monte Carlo code MCNP-4B2 [5] and the nuclear data library JENDL-3.2 [6]. The KCODE option of MCNP has been employed in criticality calculations for 3-D model of the transport cask.

3.2. Calculation Model and Conditions

It was found that the input cards of the primary results as shown in the reference [7] had some mistakes. The lack of the S(α,β) identifier affects the k_{eff} results significantly, and the re-calculated results described in the next chapter show that the old k_{eff} results are underestimated by about 1%. In the re-calculations, the input cards were corrected and modified. The three major modifications are summarized below. A sample input is shown in Appendix I.

(1) The radial 1/8 symmetry of the cask configuration as shown by dashed line in Fig. 1 is modeled explicitly in the input cards. It contributes to reduce the number of initial source points, namely, computer memory. All calculations are carried out on EWS: SUN/Blade100 (Solaris 8) where the MCNP is installed with the dynamic memory option. The dynamic storage of the sample input as shown in the appendix is 6810117 words, which is still more than the default value of the static memory parameter (MDAS = 4000000).

(2) The 32 axial equidistant cells (not 21 non-equidistant cells) are explicitly specified in the input cards in order to show the fission source distribution smoothly. In addition, the compositions of 21 non-equidistant zones are redistributed to the corresponding 32 equidistant cells.

(3) The initial guess for fission source is flat and distributed uniformly in all fissile fuel cells for all cases (symmetric, uniform, asymmetric cases).

In addition, calculation conditions are reexamined. At first, we assume 300 skipped cycles to check the axial fission source convergence for a pin cell configuration. We have to increase the skipped cycles to reach convergence in some cases of slow convergence. The number of active histories, namely, the product of the number of scored cycles and the number of histories per cycle, is taken to be 2,000,000 in order to estimate k_{eff} (1σ is about 0.0005) and the end effect (more or less 1%) except for the uniform burnup cases. It is necessary to increase the number of active histories in cases of uniform burnup to obtain a converged fission source distribution supposed to be a cosine-like curve in shape. The combination of the number of skipped cycles and the number of histories per cycle is determined as a result of convergence check for fission source distribution, which is described in section 4.2.

The numbers of neutron history for the final estimation are listed in Table 5.

Table 5 Numbers of neutron history

Numbers of history*	Cases	Comments
20000 x (300 + 100)	Symmetric 4 cases	At 32 & 50MWd/kgU for both AC-only and AC+FP approach
5000 x (300 + 4000)	Uniform 4 cases	
5000 x (300 + 400)	Asymmetric cases except below	1σ for k_{eff} is nearly equal to 0.0005
5000 x (1500 + 400)	B32C05A233333, B32C05A333333 for AC+FP approach	Fission source slow convergence needs many skipped cycles.
5000 x (4500 + 400)	B32C05A233333 for AC-only app.	
5000 x (6000 + 400)	B32C05A333333 for AC-only app.	

*: Number of histories per cycle x (number of skipped cycles + number of scored cycles)

4. Calculated Results

4.1. Prior Examination of Skipped Cycles Based on the Pin Cell Configuration

It is important to check the slow convergence caused by the axial burnup distribution in the benchmark. The aim in this section is to determine the number of the skipped cycles enough to reach convergence of fission source distribution. Hence, we have examined the convergence of the fission source distribution for an infinite array system of pin cells that is modeled as full axial structure of the cask for the Phase II-C. We adopt the pin cell configuration prior to the realistic cask because it has the advantage that effects caused by the axial burnup distribution can be distinguished from effects of the radial structure (18x18-24 fuel lattice, basket wall of B-SS and water gap, 21 fuel assemblies arranged in a 5x5 array, cask wall, and so on). The simple configuration decreases the probability of units without neutron generation points arisen and reduces the calculation time to process the configuration when the Monte Carlo simulations are executed.

As representative cases, the symmetric case: B32C05Symmetric, the uniform case: B32C05Uniform and one of the asymmetric cases: B32C05A222222 are analyzed by the AC+FP approach. Criticality calculations are performed by varying the number of skipped cycles with other calculation conditions of 20,000 histories per cycle, 100 scored cycles, and flat and uniform initial guess of fission source. Figure 8 shows calculated k_{eff} per skipped cycles. Increase of skipped cycles of more than 100 affects slightly the k_{eff} trends for the three cases as shown in Fig. 8. In the following sections, we examine the number of skipped cycles to reach convergence of the fission source distribution for the three cases, respectively.

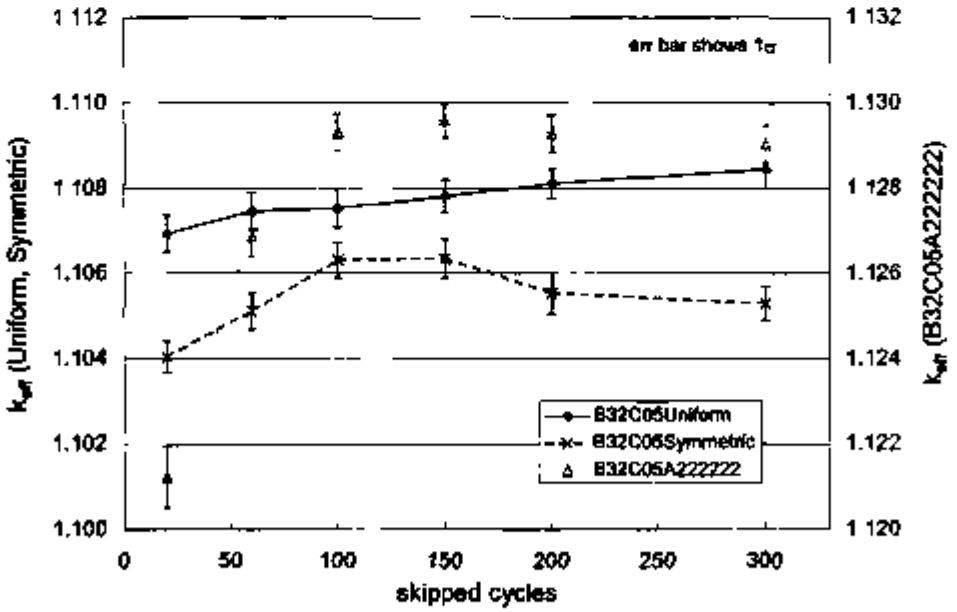

Fig. 8 Calculated k_{eff} vs. skipped cycles for the pin cell model based on Phase II-C [20,000 histories/cycle, 100 cycles scored]

4.1.1. Symmetric Burnup Case

Figure 9 shows calculated results of fission source distributions with various numbers of skipped cycles for the symmetric burnup case identified by B32C05Symmetric.

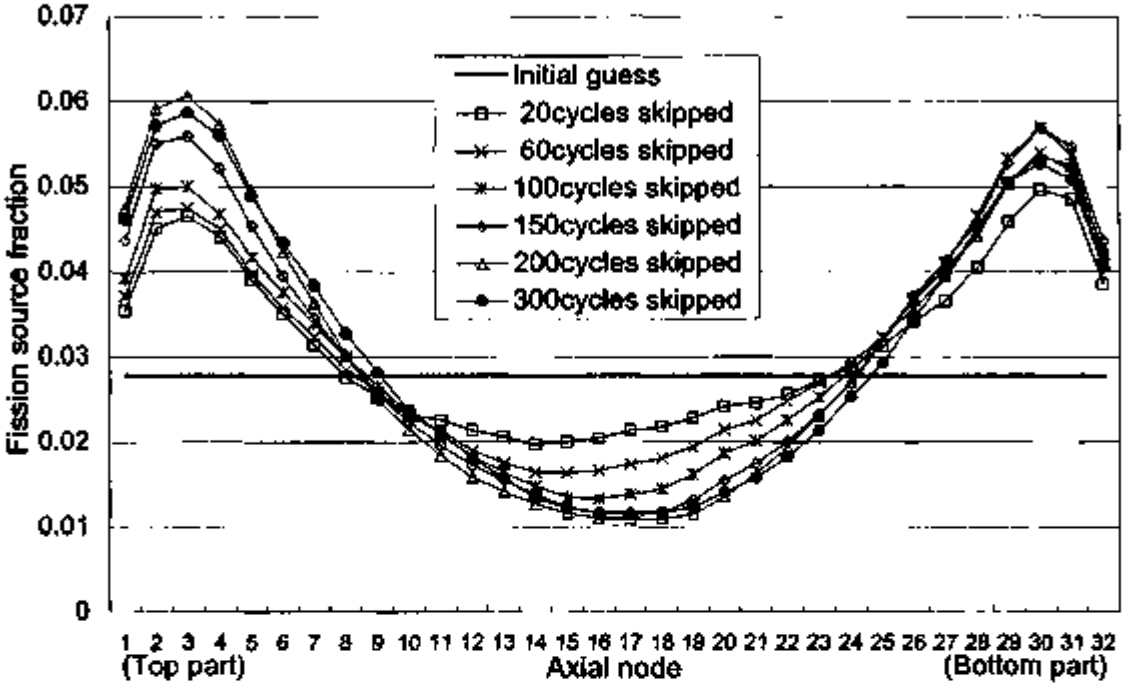

Fig. 9 Fission source distributions of B32C05Symmetric for various skipped cycles based on the pin cell model [20,000 histories/cycle, (20-300) skipped, 100 cycles scored]

As shown in Fig. 9, it is found that the initial guess affects the fission source in case of insufficient skipped cycles. The fission source at middle parts of the fuel decreases gradually with the increase of skipped cycles, and becomes almost constant for more than 150 skipped cycles. On the other hand, it seems that fission source at the top and bottom parts increases with the increase of skipped cycles, and still oscillates slightly even for 300 skipped cycles. Let's study the trends of fission fractions at the 3 parts (top, middle and bottom), which are obtained by summing those of six nodes at the top and bottom parts, and twelve nodes at the middle part shown in Fig. 9. As shown in Fig. 10, the fission fractions are almost constant for more than 200 scored cycles. Even though the burnup distribution is axially symmetric, the fission source is not symmetric such that the fission fraction at the top part is greater than that at the bottom part. It may be caused by a difference of the reflector effect between the upper and lower structures. The reactivity difference however, is found to be so small that it becomes very difficult to estimate accurately how it affects the fission source distribution as a result of some calculations.

Therefore, we conclude that 300 cycles suffice as the number of skipped cycles for the axially symmetric burnup case to estimate the fission source distribution. The combination of the number of histories per cycle and the number of scored cycles and its effect on the fission source distribution will be discussed in the next section based on the cask configuration.

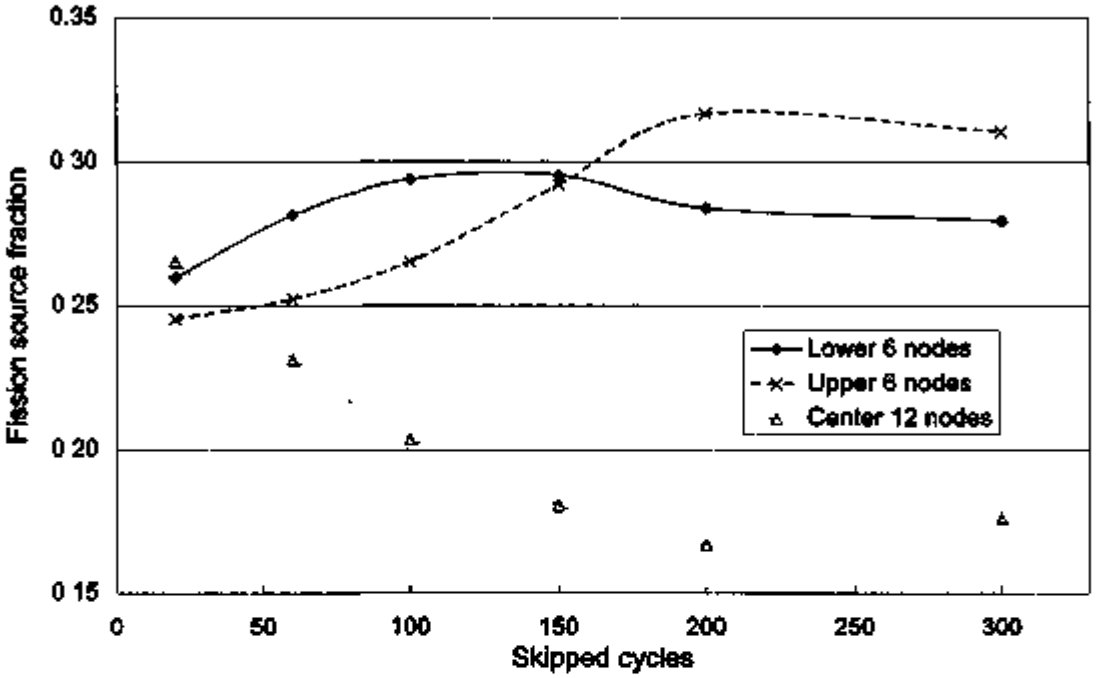

Fig. 10 Fission fractions of 6 nodes at the top and bottom parts and the center 12 nodes for various skipped cycles based on the pin cell model of B32C05Symmetric

4.1.2. Uniform Burnup Case

Figure 11 shows calculated results of fission source distributions with various numbers of skipped cycles for the uniform burnup case identified by B32C05Uniform.

As shown in Fig. 11, it is found that the fission source at the middle part is affected by the initial guess of flat distribution in case of insufficient skipped cycles. It is supposed to become near cosine-like in shape with increase of the skipped cycles because the reflector structure difference between top and bottom parts little affects the fission source distribution. But, no matter by how many the skipped cycles increase, the fission source distribution could not be represented by a smooth curve. It is necessary to increase the total scored histories, namely the product of the number of the histories per cycles and the number of the scored cycles, in order to obtain a smooth fission source distribution like a cosine curve.

Therefore, we conclude that 300 skipped cycles are enough for the uniform burnup case to estimate the fission source distribution. The results for the increase of the total scored histories will

be provided in the subsection 4.3.2 based on the cask configuration.

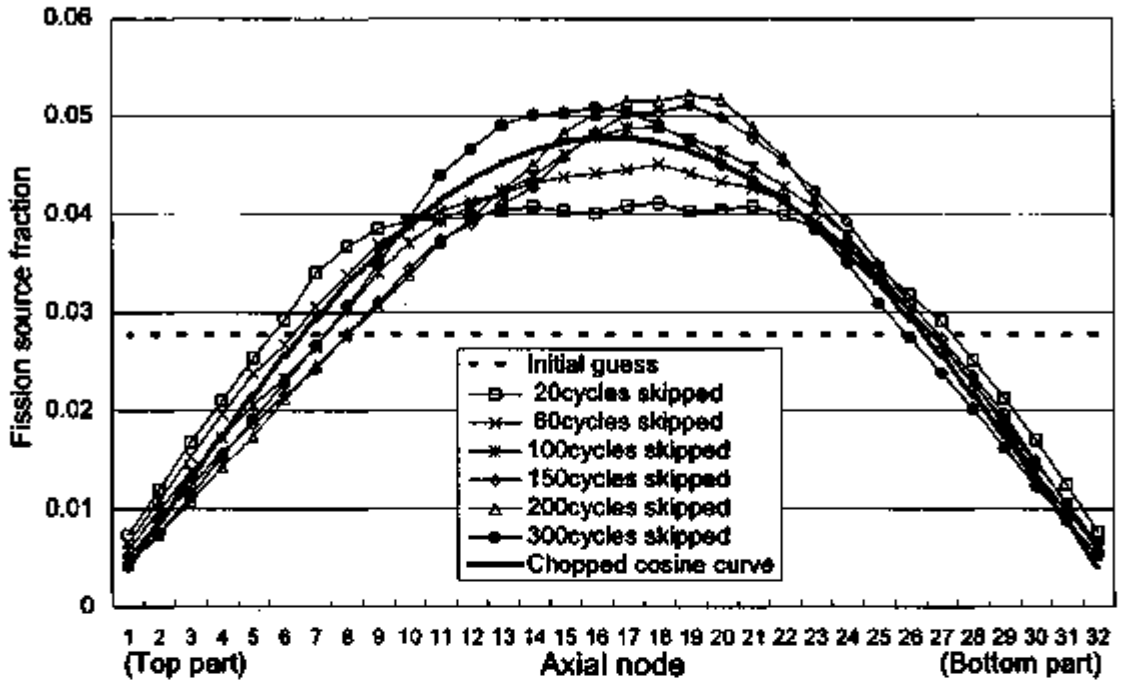

Fig. 11 Fission source distributions of B32C05Uniform for various skipped cycles based on the pin cell model [20,000 histories/cycle, (20-300) skipped, 100 cycles scored]

4.1.3. Asymmetric Burnup Case

Figure 12 shows calculated results of fission source distributions with various numbers of skipped cycles for the asymmetric burnup case identified by B32C05A222222.

Regarding the asymmetric burnup cases, the fission source distribution localizes on the top part because of its low burnup. As shown in Fig. 12, the peak value at the top part increases and the source level at the bottom part decreases with increase of the skipped cycles. Figure 13 shows the fission fractions of 4 nodes at the top and bottom parts. The fission fraction at the top 4 nodes becomes almost constant at more than 150 skipped cycles. The fission fraction at the bottom 4 nodes is shown by the logarithm axis on the right hand side in Fig. 13 because of its very low source level. It is still decreasing at 300 skipped cycles with increase of skipped cycles as shown in Fig. 13. But the change of the fission source at the bottom part is very small and does not affect the k_{eff} estimation. Therefore, we regard the fission source distribution as converged at the skipped cycles of 300 or more.

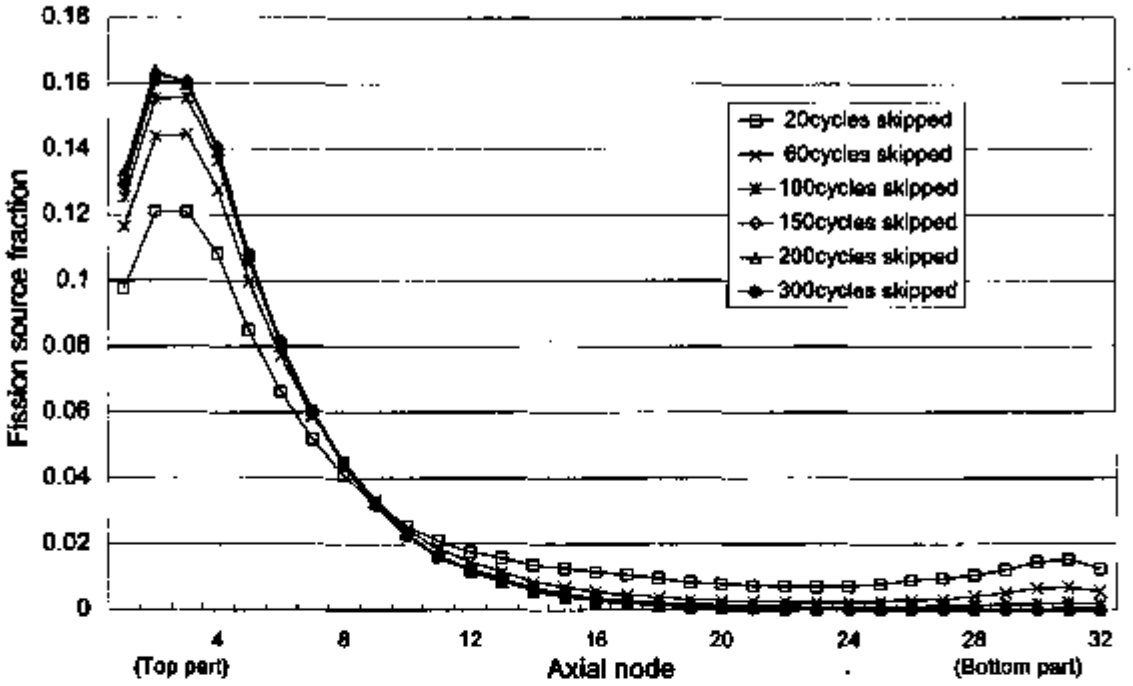

Fig. 12 Fission source distributions of B32C05A222222 for various skipped cycles based on the pin cell model [20,000 histories/cycle, (20-300) skipped, 100 cycles scored]

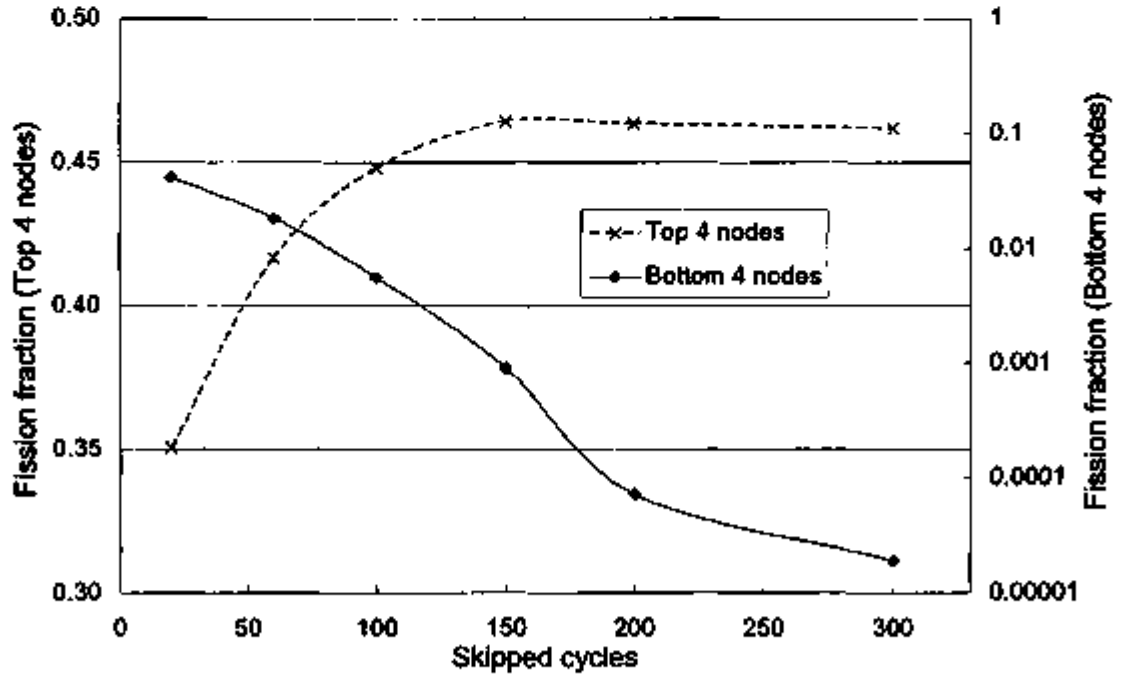

Fig. 13 Fission fractions of 4 nodes at the top and bottom parts for various skipped cycles based on the pin cell model of B32C05A222222

4.2. Radial Fission Distribution Based on Single Assembly and Color Set Configurations

In order to check the radial convergence of fission source distribution, we have also examined the single assembly configuration and 2x2 multi assembly configuration named color set configuration, here. In the color set configuration, three fuel assemblies and a water channel are considered as shown in Fig. 14. The radial boundary conditions are reflective, and the 1/8 radial symmetry is also considered for both configurations.

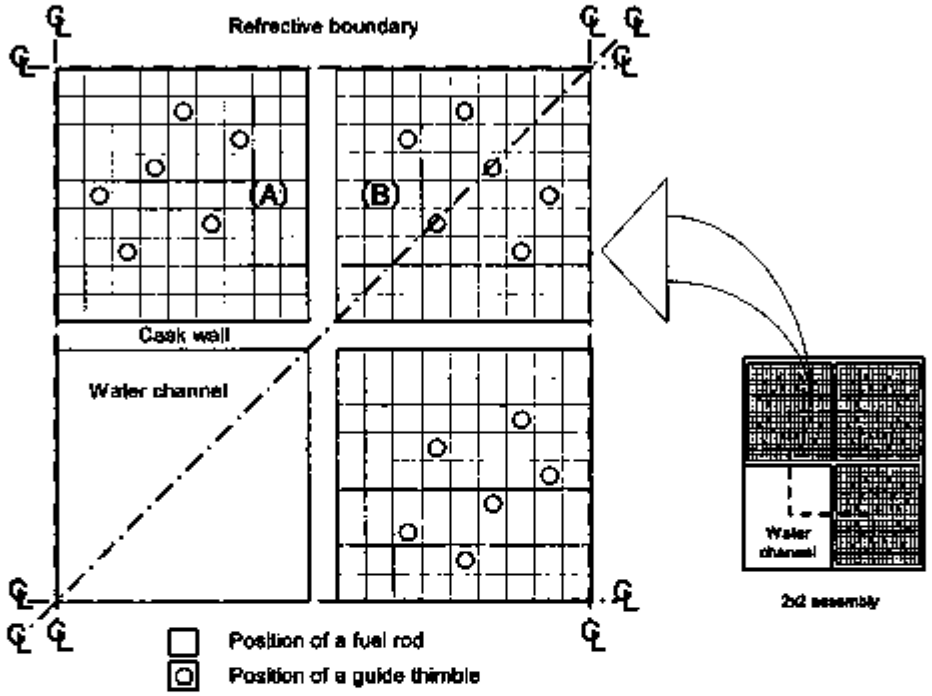

Fig. 14 Calculation model of the color set configuration

The calculated results of the radial fission source distribution for the single assembly configuration are shown in Fig. 15, 16 and 17 corresponding to the case ID of B32C05Symmetric, B32C05Uniform and B32C05A222222, respectively. In Fig.15 to 17, the calculation conditions are 150 skipped cycles and 20000 histories per cycle, and the results for both 10 and 100 scored cycles are shown.

As shown in Fig. 15 to 17, the radial fission source distributions for the three cases inside the assembly are almost the same as a chopped cosine curve in shape in spite of the axial fission source distribution difference, and they have already converged with the number of 150 skipped cycles.

The calculated result of the radial fission source distribution for the color set configuration is shown in Fig. 18 corresponding to the case ID of B32C05A222222. The calculation conditions are 300 skipped cycles and 20000 histories per cycle, and the results for both 10 and 100 scored cycles are shown. As shown in Fig. 18, the averaged fission source inside the quarter assembly (B) shown in Fig.14 is greater than that inside the eighth assembly (A) shown in Fig. 14. And the radial fission

source distributions inside the assemblies are similar to a chopped cosine curve in shape

The radial fission source distribution for the color set configuration not only inside the assembly but also assembly-wise averages has already converged as shown in Fig 18

These facts show that the radial source convergence is faster than the axial one In addition, the calculation time increases very much in order to print out the pin-wise fission source Hence, for the cask configuration, only the axial convergence is checked in the next section

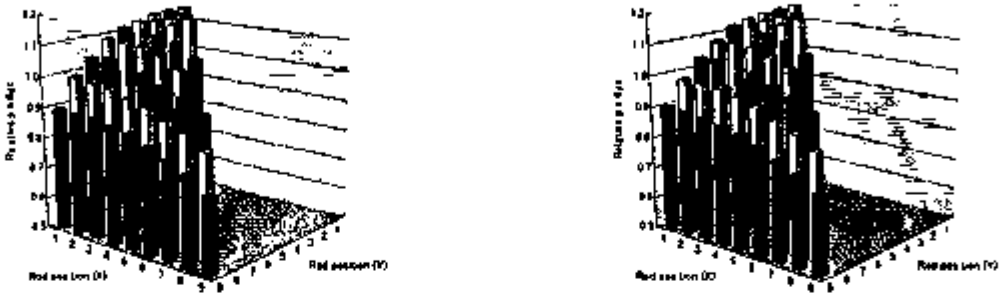

(a) 10 scored cycles (b) 100 scored cycles

Fig 15 Radial fission source distribution of single assembly configuration for B32C05Symmetric (difference of colors only means to distinguish between Y axis rod position)

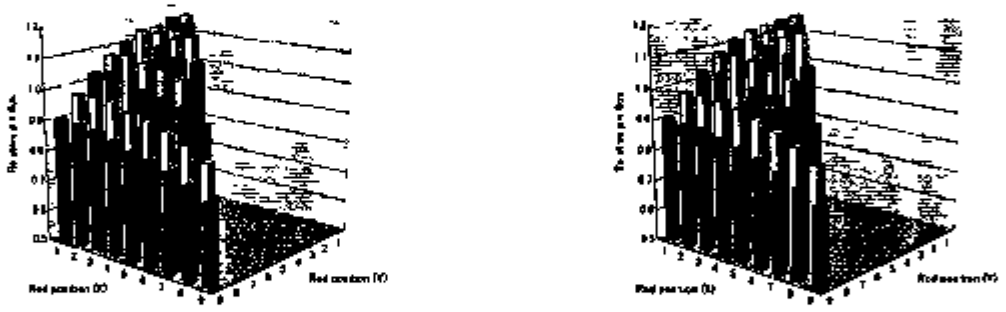

(a) 10 scored cycles (b) 100 scored cycles

Fig 16 Radial fission source distribution of single assembly configuration for B32C05Uniform (difference of colors only means the same as the other figures)

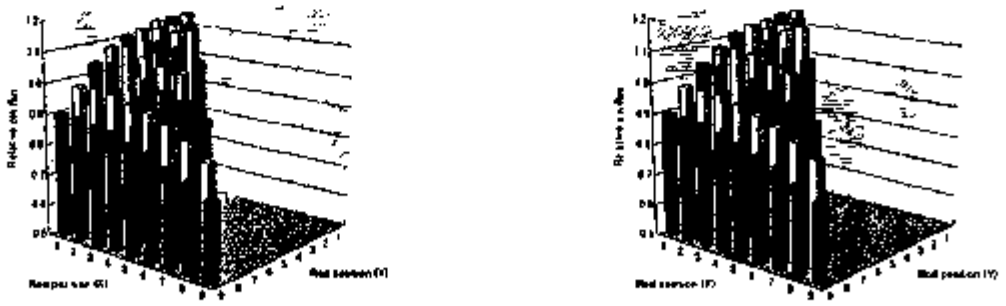

(a) 10 scored cycles (b) 100 scored cycles

Fig 17 Radial fission source distribution of single assembly configuration for B32C05A222222

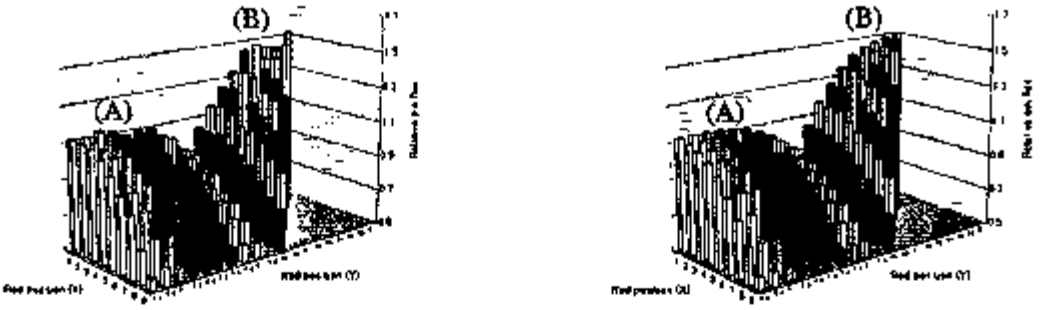

(a) 10 scored cycles (b) 100 scored cycles

Fig. 18 Radial fission source distribution of color set configuration for B32C05A222222

4.3. Convergence Check of Axial Fission Source Distribution Based on Cask Configuration

As a result of the prior examinations described in the previous sections, we determine the number of skipped cycles to be set at 300 in all cases of the cask calculation. Calculations for the Phase II-C cask configuration are carried out. As calculation conditions, the combination of the number of histories per cycle and the number of scored cycles are examined. Then, we check the axial source convergence and reset the calculation conditions to improve convergence as described in the section 3.2.

4.3.1. Symmetric Burnup Case

The calculation conditions of 3-D cask model described in Chapter 2 for B32C05Symmetric based on the AC+FP approach are examined as listed in Table 6. The calculated results for the axial fission source are shown in Fig. 19

Table 6 Calculation conditions for B32C05Symmetric examined

No.	Skipped cycles	Scored cycles	Histories per cycle	Total scored histories
1	300	4,000	500	2,000,000
2	300	2,000	1,000	2,000,000
3	300	400	5,000	2,000,000
4	300	2,000	5,000	10,000,000
5	300	100	20,000	2,000,000

As shown in Fig. 19, it is found that the results for each condition are quite different. In order to check the fission source convergence, for instance, the fission source trends per scored cycle for No. 4 and 5 are shown in Fig. 20 and Fig. 21, respectively. As shown in Fig. 20, the fission source

distribution changes with the increase of scored cycles. The same trend is observed for the calculation conditions of No. 2 and 3. In these cases, the number of histories per cycle is so small that the fission source distribution trends become unstable. On the other hand, 20,000 histories per cycle in case No. 5 is enough for the fission source distribution trend to be stable as shown in Fig.21.

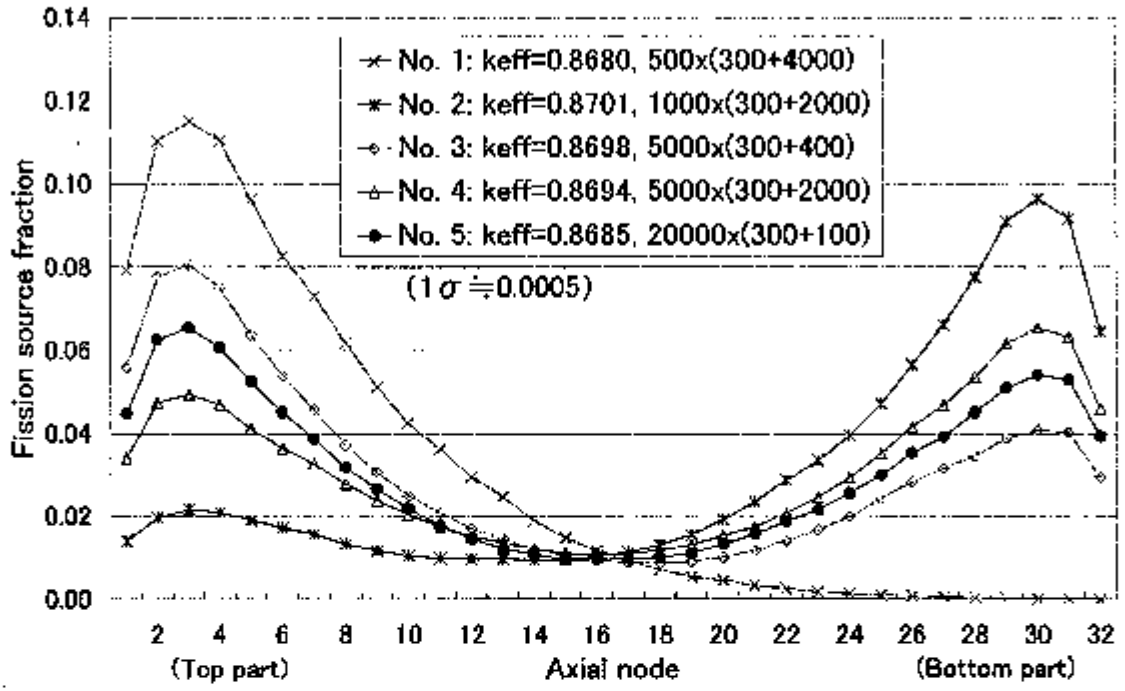

Fig. 19 Fission source distributions of B32C05Symmetric for various conditions

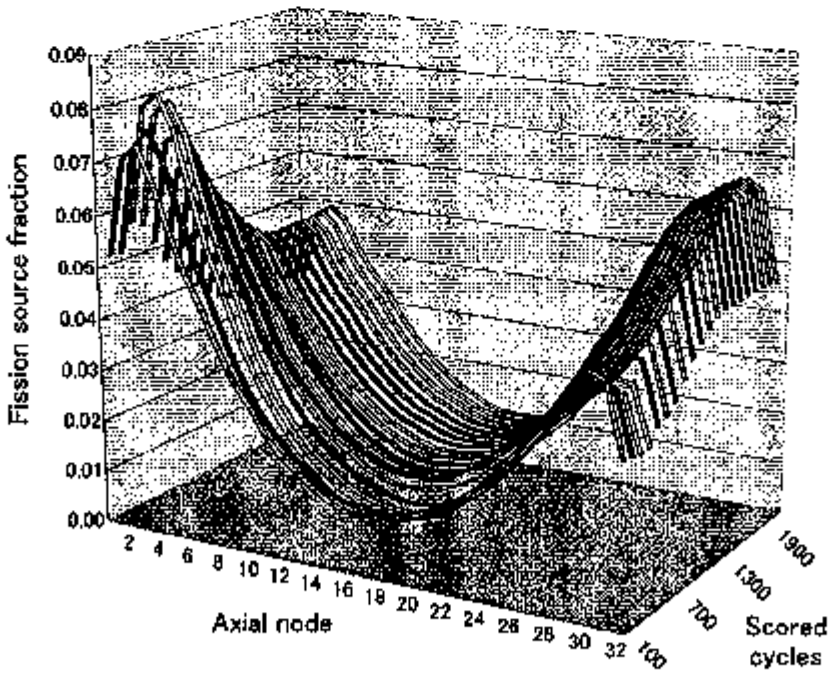

Fig. 20 Fission source distribution trend of B32C05Symmetric (calculation condition No. 4)

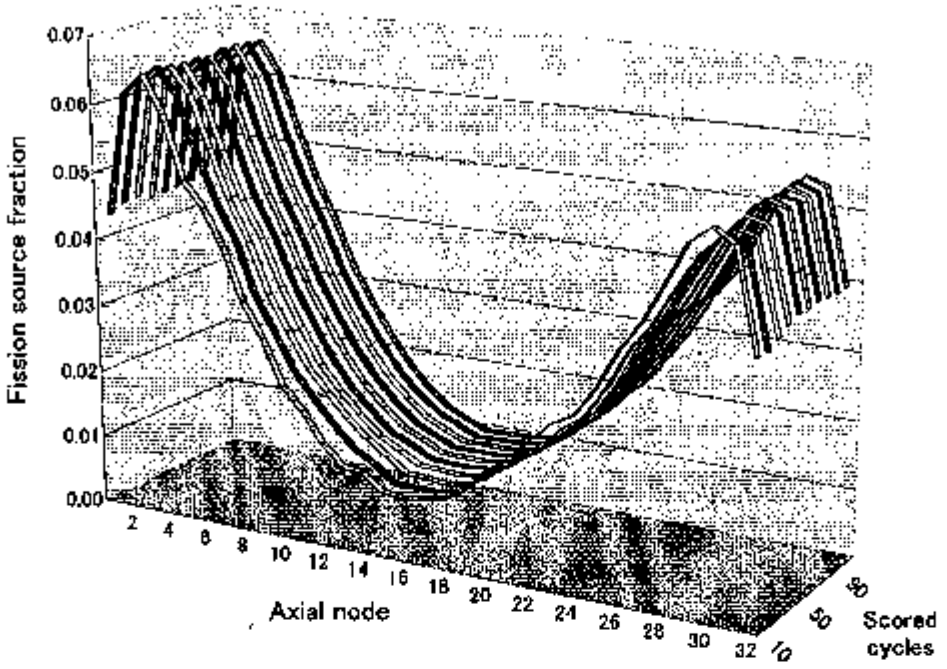

Fig. 21 Fission source distribution trend of B32C05Symmetric (calculation condition No. 5)

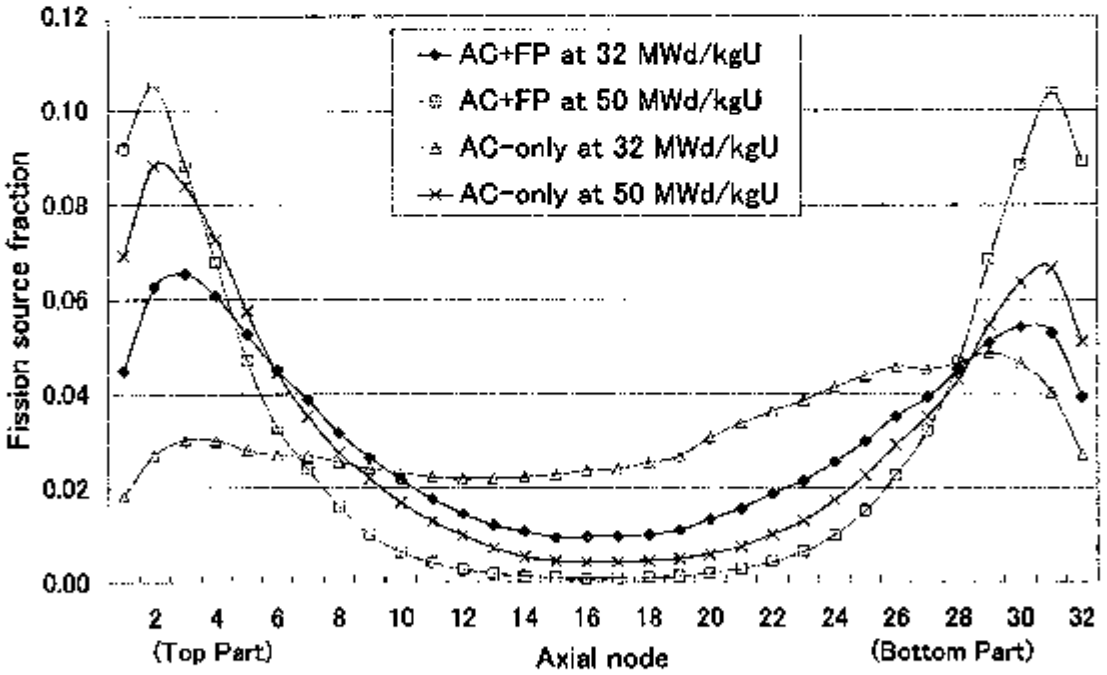

Fig. 22 Calculated results for fission source distribution in cases of the symmetric burnup

Therefore, we determine the calculation conditions for all symmetric cases to be set as No. 5 in Table 6. The calculated results for the fission source distributions are almost symmetric as shown in Fig. 22.

4.3.2. Uniform Burnup Case

The calculation conditions of 3-D cask model for B32C05Uniform based on the AC+FP approach are examined as listed in Table 7. The calculated results for the axial fission source are shown in Fig. 23

Table 7 The calculation conditions for B32C05Uniform examined

No.	Skipped cycles	Scored cycles	Histories per cycle	Total scored histories
1	300	1,000	2,000	2,000,000
2	300	400	5,000	2,000,000
3	300	100	20,000	2,000,000

The converged fission source distributions for the uniform burnup case are expected to be cosine-like in shape, and the results of the fission source distribution for each condition are a little bit different from cosine curve as shown in Fig. 23. It is necessary to increase the total scored histories in order to obtain smoother and more cosine-like shape. The calculated results of all uniform cases for condition No.2 in Table 7 and for the case of increased histories are shown in Fig. 24(a) and Fig. 24(b), respectively. The calculation condition of the latter, that is 300 skipped cycles, 4,000 scored cycles and 5,000 histories per cycle are considered appropriate to give the final results for the uniform burnup cases in this report.

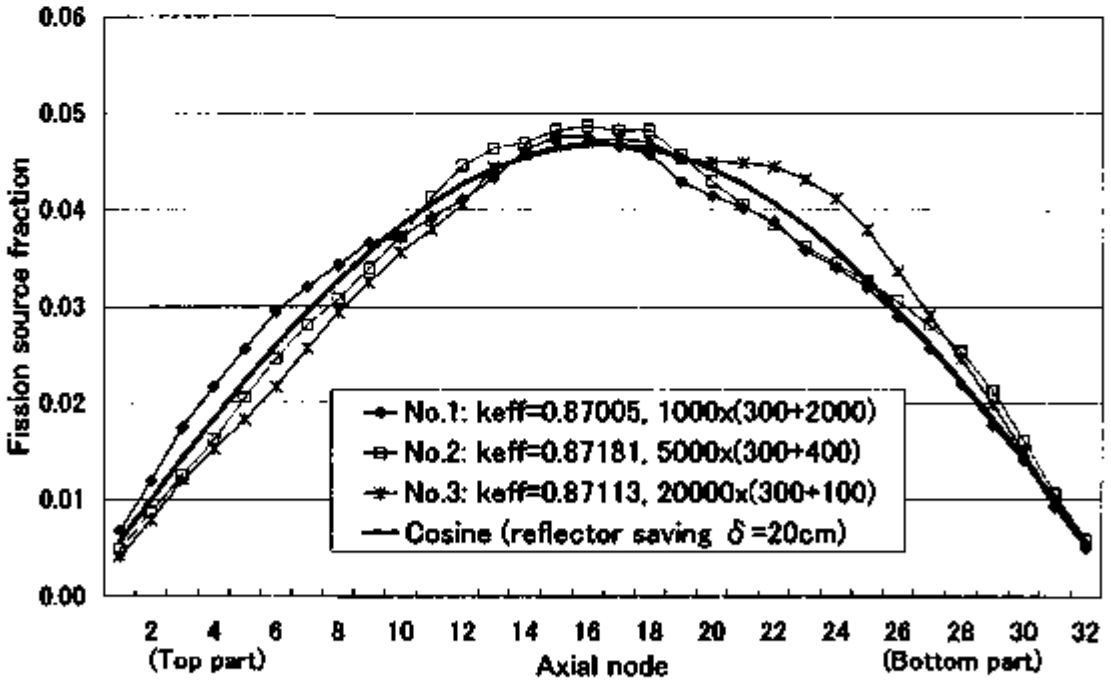

Fig. 23 Calculated results for fission source distribution in cases of the uniform burnup

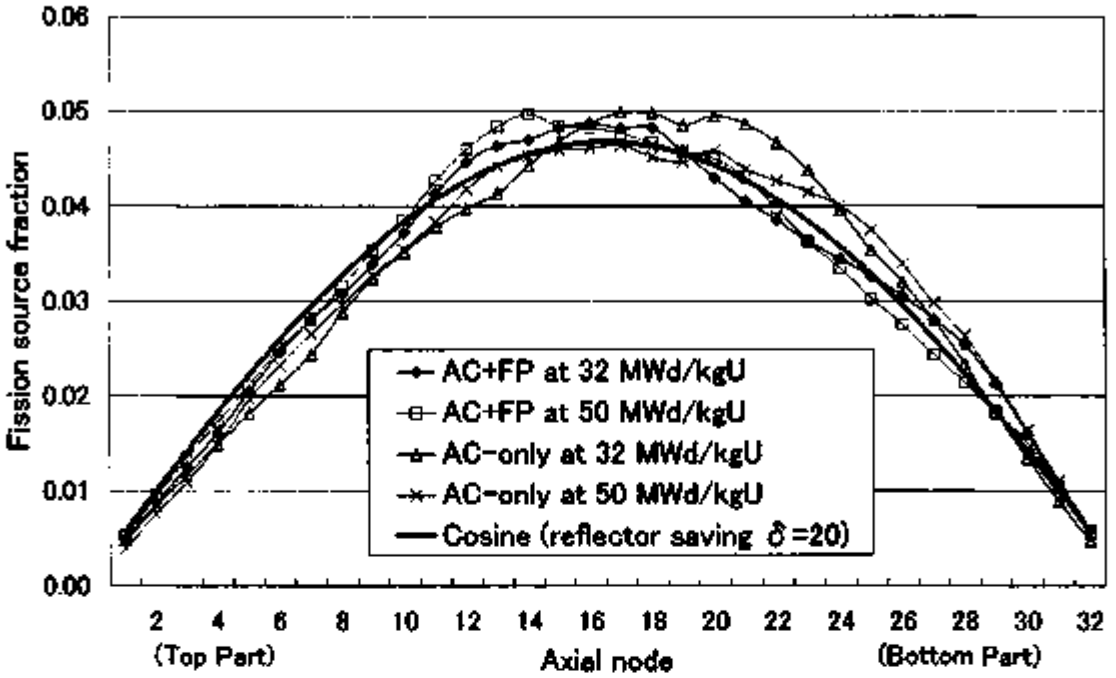

(a) Not final results: 5000 histories per cycle x (300 skipped cycles + 400 scored cycles)

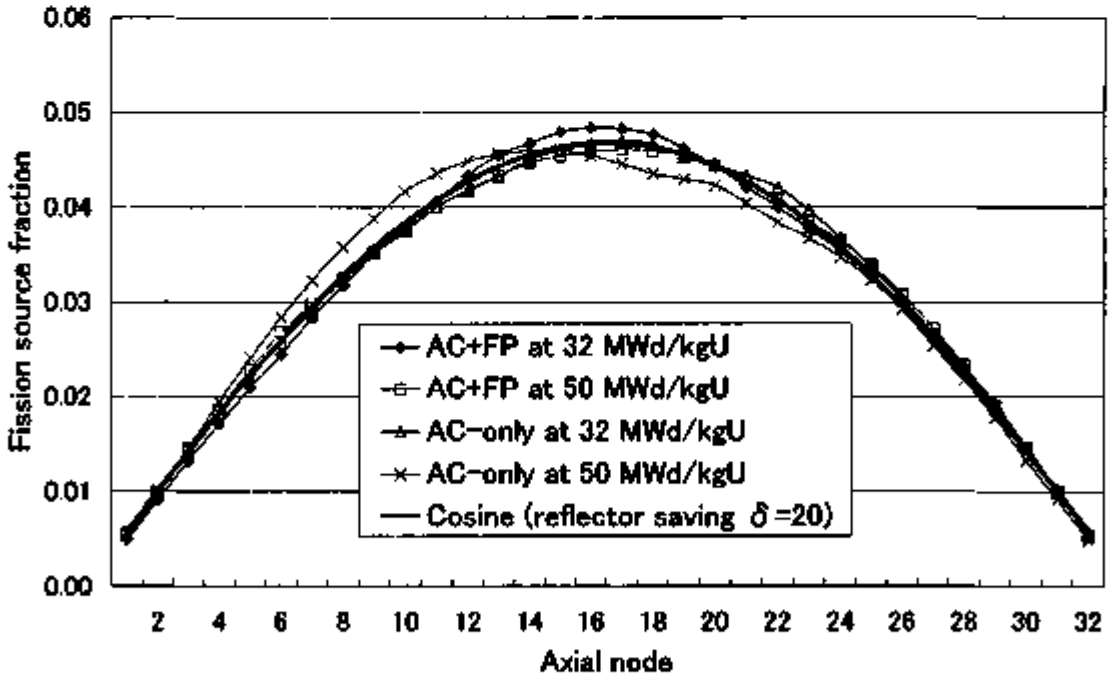

(b) Final results: 5000 histories per cycle x (300 skipped cycles + 4000 scored cycles)

Fig. 24 Calculated results for fission source distribution in cases of the uniform burnup

In order to check the fission source convergence of final results, the fission source trend per scored cycle of B32C05Uniform, for instance, is shown in Fig. 25. As shown in Fig. 25, the fission source distribution is observed to reach near convergence at 4000 scored cycles.

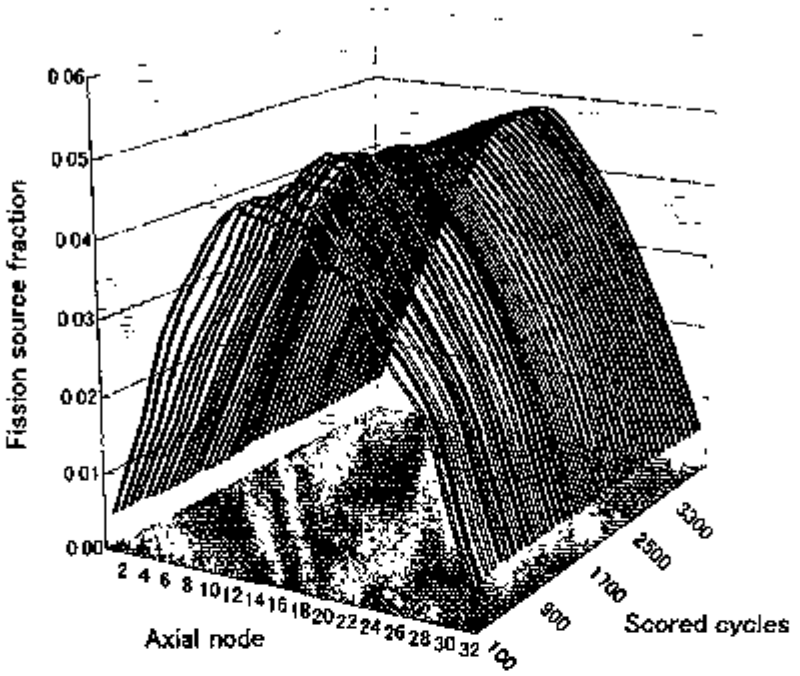

Fig. 25 Fission source distribution trend of B32C05Uniform in case of 5000 histories per cycle

4.3.3. Asymmetric Burnup Case

It is desirable to examine various calculation conditions for the asymmetric burnup cases in the same way as the previously mentioned cases of symmetric and uniform burnup. From the viewpoints of calculation time, we carry out calculations of only two different conditions such as 1,000 histories per cycle x 2000 scored cycles and 5,000 histories per cycle x 400 scored cycles. Both are with 300 skipped cycles. For most cases, the fission source distribution trends for the latter condition are slightly more stable than the former, and they reach near convergence. But it was found that there exist four cases of insufficiently converged fission source. As a function of the burnup A. O. (see subsection 2.2.3.), the maximum and the standard deviation for differences of fission source distribution between two conditions are shown in Fig. 26. In general, both conditions give almost the same result of fission source distribution except the insufficiently converged cases such as B32C05A233333 and B32C05A333333 for the both AC+FP and AC-only approaches as shown in Fig. 26. This is caused by their slightly asymmetric burnup. So, the skipped cycles are reexamined for them to reach convergence based on the cask configuration. The calculated results of the four cases for more than 300 skipped cycles are shown in Fig. 27 to Fig. 30, respectively. It is found that

the largest number of skipped cycles shown in each figure gives almost converged fission source distribution of the corresponding four cases. In order to check the fission source convergence of final results, the fission source trends per scored cycle of the four cases are shown in Fig. 31 to Fig. 34.

Therefore, the calculation conditions for all cases are finally determined as listed in Table 5.

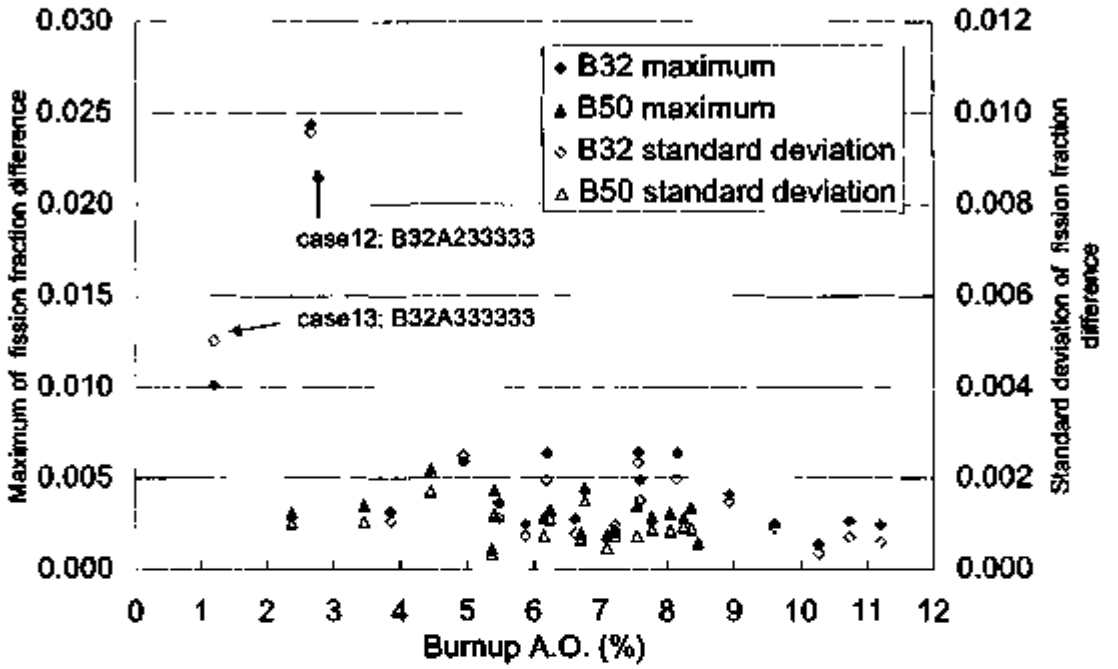

(a) AC+FP approach

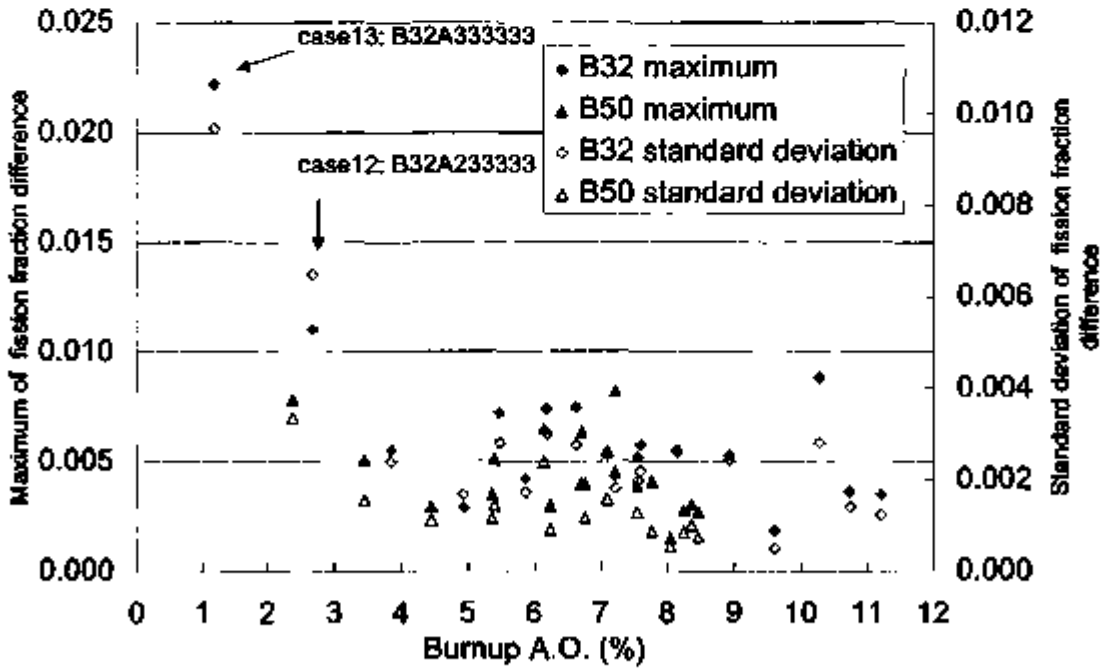

(b) AC-only approach

Fig. 26 Fission source differences between 2 conditions in cases of asymmetric burnup

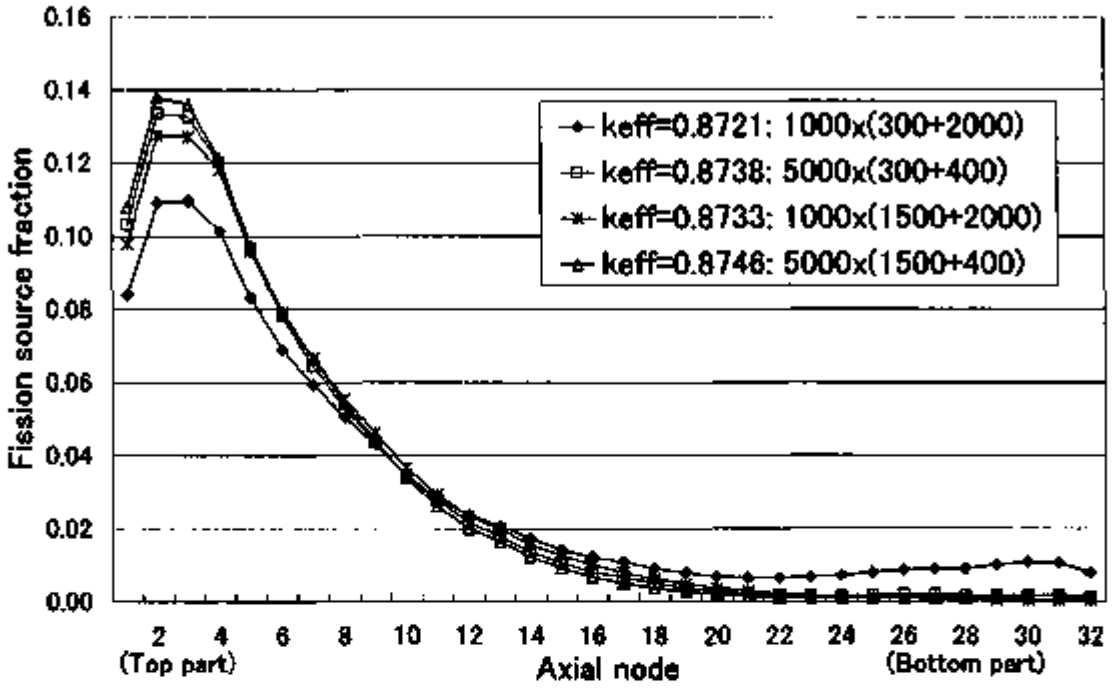

Fig. 27 Reexamination of calculation conditions for B32C05A233333 based on the AC+FP approach

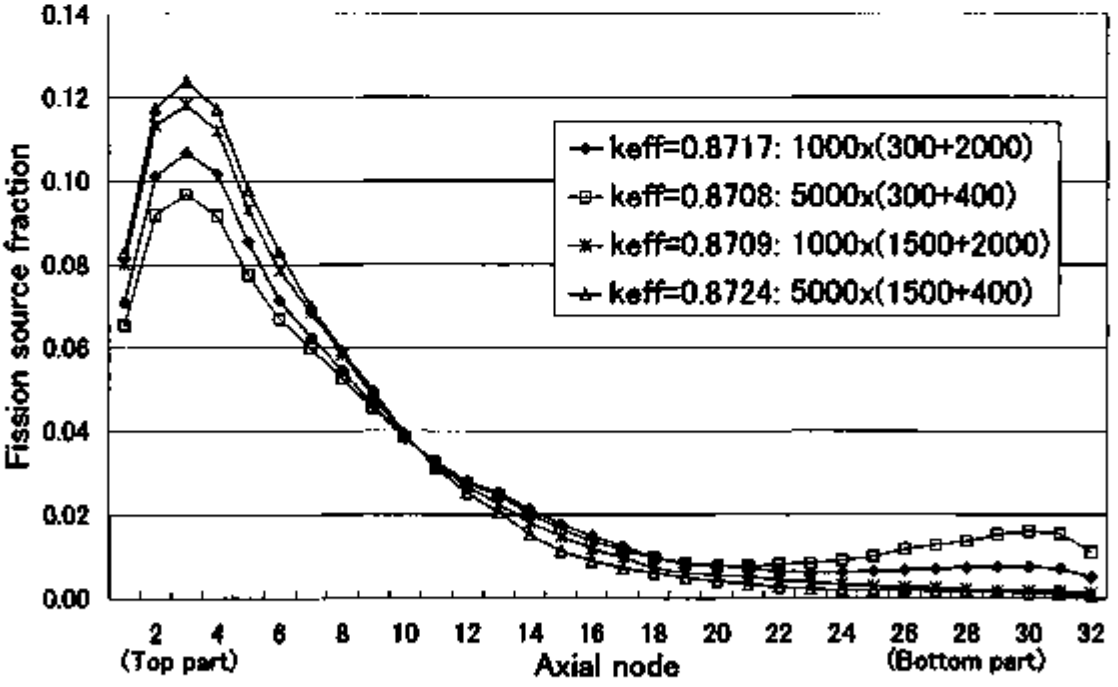

Fig. 28 Reexamination of calculation conditions for B32C05A333333 based on the AC+FP approach

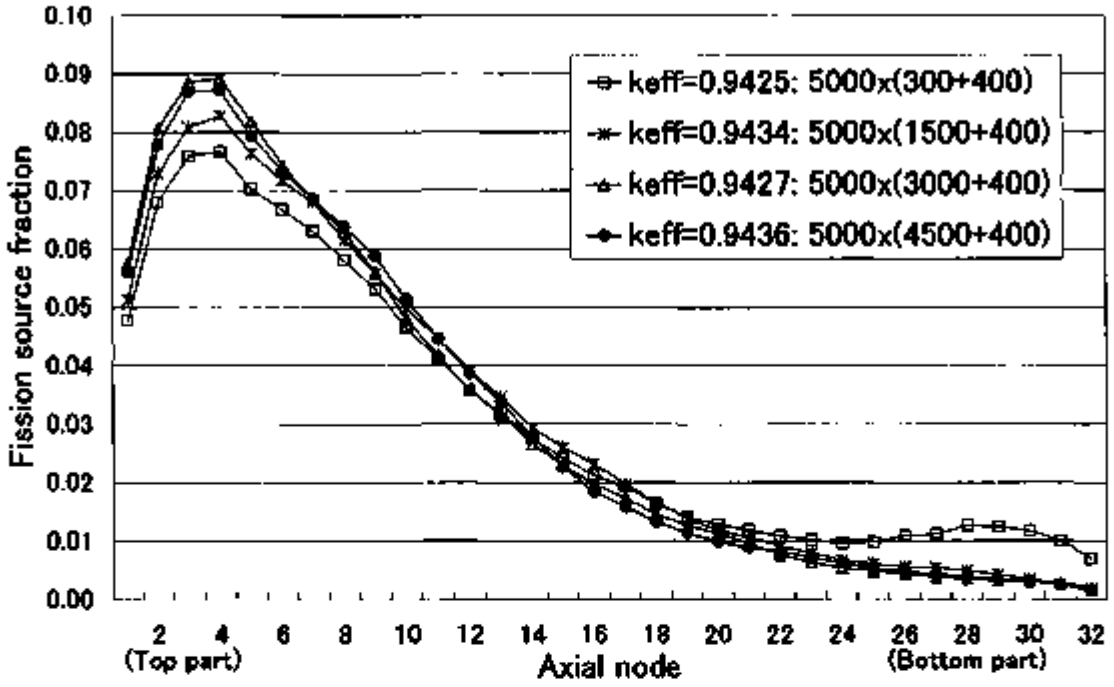

Fig. 29 Reexamination of calculation conditions for B32C05A233333 based on the AC-only approach

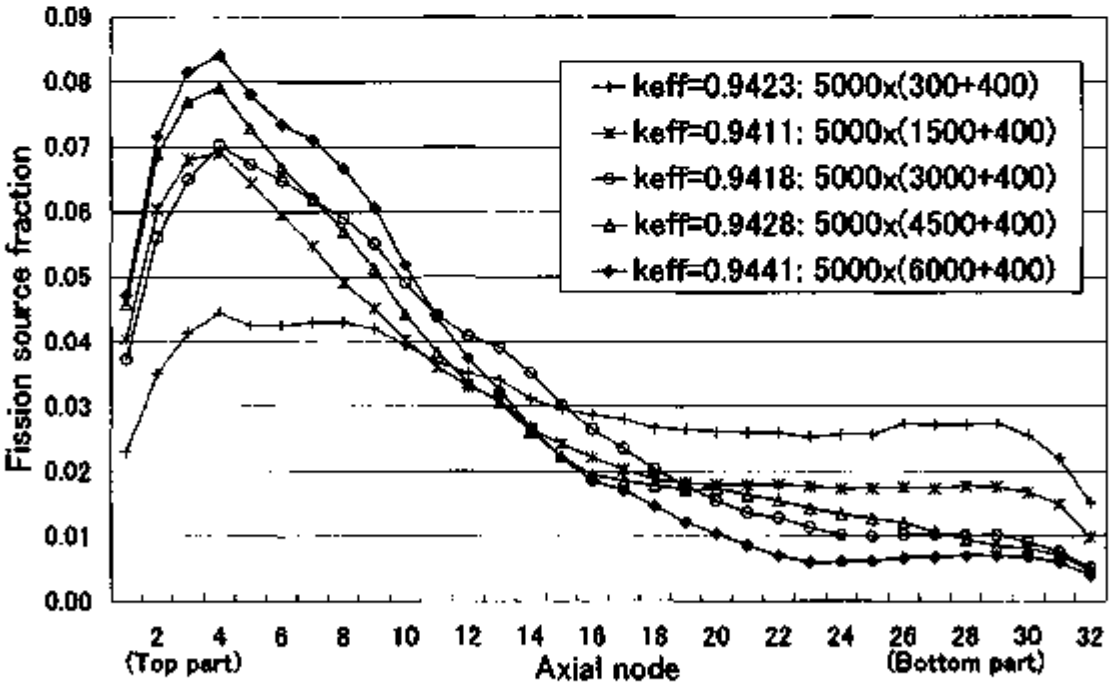

Fig. 30 Reexamination of calculation conditions for B32C05A333333 based on the AC-only approach

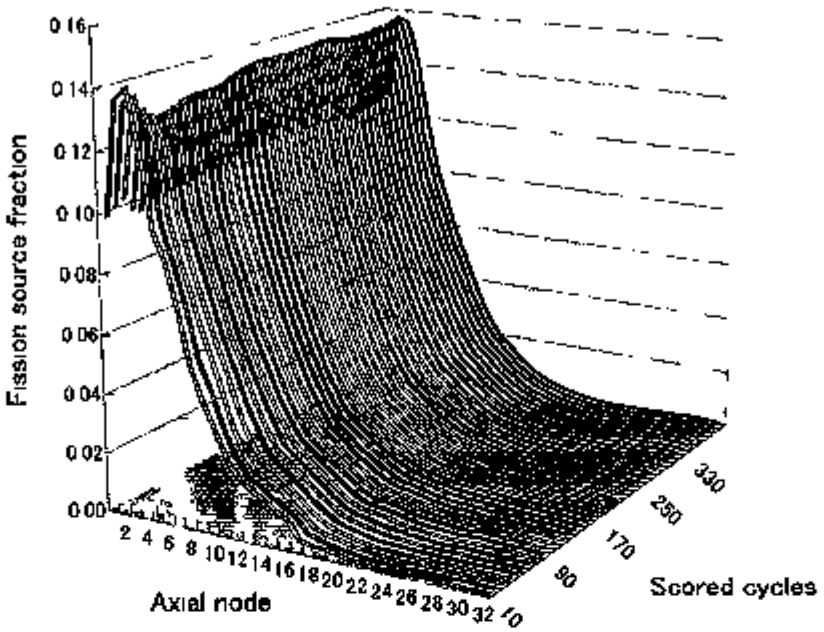

Fig 31 Fission source distribution trend of B32C05A233333 in case of 1500 skipped cycles and 5000 histories per cycle, based on AC+FP approach

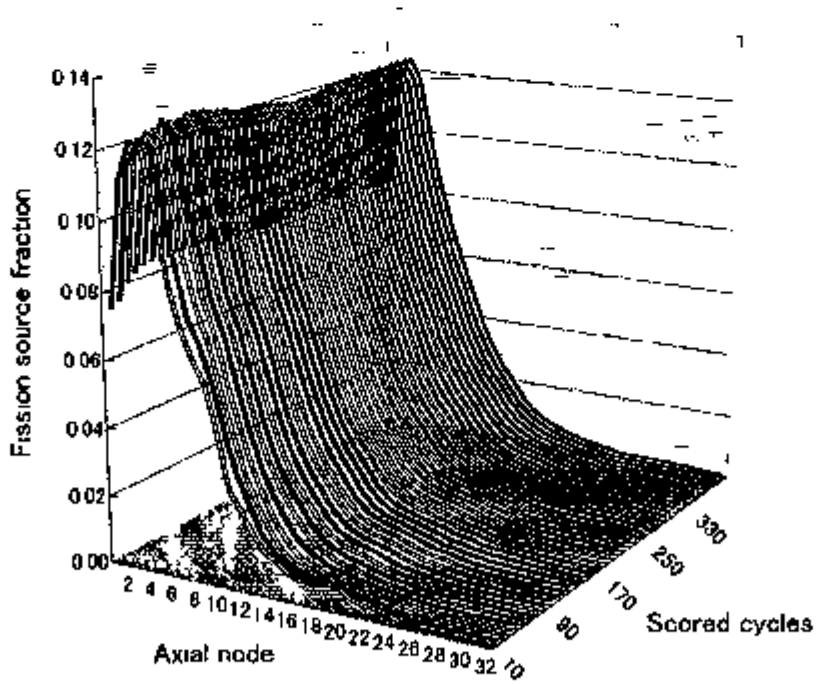

Fig 32 Fission source distribution trend of B32C05A333333 in case of 1500 skipped cycles and 5000 histories per cycle, based on AC+FP approach

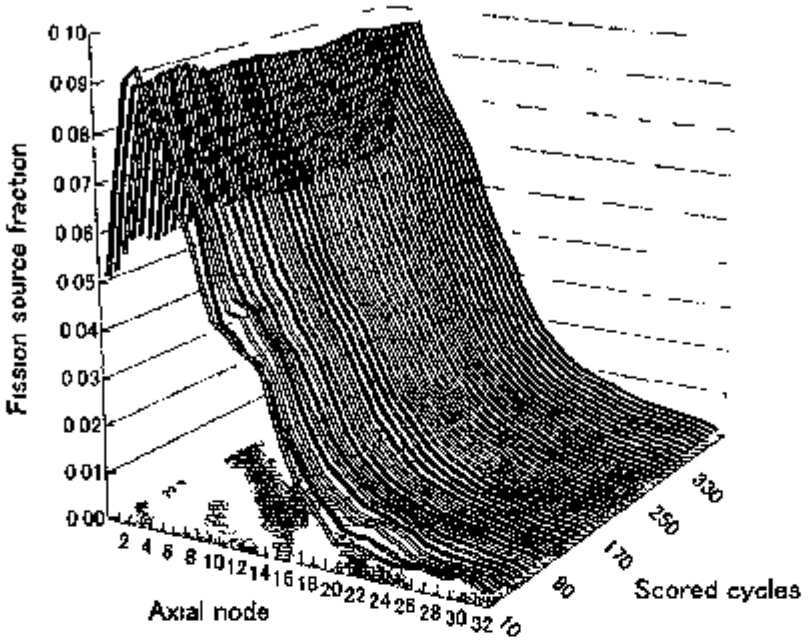

Fig 33 Fission source distribution trend of B32C05A233333 in case of 4500 skipped cycles and 5000 histories per cycle, based on AC-only approach

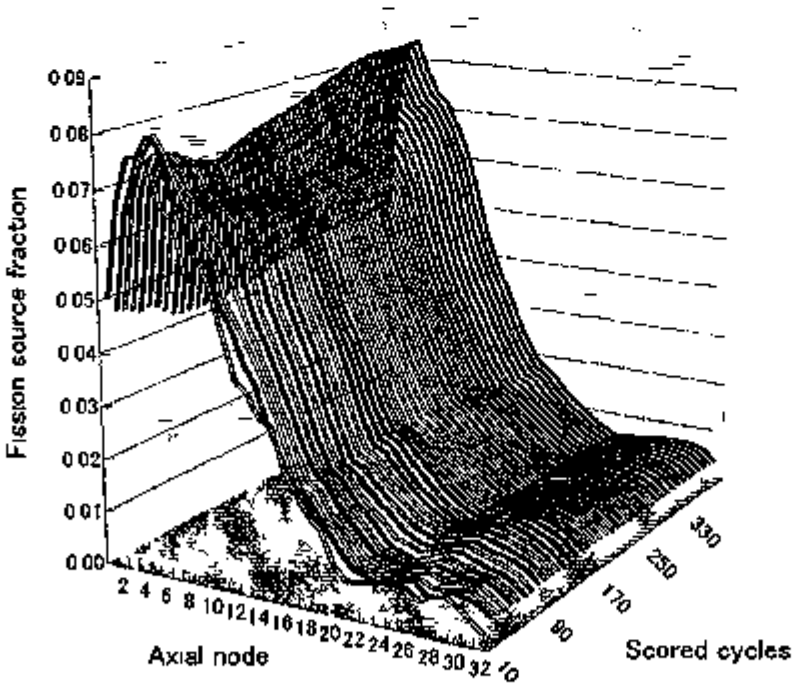

Fig 34 Fission source distribution trend of B32C05A333333 in case of 6000 skipped cycles and 5000 histories per cycle, based on AC-only approach

4.4. Final Results

4.4.1. k_{eff} and End Effect

Calculated k_{eff} results, one standard deviations and end effects for the final estimations are listed in Table 8. Here, the end effect is defined as a reactivity difference between the uniform burnup case and the others in consideration of the axial burnup profiles as formulated below.

$$\text{End effect}\,(\%\Delta k/k) = 100 \times \frac{k_{eff}\,(\text{axial burnup profile}) - k_{eff}\,(\text{uniform burnup})}{k_{eff}\,(\text{uniform burnup})}$$

Table 8 Calculated k_{eff} results for both AC+FP and AC-only approaches

Case ID	Serial No.	Burnup A.O. (%)	AC+FP approach			AC-only approach		
			k_{eff}	1σ	End effect (%Δk/k)	k_{eff}	1σ	End effect (%Δk/k)
B32C05Symmetric	--	0.00	0.86848	0.00051	-0.36	0.94071	0.00045	-0.53
B32C05Uniform	--	0.00	0.87166	0.00015	——	0.94571	0.00016	——
B32C05A222222	1	7.21	0.88971	0.00050	2.07	0.95218	0.00048	0.68
B32C05A111111	2	11.20	0.90013	0.00050	3.27	0.96120	0.00050	1.64
B32C05A111112	3	10.73	0.90042	0.00051	3.30	0.96001	0.00055	1.51
B32C05A111122	4	10.27	0.89959	0.00049	3.20	0.96077	0.00051	1.59
B32C05A111222	5	9.60	0.89709	0.00047	2.92	0.95874	0.00050	1.38
B32C05A112222	6	8.93	0.89390	0.00050	2.55	0.95695	0.00048	1.19
B32C05A122222	7	8.14	0.89102	0.00049	2.22	0.95332	0.00048	0.80
B32C05A222223	8	6.62	0.88674	0.00049	1.73	0.95265	0.00052	0.73
B32C05A222233	9	5.87	0.88630	0.00049	1.68	0.95158	0.00049	0.62
B32C05A222333	10	4.93	0.88410	0.00047	1.43	0.94881	0.00048	0.33
B32C05A223333	11	3.86	0.87746	0.00049	0.67	0.94411	0.00047	-0.17
B32C05A233333	12	2.68	0.87327	0.00047	0.18	0.94357	0.00052	-0.23
B32C05A333333	13	1.19	0.87093	0.00047	-0.08	0.94408	0.00049	-0.17
B32C05A122223	14	7.55	0.88986	0.00049	2.09	0.95247	0.00050	0.71
B32C05A112233	15	7.59	0.89203	0.00049	2.34	0.95273	0.00052	0.74
B32C05A322221	16	6.19	0.88671	0.00049	1.73	0.95300	0.00049	0.77
B32C05A332211	17	5.48	0.88283	0.00048	1.28	0.95254	0.00050	0.72
B50C05Symmetric	--	0.00	0.75590	0.00047	2.03	0.84242	0.00047	0.76
B50C05Uniform	--	0.00	0.74084	0.00013	-----	0.83610	0.00014	-----
B50C05A222222	18	7.21	0.78772	0.00046	6.33	0.86562	0.00047	3.53
B50C05A111111	19	8.46	0.79403	0.00046	7.18	0.87013	0.00049	4.07
B50C05A111112	20	8.35	0.79362	0.00046	7.12	0.87012	0.00050	4.07
B50C05A111122	21	8.24	0.79372	0.00045	7.14	0.87093	0.00049	4.17
B50C05A111222	22	8.04	0.79299	0.00044	7.04	0.86943	0.00047	3.99
B50C05A112222	23	7.77	0.79037	0.00047	6.69	0.86867	0.00048	3.90
B50C05A122222	24	7.54	0.78843	0.00047	6.42	0.86630	0.00045	3.61
B50C05A222223	25	6.76	0.78679	0.00047	6.20	0.86569	0.00048	3.54
B50C05A222233	26	6.15	0.78565	0.00043	6.05	0.86415	0.00047	3.35
B50C05A222333	27	5.41	0.78221	0.00045	5.58	0.86155	0.00050	3.04
B50C05A223333	28	4.45	0.77597	0.00043	4.74	0.85658	0.00050	2.45
B50C05A233333	29	3.46	0.76778	0.00046	3.64	0.85038	0.00050	1.71
B50C05A333333	30	2.38	0.76141	0.00046	2.78	0.84740	0.00046	1.35
B50C05A122223	31	7.09	0.78910	0.00046	6.51	0.86599	0.00046	3.57
B50C05A112233	32	6.70	0.79017	0.00044	6.66	0.86763	0.00049	3.77
B50C05A322221	33	6.24	0.78211	0.00044	5.57	0.86290	0.00048	3.21
B50C05A332211	34	5.36	0.77461	0.00047	4.56	0.85828	0.00044	2.65

The relation between k_{eff} and burnup A. O. is shown in Fig. 35 to Fig. 38. Here, the error bars show 3σ of k_{eff}. The fitting lines are obtained by the following equations as shown in Fig. 35 to Fig. 38.

$$k_{eff}\,[32\text{MWd/kgU, AC+FP approach}] = 0.0031 \times \text{Burnup A. O. (\%)} + 0.8672$$

$$k_{eff}\,[50\text{MWd/kgU, AC+FP approach}] = 0.0049 \times \text{Burnup A. O. (\%)} + 0.7531$$

$$k_{eff}\,[32\text{MWd/kgU, AC-only approach}] = 0.0019 \times \text{Burnup A. O. (\%)} + 0.9399$$

$$k_{eff}\,[50\text{MWd/kgU, AC-only approach}] = 0.0036 \times \text{Burnup A. O. (\%)} + 0.8406$$

As shown in Fig. 35 to Fig. 38, it is found that k_{eff} in case of 32 MWd/kgU decreases by considering the axial burnup profile at 0 burnup A. O. both for the AC+FP and AC-only approaches. On the other hand, in case of 50 MWd/kgU, k_{eff} increases at 0 burnup A. O. This is explained as follows. The consideration of axial burnup profile makes the fission source distribution to be localized in the top and the bottom parts. In case of low burnup, the localization of fission source distribution increases the negative reactivity of neutron leakage that is supposed to be major effect. At 32 MWd/kgU for symmetric burnup profile, total reactivity is somewhat negative. With increase of average burnup, the burnup difference between the end part of low burnup and the middle part of high burnup increases, and the localization of fission source distribution to the low burnup is also enhanced. Therefore, the increase of average burnup contributes to the positive reactivity effect. In a certain point of average burnup more than 32 MWd/kgU, the positive reactivity effect seems to be greater than the negative one. Hence, the total reactivity at 50 MWd/kgU for symmetric burnup profile becomes positive.

The burnup difference between the top part of highest burnup and the other part increases with the increase of burnup A. O., namely, with increase of the axial asymmetry of burnup profile, and the localization of fission source distribution is also enhanced. So, k_{eff} increases almost linearly with the increase of burnup A. O at both 32 and 50 MWd/kgU. The discrepancy between k_{eff} results and the fitting line seems to be large in comparison with 3σ of k_{eff}. One of the reasons is supposed to be that the burnup shape inside the upper part affects the k_{eff} results because the burnup A.O. represents the region averaged burnup difference, but does not reflect the fine burnup shape inside the top part.

It is obviously seen that the AC-only approach is conservative in comparison with the AC+FP approach. The k_{eff} margin at both 32 and 50 MWd/kgU is at least 4 $\%\Delta k/k$.

The relation between the end effect and the burnup A. O. is shown in Fig. 39. The fitting lines are also shown in Fig. 39. The same tendency as k_{eff} is observed in Fig. 39. Both the increase of average burnup and the consideration of FP contribute to the increase of not only the end effect itself but also the tendency of dependence on the burnup A. O.

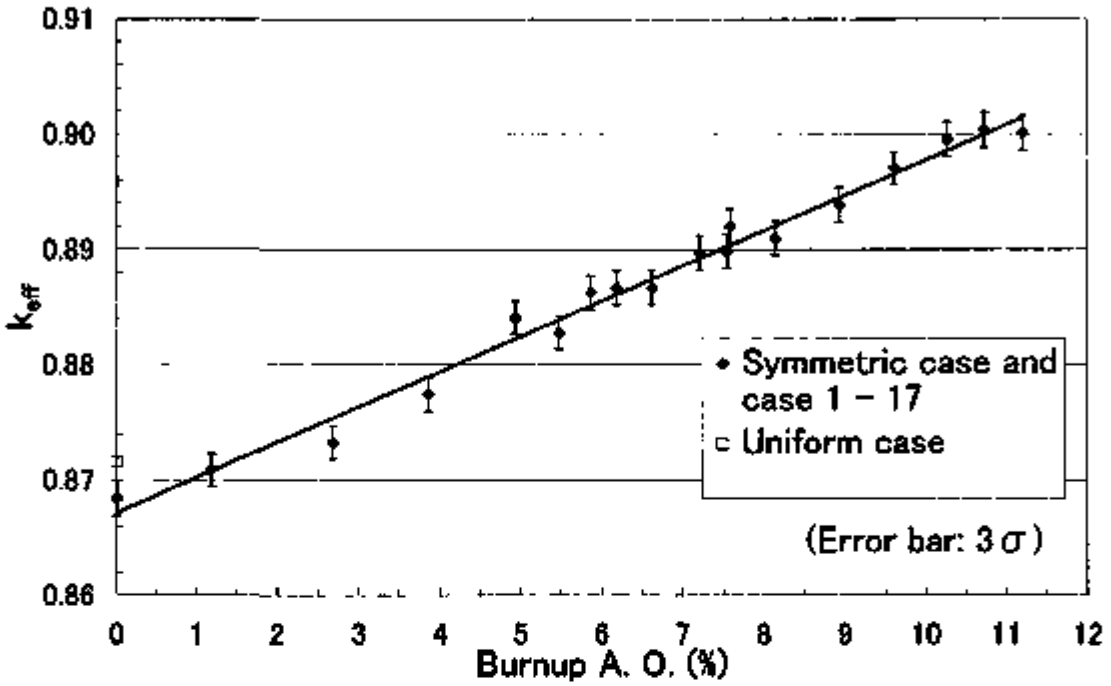

Fig. 35 k_{eff} vs. burnup A. O. at 32 MWd/kgU based on AC+FP approach

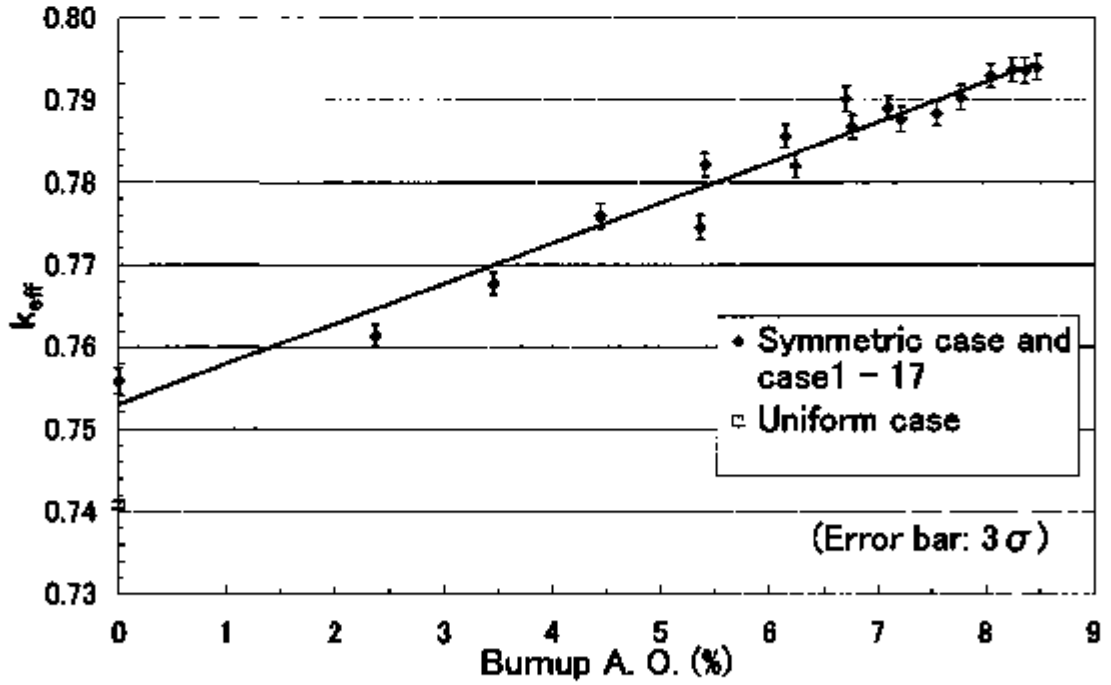

Fig. 36 k_{eff} vs. burnup A. O. at 50 MWd/kgU based on AC+FP approach

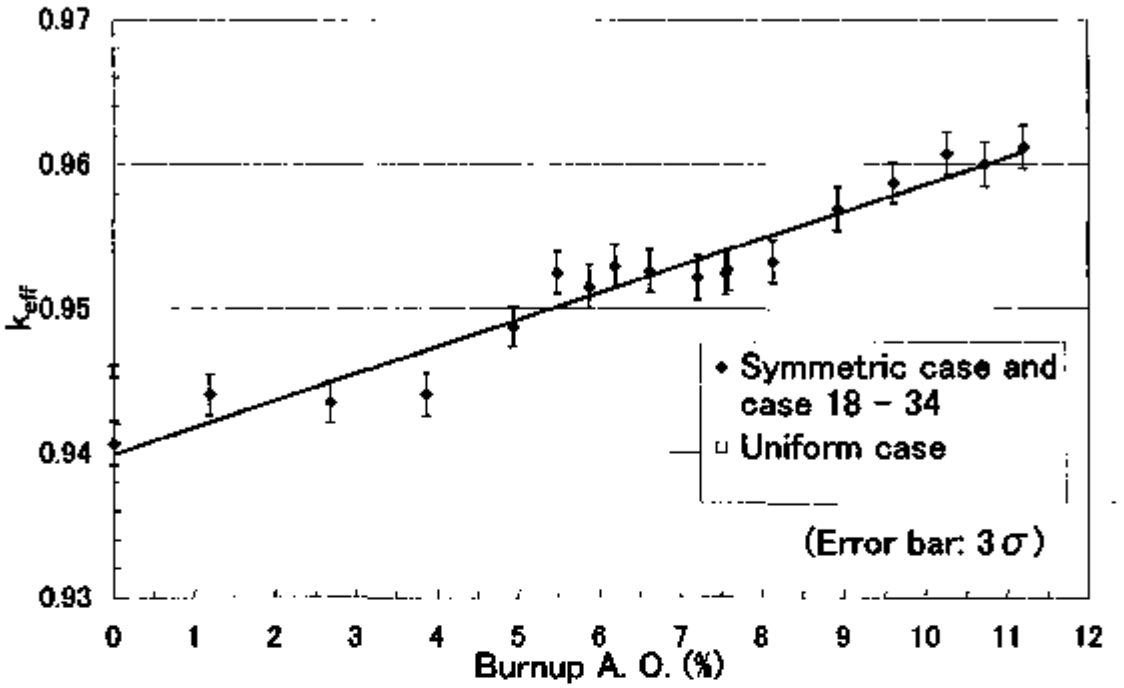

Fig. 37 k_{eff} vs. burnup A. O. at 32 MWd/kgU based on AC-only approach

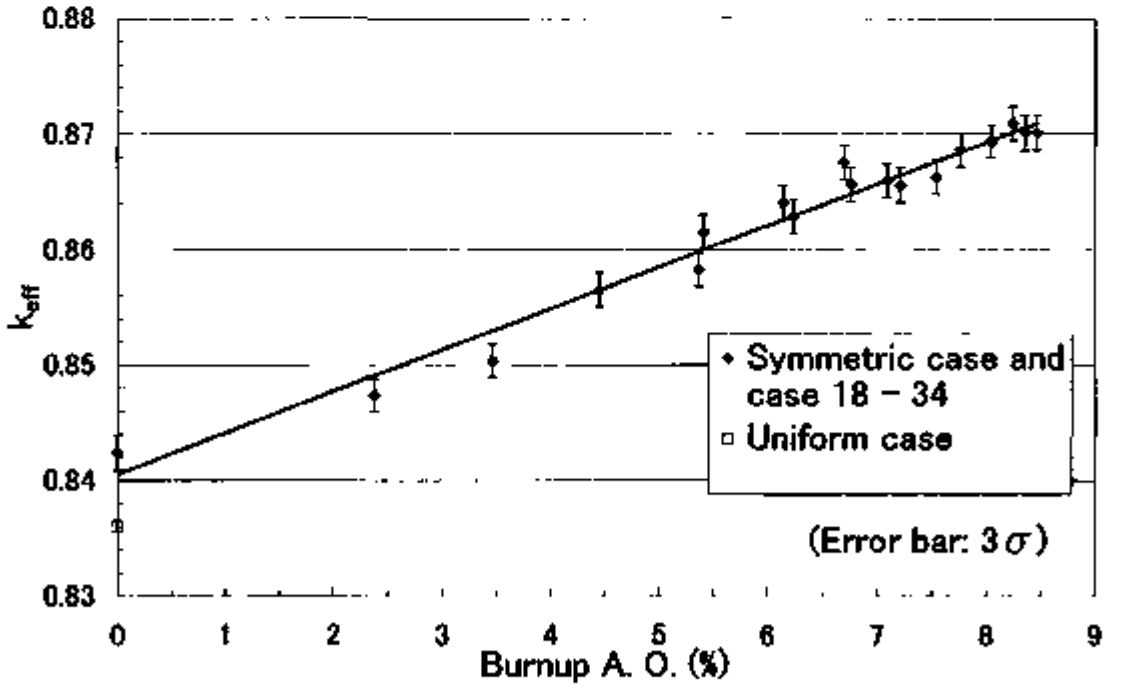

Fig. 38 k_{eff} vs. burnup A. O. at 50 MWd/kgU based on AC-only approach

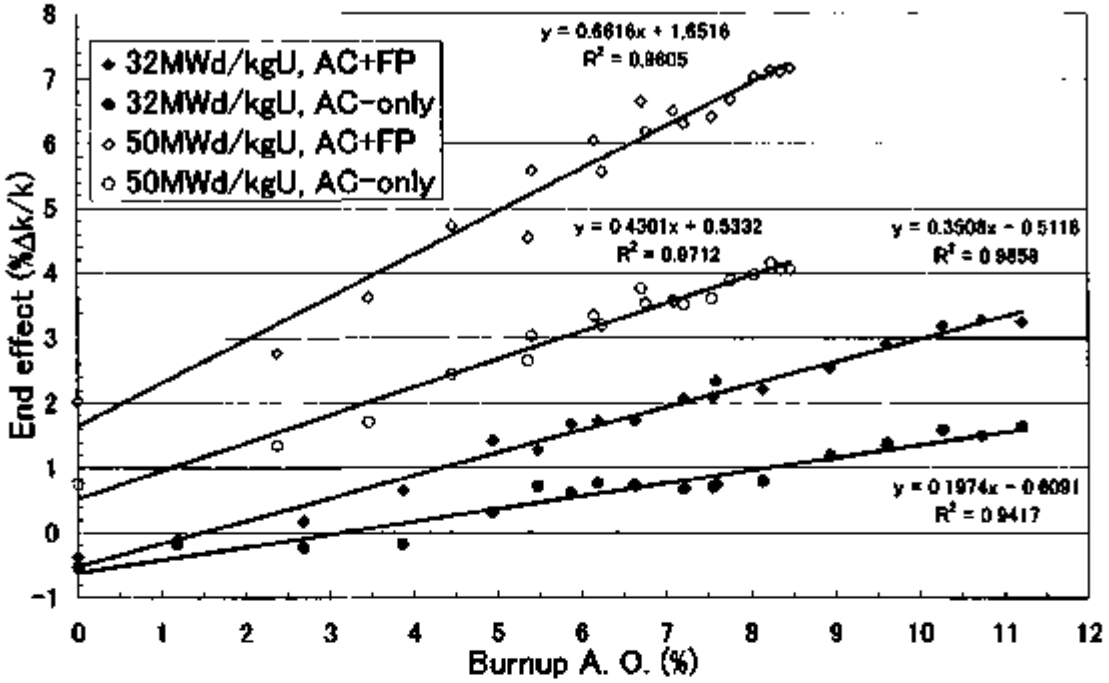

Fig. 39 End effect vs. burnup A. O.

4.4.2. Fission Source Distribution

The calculated results of the fission source distribution for all cases are shown in Fig. 40 to Fig. 43 with both linear and semi-log scales. We cannot predict the very low source levels at the bottom end with enough reliability. Nonetheless, the precision of estimated k_{eff}'s and fission source distributions are acceptable. So, we neglect the fission source fluctuation at the bottom end in judging convergences of calculations. It is seen that the increase of average burnup and the burnup A. O., and the consideration of FP enhance the localization of the fission source distribution at the upper part and increase the maximum value. In order to illustrate this tendency, we introduce the fission A. O. defined as follows.

Fission A. O. = (Fission source average for upper 16 nodes – that for lower 16 nodes)
/ fission source average for all 32 nodes

The calculated results of the fission A. O. as a function of burnup A. O. are shown in Fig. 44 and Fig. 45. The fission A. O. increases with the increase of the burnup A. O. as shown in Fig. 44 and Fig. 45. The tendency of the fission source distribution is different from that of k_{eff}. In case of strong asymmetry of burnup profile, the fission A. O. is very large, and it is supposed to change drastically toward zero, namely as approaching to symmetric shape with a low value of burnup A. O.

The above observation shows that the localization of fission source distribution could happen drastically as the asymmetry degree increases in burnup profile.

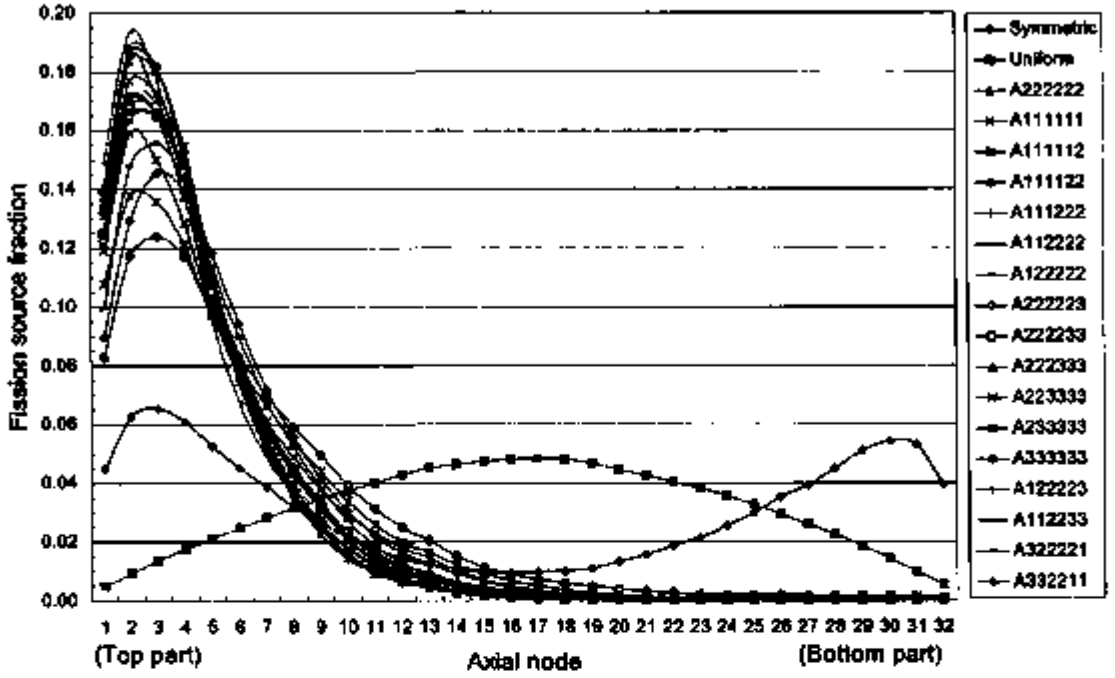

(a) Linear

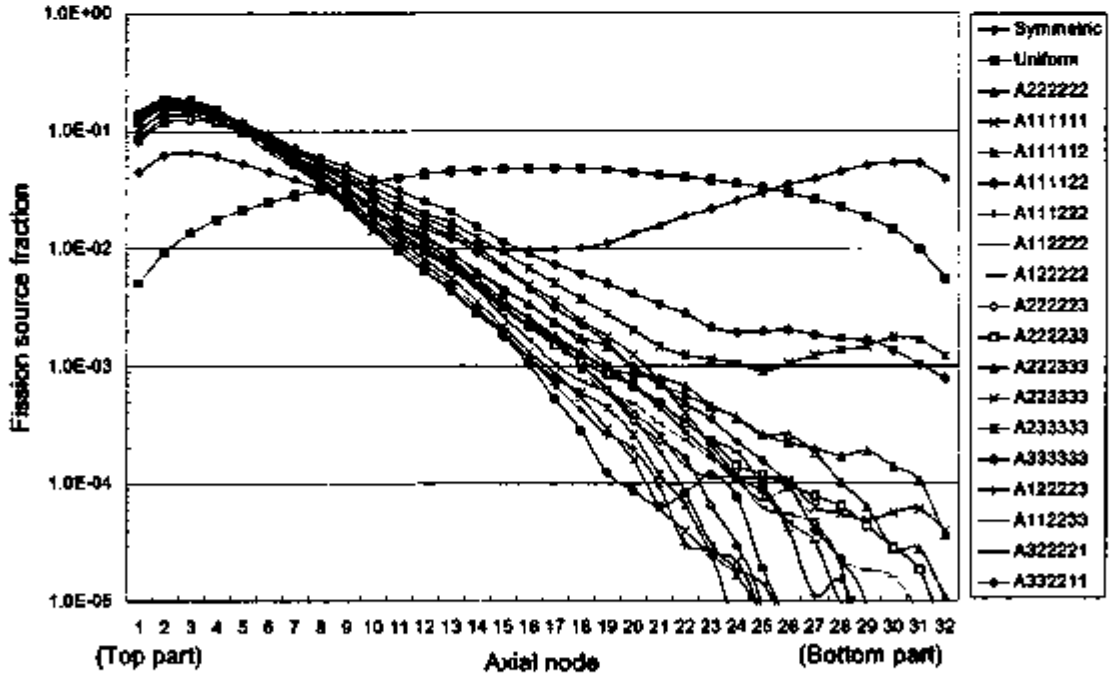

(b) Semi-log

Fig. 40 Calculated results of the fission source distribution at 32 MWd/kgU based on AC+FP approach

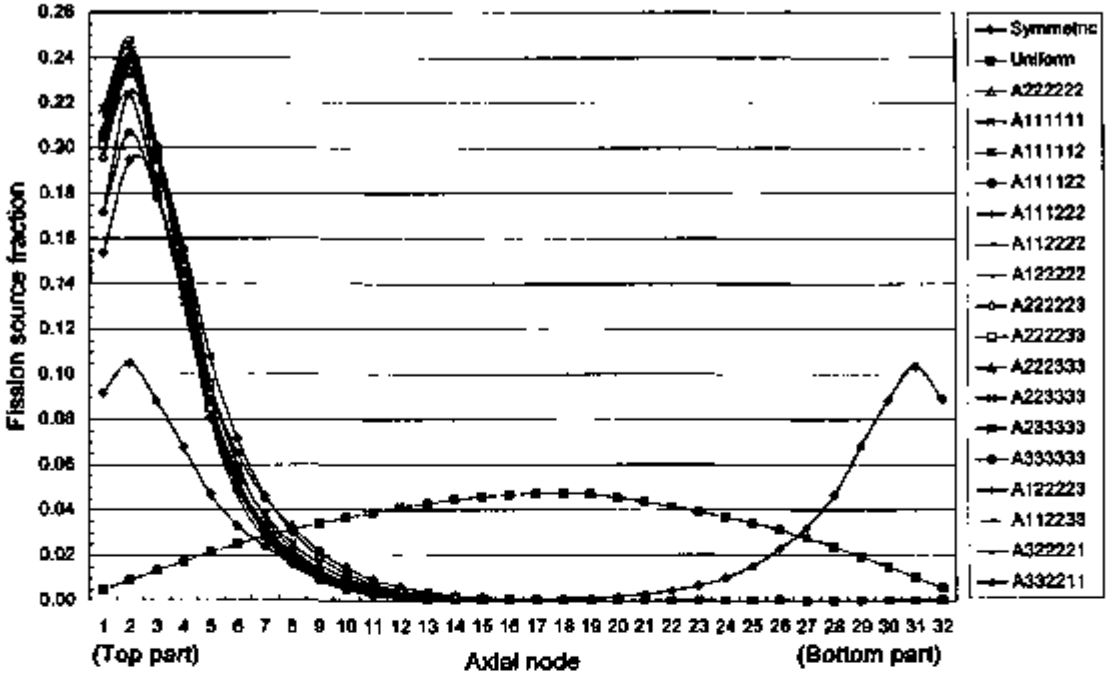

(a) Linear

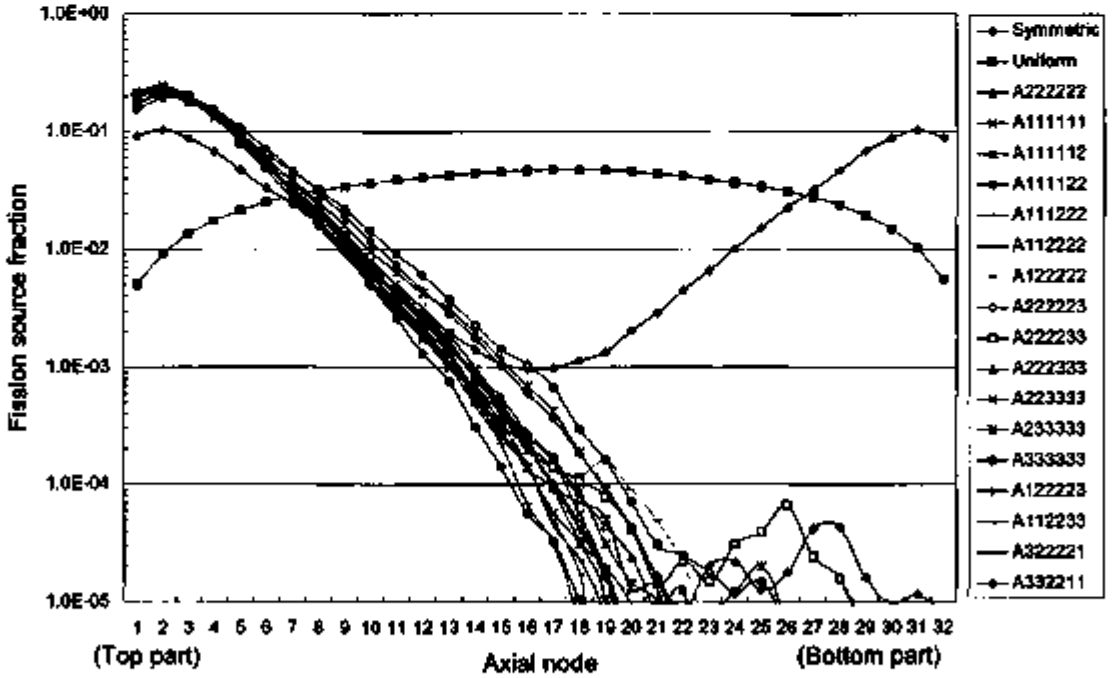

(b) Semi-log

Fig. 41 Calculated results of the fission source distribution at 50 MWd/kgU based on AC+FP approach

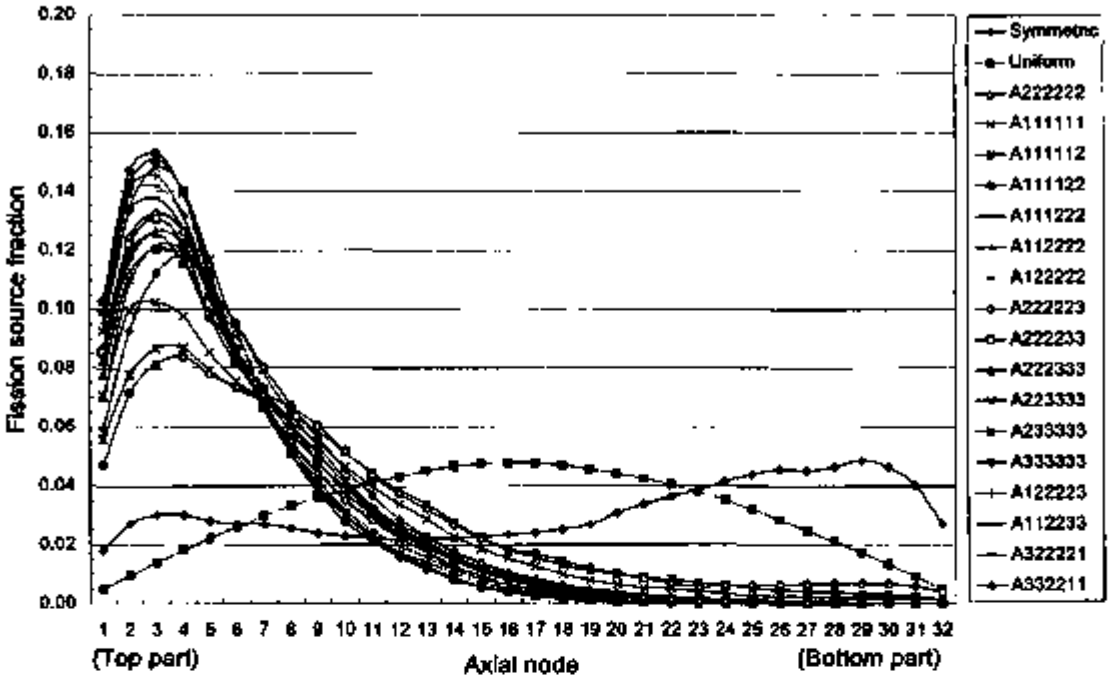

(a) Linear

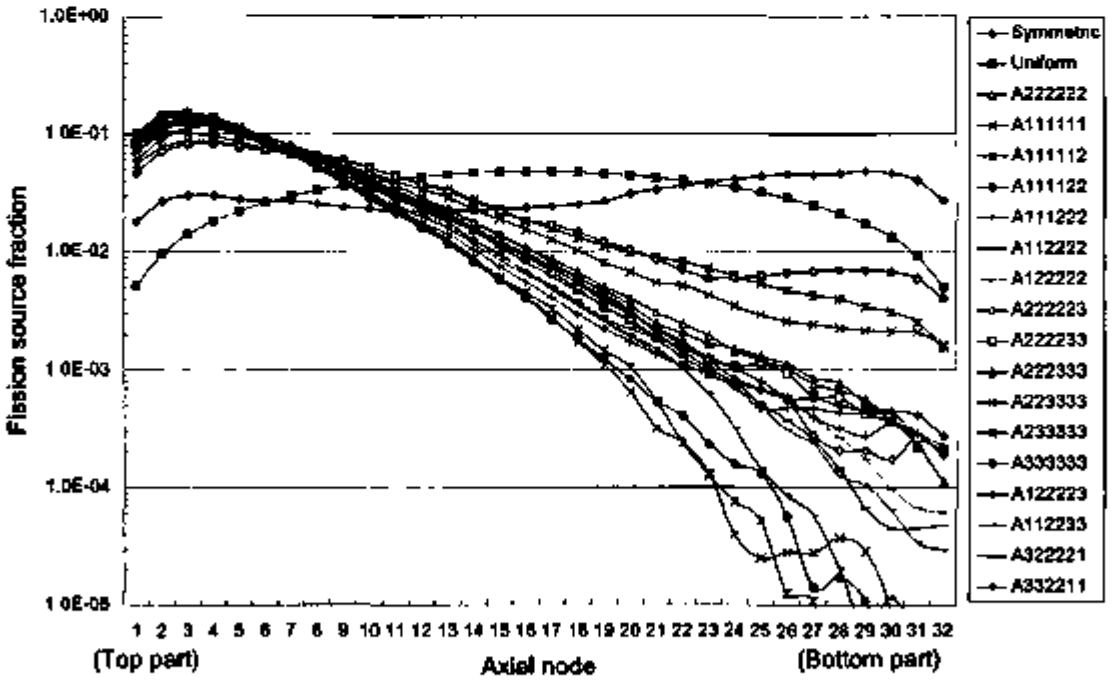

(b) Semi-log

Fig. 42 Calculated results of the fission source distribution at 32 MWd/kgU based on AC-only approach

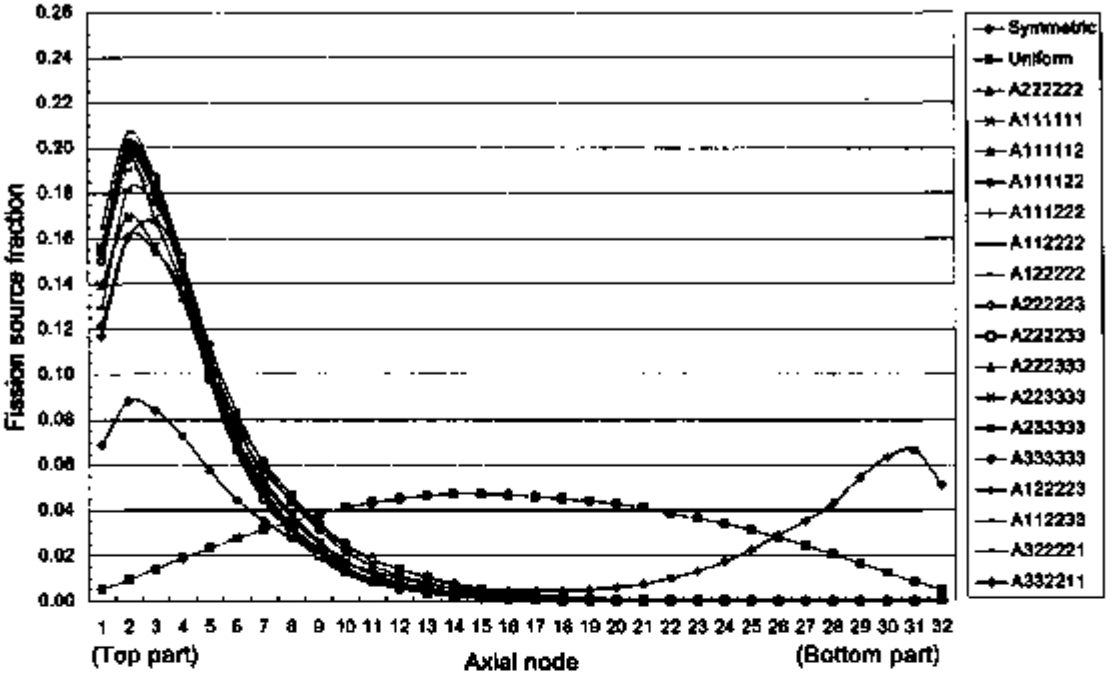

(a) Linear

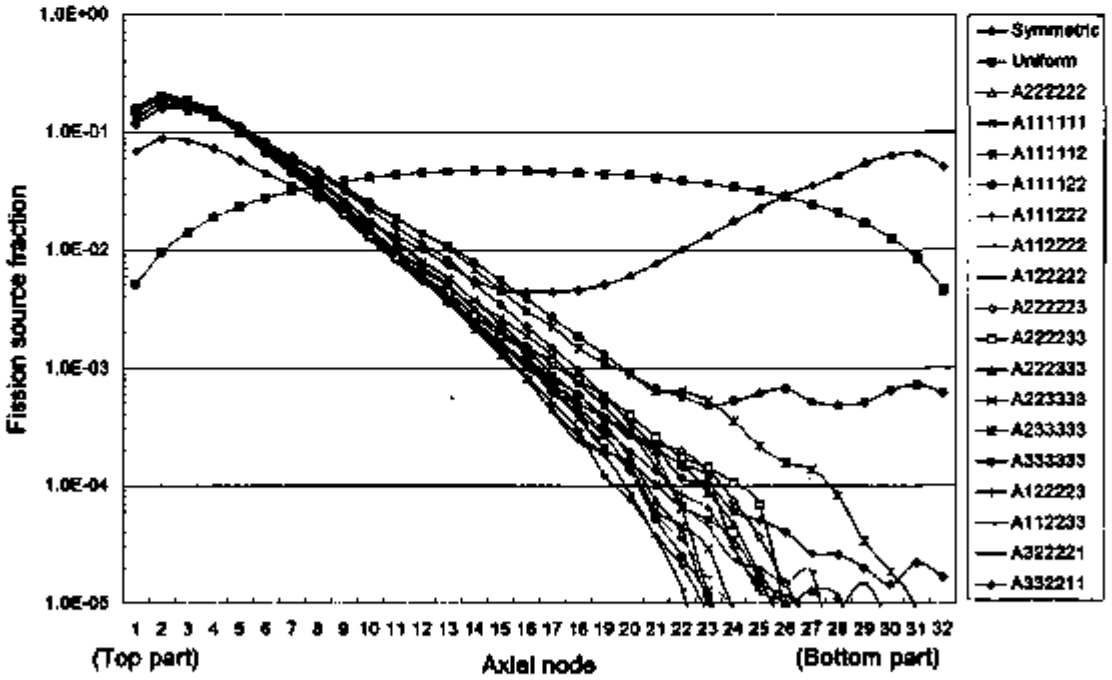

(b) Semi-log

Fig. 43 Calculated results of the fission source distribution at 50 MWd/kgU based on AC-only approach

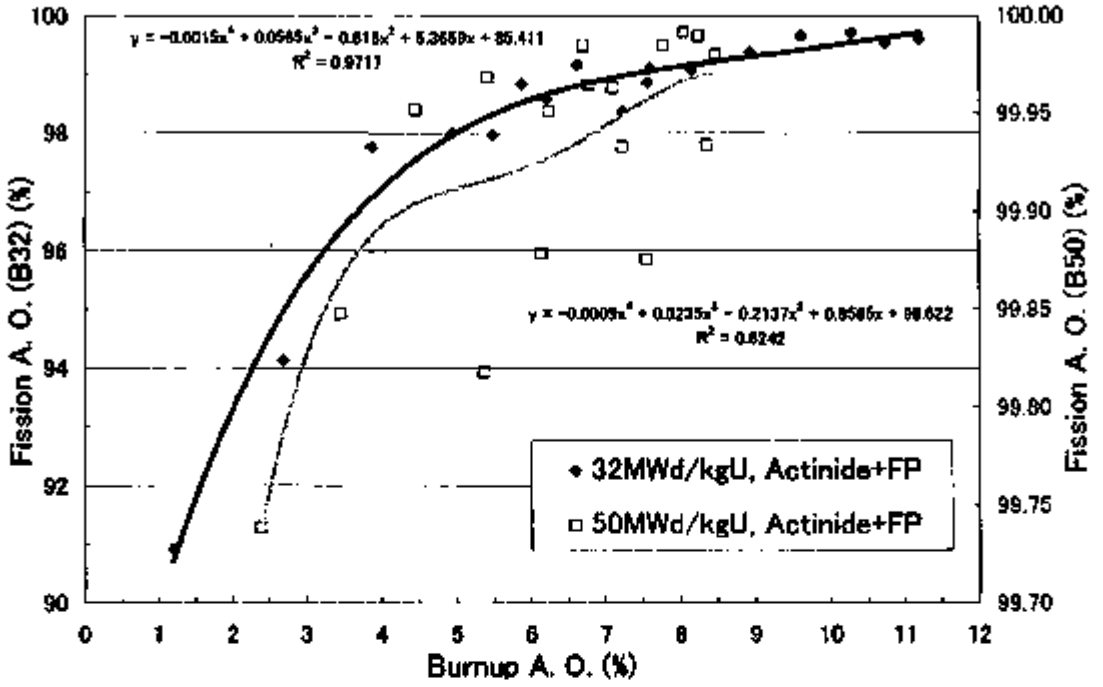

Fig. 44 Fission A. O. vs. burnup A. O. based on AC+FP approach

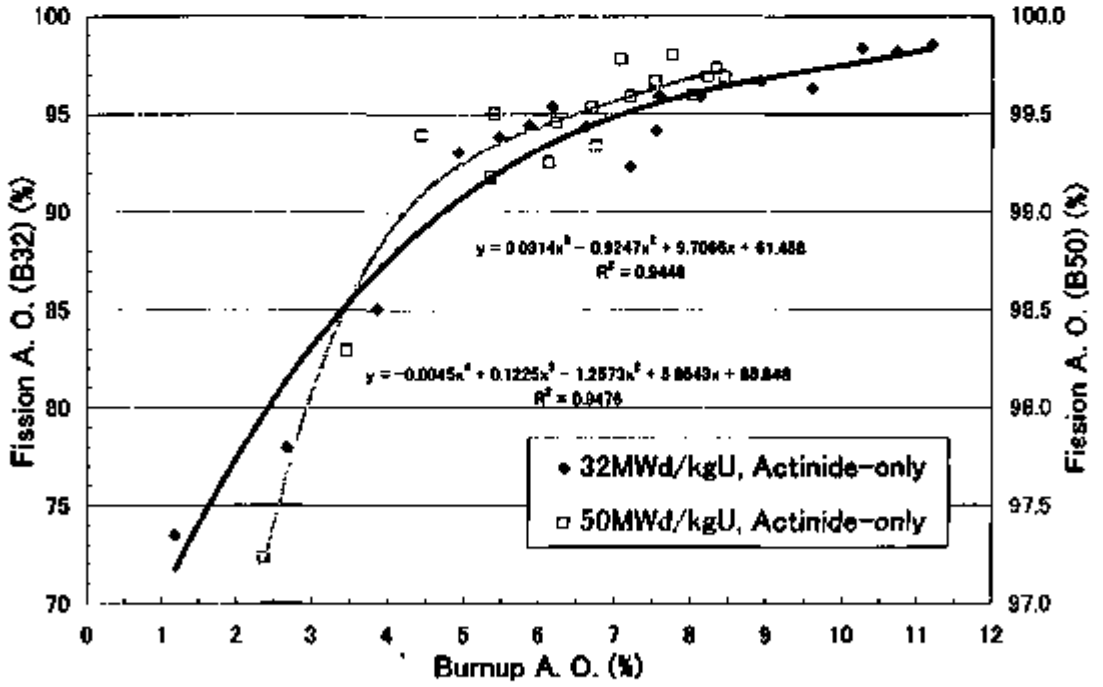

Fig. 45 Fission A. O. vs. burnup A. O. based on AC-only approach

4.4.3. Comparison of Calculation Time

The calculation time depends on not only the number of histories but also the calculation model and printout parameters to be estimated. The representative cases for the AC+FP approach adopted in this report are listed in Table 9. All calculation times listed in Table 9 are actual results for one case performed on the SUN/BLADE100 (Solaris8) machine. In case of the AC-only approach, it isn't necessary to read 15 FP nuclides data from the cross section library. So, the calculation time is reduced to about 80% of the AC+FP approach.

Table 9 Calculation time per execution for representative cases

Configuration	Numbers of history*	Calculation time
Pin cell	20000 x (300 + 100)	7.7 hr
Single assembly	20000 x (150 + 100)	6.5 hr
Color set	10000 x (300 + 200)	9.5 hr
Cask	20000 x (300 + 100)	10.0 hr
	5000 x (300 + 4000)	29.6 hr
	5000 x (300 + 400)	4.7 hr
	5000 x (1500 + 400)	12.1 hr
	5000 x (4500 + 400)	25.1 hr**
	5000 x (6000 + 400)	32.2 hr**
	1000 x (300 + 2000)	3.2 hr

*: Number of histories per cycle x (number of skipped cycles + number of scored cycles)

**: Actual results for the AC-only approach (calculations for AC+FP is not carried out)

5. Conclusion

Our study has been based on the current OECD/NEA Phase II-C benchmark problem for PWR spent fuel transport cask, which consists of a realistic set of axial burnup profiles for average burnups of 32 MWd/kgU and 50 MWd/kgU. The material compositions in each of the 21 non-equidistant material zones are provided in the benchmark in order to simulate the axial burnup profiles. Criticality calculations of 3-D model are carried out based not only on the actinide plus fission product approach specified in the benchmark, but also actinide-only approach as an extension of the Phase II-C, by using the continuous energy Monte Carlo code MCNP-4B2 with the cross section library JENDL-3.2. And the sensitivities of k_{eff}, end effect and fission source distribution to the asymmetry of the axial burnup profile are evaluated with introducing the burnup axial offset.

The adequacy of Monte Carlo calculation conditions is examined by the convergence check for the fission source distribution. In some cases recognized as very slow fission source convergence, the calculation conditions are reexamined. As a result of the final estimation, a general tendency is observed such that the end effect increases linearly with the increase of axial burnup profile asymmetry. The end effect is found to be more sensitive to the asymmetry of axial burnup profile as averaged burnup increases.

Even for slightly asymmetric axial burnup profiles, the axial fission source distribution becomes strongly asymmetric such that the peak shifts toward the top end of the fuel active zone where the local burnup is less than that of the bottom end. The peak of fission source distribution becomes higher with the increase of the asymmetry of burnup profile as well as the assembly-averaged burnup.

As far as conservatism of burnup credit criticality is concerned, the following conclusions can be drawn. The actinide plus fission product approach should be adopted carefully because an axially distributed burnup profile strongly affects the calculated k_{eff} so that the upper limit of axial asymmetry should be assumed from the real situation of burnup profile. On the other hand, the actinide-only approach assuming uniform burnup profile is still conservative with a reactivity margin of at least 4 %Δk/k as a result of the Phase II-C benchmark problem. The trade-off between simplicity by assuming the above approach and its less incentive to an introduction of burnup credit, regarding the reactivity of fission products as a safety margin, should be further considered from the economical point of view.

References

[1] M. Takano and H. Okuno, OECD/NEA Burnup Credit Criticality Benchmark – Results of Phase II A, JAERI-Research 96-003, NEA/NSC/DOC(96)01, Nuclear Energy Agency (1996).

[2] A. Nouri, Analysis of Phase II-B Results: Conceptual PWR Spent Fuel Transportation Cask, IPSN/98-05, NEA/NCS/DOC(98)1, Nuclear Energy Agency (1998).

[3] J. C. Wagner and M. D. Dehart, Review of Axial Burnup Distribution Considerations for Burnup Credit Calculations, ORNL/TM-1999/246, Oak Ridge National Laboratory (2000).

[4] M.D. DeHart, Sensitivity and Parametric Evaluations of Significant Aspects of Burnup Credit for PWR Spent Fuel Packages, ORNL/TM-12973, Oak Ridge National Laboratory (1996).

[5] MCNP – A General Monte Carlo N-Particle Transport Code, Version 4B, LA-12625-M, (1997).

[6] T. Nakagawa, *et al.*, "Japanese Evaluated Nuclear Data Library Version 3 Revision-2: JENDL-3.2," *J. Nucl. Sci. Technol.*, 32[12], pp. 1259-1271 (1995).
JENDL-3.2 can be referred to the website: http://wwwndc.tokai.jaeri.go.jp/jendl/j32/j32.html

[7] H. A. Tuan, H. Okuno and Y. Nomura, Reactivity Effect of Axial Burnup Shapes for A Realistic PWR Fuel Transport Cask, *Proceedings of the International Symposium NUCEFF 2001*, Tokai JAERI, Tokai-mura, Japan, October 31 - November 2, 2001, JAERI-Conf 2002-004, pp.407-414, Japan Atomic Energy Research Institute (2002).

Appendix I

Sample Input of MCNP-4B2 Code for the OECD/NEA Phase II-C Burnup Credit Criticality Benchmark

This is a blank page.

Sample input of MCNP-4B2 in case of B32C05A222222 based on the AC+FP approach

```
OECD/NEA BUC Benchmark Phase II-C (B32C05A222222) 1/8 Cask configuration
c   Case 1: Asymmetrically distributed axial burnup for AC + FP approach
c   1/8 Cask configuration (radially symmetric) 32 nodes in active length
c
c   Cell cards
c
c   Fuel full length with lower & upper axial region   universe 1
 50   0                          -1        -100     imp:n=1 u=1   $ inactive zone of fuel
  1   1   -6.8259446E-02        -9    100 -101     imp:n=1 u=1   $ active node 32
  2   2   -6.8154736E-02        -1    101 -102     imp:n=1 u=1   $ active node 31
  3   3   -6.8068136E-02        -1    102 -103     imp:n=1 u=1   $ active node 30
  4   4   -6.8012906E-02        -1    103 -104     imp:n=1 u=1   $ active node 29
  5   5   -6.7993318E-02        -1    104 -105     imp:n=1 u=1   $ active node 28
  6   6   -6.7995316E-02        -1    105 -106     imp:n=1 u=1   $ active node 27
  7   7   -6.8027686E-02        -1    106 -107     imp:n=1 u=1   $ active node 26
  8   7   -6.7990676E-02        -1    107 -108     imp:n=1 u=1   $ active node 25
  9   7   -6.7990676E-02        -1    108 -109     imp:n=1 u=1   $ active node 24
 10   7   -6.7990676E-02        -1    109 -110     imp:n=1 u=1   $ active node 23
 11   8   -6.8021286E-02        -1    110 -111     imp:n=1 u=1   $ active node 22
 12   9   -6.8035186E-02        -1    111 -112     imp:n=1 u=1   $ active node 21
 13   9   -6.8063186E-02        -1    112 -113     imp:n=1 u=1   $ active node 20
 14  10   -6.8086816E-02        -1    113 -114     imp:n=1 u=1   $ active node 19
 15  10   -6.8085816E-02        -1    114 -115     imp:n=1 u=1   $ active node 18
 16  11   -6.8031646E-02        -1    115 -116     imp:n=1 u=1   $ active node 17
 17  12   -6.8012916E-02        -1    116 -117     imp:n=1 u=1   $ active node 16
 18  12   -6.8012916E-02        -1    117 -118     imp:n=1 u=1   $ active node 15
 19  12   -6.8012916E-02        -1    118 -119     imp:n=1 u=1   $ active node 14
 20  13   -6.8053286E-02        -1    119 -120     imp:n=1 u=1   $ active node 13
 21  14   -6.8021006E-02        -1    120 -121     imp:n=1 u=1   $ active node 12
 22  14   -6.8021006E-02        -1    121 -122     imp:n=1 u=1   $ active node 11
 23  14   -6.8021006E-02        -1    122 -123     imp:n=1 u=1   $ active node 10
 24  15   -6.8040056E-02        -1    123 -124     imp:n=1 u=1   $ active node 9
 25  15   -6.8040056E-02        -1    124 -125     imp:n=1 u=1   $ active node 8
 26  16   -6.8049066E-02        -1    125 -126     imp:n=1 u=1   $ active node 7
 27  16   -6.8049066E-02        -1    126 -127     imp:n=1 u=1   $ active node 6
 28  17   -6.8058776E-02        -1    127 -128     imp:n=1 u=1   $ active node 5
 29  18   -6.8126946E-02        -1    128 -129     imp:n=1 u=1   $ active node 4
 30  19   -6.8126946E-02        -1    129 130      imp:n=1 u=1   $ active node 3
 31  20   -6.8271466E-02        -1    130 -131     imp:n=1 u=1   $ active node 2
 32  21   -6.8294616E-02        -1    131 132      imp:n=1 u=1   $ active node 1
 51   0                          -1    132          imp:n=1 u=1   $ inactive zone of fuel
 52 102    4.325429e-02   1 -2                     imp:n=1 u=1   $ Cladding
 53 103    1.00120e-01    2                        imp:n=1 u=1   $ Water coolant
c
c   Guide Thimble in fuel full length   universe 2
 54 103    1.00120e-01    -3                       imp:n=1 u=2   $ Water coolant
 55 102    4.320429e-02   3 -4                     imp:n=1 u=2   $ Cladding
 56 103    1.00120e-01    4                        imp:n=1 u=2   $ Water coolant
c
c   Wall of fuel cut by y=± this  universe 3
150   0                          -1        -100     imp:n=1 u=3   $ inactive zone of fuel
101   1   -6.8259446E-02         1    100  101     imp:n=1 u=3   $ active node 32
102   2   -6.8154736E-02        -1    101  102     imp:n=1 u=3   $ active node 31
103   3   -6.8068136E-02        -1    102  103     imp:n=1 u=3   $ active node 30
104   4   -6.8012906E-02        -1    103  104     imp:n=1 u=3   $ active node 29
105   5   -6.7996316E-02        -1    104  105     imp:n=1 u=3   $ active node 28
106   5   -6.7995316E-02         1    105  106     imp:n=1 u=3   $ active node 27
107   6   -6.8027056E-02         1    106  107     imp:n=1 u=3   $ active node 26
108   7   -6.7990676E-02         1    107  108     imp:n=1 u=3   $ active node 25
109   7   -6.7990676E-02         1    108  109     imp:n=1 u=3   $ active node 24
110   7   -6.7990676E-02         1    109  110     imp:n=1 u=3   $ active node 23
111   8   -6.8021286E-02         1    110  111     imp:n=1 u=3   $ active node 22
112   9   -6.8035186E-02        -1    111  112     imp:n=1 u=3   $ active node 21
113   9   -6.8063186E-02        -1    112  113     imp:n=1 u=3   $ active node 20
114  10   -6.8086816E-02        -1    113  114     imp:n=1 u=3   $ active node 19
115  10   -6.8085816E-02         1    114  115     imp:n=1 u=3   $ active node 18
116  11   -6.8031646E-02        -1    115  116     imp:n=1 u=3   $ active node 17
117  12   -6.8012916E-02         1    116  117     imp:n=1 u=3   $ active node 16
118  12   -6.8012916E-02        -1    117  118     imp:n=1 u=3   $ active node 15
119  12   -6.8012916E-02        -1    118  119     imp:n=1 u=3   $ active node 14
120  13   -6.8053286E-02        -1    119  120     imp:n=1 u=3   $ active node 13
121  14   -6.8021006E-02         1    120  121     imp:n=1 u=3   $ active node 12
122  14   -6.8021006E-02         1    121  122     imp:n=1 u=3   $ active node 11
123  14   -6.8021006E-02        -1    122  123     imp:n=1 u=3   $ active node 10
124  15   -6.8040056E-02        -1    123  124     imp:n=1 u=3   $ active node 9
125  15   -6.8040056E-02        -1    124  125     imp:n=1 u=3   $ active node 8
126  16   -6.8049066E-02         1    125  126     imp:n=1 u=3   $ active node 7
127  16   -6.8049066E-02         1    126  127     imp:n=1 u=3   $ active node 6
128  17   -6.8058776E-02        -1    127  128     imp:n=1 u=3   $ active node 5
129  18   -6.8126946E-02        -1    128  129     imp:n=1 u=3   $ active node 4
130  19   -6.8126946E-02         1    129  130     imp:n=1 u=3   $ active node 3
131  20   -6.8274656E-02        -1    130  131     imp:n=1 u=3   $ active node 2
132  21   -6.8294616E-02        -1    131  132     imp:n=1 u=3   $ active node 1
151   0                          -1    132          imp:n=1 u=3   $ inactive zone of fuel
152 102    4.325429e-02   1 -2                     imp:n=1 u=3   $ Cladding
153 103    1.00120e-01    2                        imp:n=1 u=3   $ Water coolant
c
c   Half of GT cut by y=± this  universe 4
154 103    1.00120e-01    -3                       imp:n=1 u=4   $ Water coolant
155 102    4.320429e-02   3 -4                     imp:n=1 u=4   $ Cladding
156 103    1.00120e-01    4                        imp:n=1 u=4   $ Water coolant
c
c   Half assembly filled with Fuel & GT   universe 5
 57   0    -8.5   -9.7  imp:n=1 lat=1 u=5 fill=-6:6 -6:6 0:0
                        3 3 3 3 3 3 3 3 3 3 3 3 3
                       3 3 3 3 3 3 3 3 3 3 3 3 3 3 3
                      3 3 3 3 3 3 3 3 3 3 3 3 3 3 3 3 3
                     3 3 3 3 3 3 3 3 3 3 3 3 3 3 3 3 3 3 3
                    3 3 3 3 3 3 3 3 3 3 3 3 3 3 3 3 3 3 3 3 3
                   3 3 3 3 3 3 3 3 3 3 3 3 3 3 3 3 3 3 3 3 3 3 3
                  3 3 3 3 3 3 3 3 3 3 3 3 3 3 3 3 3 3 3 3 3 3 3 3 3
                 3 3 3 3 3 3 3 3 3 3 3 3 3 3 3 3 3 3 3 3 3 3 3 3 3 3 3
                3 3 3 3 3 3 3 3 3 3 3 3 3 3 3 3 3 3 3 3 3 3 3 3 3 3 3 3 3
               3 3 3 3 3 3 3 3 3 3 3 3 3 3 3 3 3 3 3 3 3 3 3 3 3 3 3 3 3 3 3
              3 3 3 3 3 3 3 3 3 3 3 3 3 3 3 3 3 3 3 3 3 3 3 3 3 3 3 3 3 3 3 3 3
             3 3 3 3 3 3 3 3 3 3 3 3 3 3 3 3 3 3 3 3 3 3 3 3 3 3 3 3 3 3 3 3 3 3 3
            3 3 3 3 3 3 3 3 3 3 3 3 3 3 3 3 3 3 3 3 3 3 3 3 3 3 3 3 3 3 3 3 3 3 3 3 3
           3 3 3 3 3 3 3 3 3 3 3 3 3 3 3 3 3 3 3 3 3 3 3 3 3 3 3 3 3 3 3 3 3 3 3 3 3 3 3
          3 3 3 3 3 3 3 3 3 3 3 3 3 3 3 3 3 3 3 3 3 3 3 3 3 3 3 3 3 3 3 3 3 3 3 3 3 3 3 3 3
         3 3 3 3 3 3 3 3 3 3 3 3 3 3 3 3 3 3 3 3 3 3 3 3 3 3 3 3 3 3 3 3 3 3 3 3 3 3 3 3 3 3 3
        3 3 3 3 3 3 3 3 3 3 3 3 3 3 3 3 3 3 3 3 3 3 3 3 3 3 3 3 3 3 3 3 3 3 3 3 3 3 3 3 3 3 3 3 3
       3 3 3 3 3 3 3 3 3 3 3 3 3 3 3 3 3 3 3 3 3 3 3 3 3 3 3 3 3 3 3 3 3 3 3 3 3 3 3 3 3 3 3 3 3 3 3
      3 3 3 3 3 3 3 3 3 3 3 3 3 3 3 3 3 3 3 3 3 3 3 3 3 3 3 3 3 3 3 3 3 3 3 3 3 3 3 3 3 3 3 3 3 3 3 3 3
     3 3 3 3 3 3 3 3 3 3 3 3 3 3 3 3 3 3 3 3 3 3 3 3 3 3 3 3 3 3 3 3 3 3 3 3 3 3 3 3 3 3 3 3 3 3 3 3 3 3 3
    3 3 3 3 3 3 3 3 3 3 3 3 3 3 3 3 3 3 3 3 3 3 3 3 3 3 3 3 3 3 3 3 3 3 3 3 3 3 3 3 3 3 3 3 3 3 3 3 3 3 3 3 3
   3 3 3 3 3 3 3 3 3 3 3 3 3 3 3 3 3 3 3 3 3 3 3 3 3 3 3 3 3 3 3 3 3 3 3 3 3 3 3 3 3 3 3 3 3 3 3 3 3 3 3 3 3 3 3
  3 3 3 3 3 3 3 3 3 3 3 3 3 3 3 3 3 3 3 3 3 3 3 3 3 3 3 3 3 3 3 3 3 3 3 3 3 3 3 3 3 3 3 3 3 3 3 3 3 3 3 3 3 3 3 3 3
 3 3 3 3 3 3 3 3 3 3 3 3 3 3 3 3 3 3 3 3 3 3 3 3 3 3 3 3 3 3 3 3 3 3 3 3 3 3 3 3 3 3 3 3 3 3 3 3 3 3 3 3 3 3 3 3 3 3 3
c
c   Full assembly filled with Fuel & GT   universe 6
 58   0    -8.5   -9.7  imp:n=1 lat=1 u=6 fill=-6:6 -6:6 0:0
                        1 1 1 1 1 1 1 1 1 1 1 1 1
                       1 1 1 1 1 1 1 1 1 1 1 1 1 1 1
                      1 1 1 1 1 1 1 1 1 1 1 1 1 1 1 1 1
                     1 1 1 1 1 1 1 1 1 1 1 1 1 1 1 1 1 1 1
                    1 1 1 1 1 1 1 1 1 1 1 1 1 1 1 1 1 1 1 1 1
                   1 1 1 1 1 1 1 1 1 1 1 1 1 1 1 1 1 1 1 1 1 1 1
                  1 1 1 1 1 1 1 1 1 1 1 1 1 1 1 1 1 1 1 1 1 1 1 1 1
                 1 1 1 1 1 1 1 1 1 1 1 1 1 1 1 1 1 1 1 1 1 1 1 1 1 1 1
                1 1 1 1 1 1 1 1 1 1 1 1 1 1 1 1 1 1 1 1 1 1 1 1 1 1 1 1 1
               1 1 1 1 1 1 1 1 1 1 1 1 1 1 1 1 1 1 1 1 1 1 1 1 1 1 1 1 1 1 1
              1 1 1 1 1 1 1 1 1 1 1 1 1 1 1 1 1 1 1 1 1 1 1 1 1 1 1 1 1 1 1 1 1
             1 1 1 1 1 1 1 1 1 1 1 1 1 1 1 1 1 1 1 1 1 1 1 1 1 1 1 1 1 1 1 1 1 1 1
            1 1 1 1 1 1 1 1 1 1 1 1 1 1 1 1 1 1 1 1 1 1 1 1 1 1 1 1 1 1 1 1 1 1 1 1 1
           1 1 1 1 1 1 1 1 1 1 1 1 1 1 1 1 1 1 1 1 1 1 1 1 1 1 1 1 1 1 1 1 1 1 1 1 1 1 1
          1 1 1 1 1 1 1 1 1 1 1 1 1 1 1 1 1 1 1 1 1 1 1 1 1 1 1 1 1 1 1 1 1 1 1 1 1 1 1 1 1
         1 1 1 1 1 1 1 1 1 1 1 1 1 1 1 1 1 1 1 1 1 1 1 1 1 1 1 1 1 1 1 1 1 1 1 1 1 1 1 1 1 1 1
        1 1 1 1 1 1 1 1 1 1 1 1 1 1 1 1 1 1 1 1 1 1 1 1 1 1 1 1 1 1 1 1 1 1 1 1 1 1 1 1 1 1 1 1 1
       1 1 1 1 1 1 1 1 1 1 1 1 1 1 1 1 1 1 1 1 1 1 1 1 1 1 1 1 1 1 1 1 1 1 1 1 1 1 1 1 1 1 1 1 1 1 1
      1 1 1 1 1 1 1 1 1 1 1 1 1 1 1 1 1 1 1 1 1 1 1 1 1 1 1 1 1 1 1 1 1 1 1 1 1 1 1 1 1 1 1 1 1 1 1 1 1
     1 1 1 1 1 1 1 1 1 1 1 1 1 1 1 1 1 1 1 1 1 1 1 1 1 1 1 1 1 1 1 1 1 1 1 1 1 1 1 1 1 1 1 1 1 1 1 1 1 1 1
    1 1 1 1 1 1 1 1 1 1 1 1 1 1 1 1 1 1 1 1 1 1 1 1 1 1 1 1 1 1 1 1 1 1 1 1 1 1 1 1 1 1 1 1 1 1 1 1 1 1 1 1 1
   1 1 1 1 1 1 1 1 1 1 1 1 1 1 1 1 1 1 1 1 1 1 1 1 1 1 1 1 1 1 1 1 1 1 1 1 1 1 1 1 1 1 1 1 1 1 1 1 1 1 1 1 1 1 1
  1 1 1 1 1 1 1 1 1 1 1 1 1 1 1 1 1 1 1 1 1 1 1 1 1 1 1 1 1 1 1 1 1 1 1 1 1 1 1 1 1 1 1 1 1 1 1 1 1 1 1 1 1 1 1 1 1
 1 1 1 1 1 1 1 1 1 1 1 1 1 1 1 1 1 1 1 1 1 1 1 1 1 1 1 1 1 1 1 1 1 1 1 1 1 1 1 1 1 1 1 1 1 1 1 1 1 1 1 1 1 1 1 1 1 1 1
c
 59   0     9 10 11 12 204  205  imp:n=1 u=7 fill=-3:0 0:0 0:0   $ Half assembly
 60 105     9 31822e-02     9 -10 11 -12   203 -204   imp:n=1 u=7 $ Lower hardware
 61 106     9 31822e-02     9 -10 11 -12   205 -206   imp:n=1 u=7 $ Upper hardware
 62 103     1 00120e-01    13 -14 15 -16
                          #(9 -10 11 -12   203 -206) imp:n=1 u=7 $ Water gap
 63 109     8 7627640e-02  17 -15 19 -20
                          #(13 -14 15 -16)          imp:n=1 u=7 $ B-SS Basket
c
 64   0     9 10 11 12 204 -205  imp:n=1 u=8 fill=-3:0 0:0 0:0   $ Full assembly
 65 106     9 31822e-02     9 -10 11 -12   203 -204   imp:n=1 u=8 $ Lower hardware
 66 106     9 31822e-02     9 -10 11 -12   205 -206   imp:n=1 u=8 $ Upper hardware
 67 103     1 00120e-01    13 -14 15 -16
                          #(9 -10 11 -12   203 -206) imp:n=1 u=8 $ Water gap
 68 105     8 7627640e-02  17 -15 19 -20
                          #(13 -14 15 -16)          imp:n=1 u=8 $ B-SS Basket
c
c Water channel (Basket without fuel assembly
 69 103     1 00120e-01    13 -14 15 -16  imp:n=1 u=9 $ Water gap
 70 105     8 7627640e-02  17 -15 19 -20
                          #(13 -14 15 -16) imp:n=1 u=9 $ B-SS Basket
c
c 1/8 Cask configuration
 71   0    -22 21 24 23   imp:n=1 lat=1 u=10 fill=0 2 0 3 0 0
                                  7 0 0
                                 8 7 6
                                  5 4 9
                                    9 9 9
 72   0     29 -30 27  28 202 -207  30   imp:n=1 fill=10                $ 21/8
Assemblies
 73 103     1 00120e-01    26 -40 #(25 -26 27 -28) 202 -207  30   imp:n=1  $ Water
flooded inside cask
 74 104     8.53470e-02    25 -41  (40 -202  207) 201 -205 30   imp:n=1  $ Cask shell
SS Valve and Upper & lower lids
c   Boundary
999   0     29  41  -201  205  -30     imp:n=0

c
c   Surface cards
c
   1   cz    0.411000          $ Fuel diameter  Clad inner diameter  0.822 cm
   2   cz    0.478000          $ Clad outer diameter                0.956 cm
   3   cz    0.559000          $ Guide Thimble inner diameter       1.118 cm
   4   cz    0.616000          $ Guide Thimble outer diameter       1.232 cm
c
   5   px   -0.635000          $ Pin cell pitch 1.27 cm  fuel lattice element
   6   px    0.635000          $ Pin cell pitch 1.27 cm, fuel lattice element
   7   py   -0.635000          $ Pin cell pitch 1.27 cm  fuel lattice element
   8   py    0.635000          $ Pin cell pitch 1.27 cm, fuel lattice element
c
   9   px  -11.43              $ HW  16x16 array 1.27x16= 22.86 cm
  10   px   11.43              $ HW, 16x16 array 1.27x16= 22.86 cm
  11   py  -11.43              $ HW, 16x16 array 1.27x16= 22.86 cm
  12   py   11.43              $ HW, 16x16 array 1.27x16= 22.86 cm
c
  13   px  -11.76              $ Water Gap between FA and B-SS 23.5 cm
  14   px   11.76              $ Water Gap between FA and B-SS 23.5 cm
  15   py  -11.76              $ Water Gap between FA and B-SS 23.5 cm
  16   py   11.76              $ Water Gap between FA and B-SS 23.5 cm
c
  17   px  -12.25              $ Basket pitch 24.5 cm (B-SS thickness 1cm)
  18   px   12.25              $ Basket pitch 24.5 cm (B-SS thickness 1cm)
  19   py  -12.25              $ Basket pitch 24.5 cm (B-SS thickness 1cm)
  20   py   12.25              $ Basket pitch 24.5 cm (B-SS thickness 1cm)
c
  21   px  -12.25              $ 21/8 Assembly universe Basket pitch 24.5 cm (B-SS
thickness 1cm)
  22   px   12.25              $ 21/8 Assembly universe Basket pitch 24.5 cm (B-SS
thickness 1cm)
  23   py  -12.25              $ 21/8 Assembly universe Basket pitch 24.5 cm (B-SS
thickness 1cm)
  24   py   12.25              $ 21/8 Assembly universe Basket pitch 24.5 cm (B-SS
thickness 1cm)
c
  25*  px    0.00              $ 21/8 Assembly window Basket pitch 24.5 cm (B-SS
thickness 1cm)
  26   px   37.25              $ 21/8 Assembly window 24.5 * 3/2 - 0.5 = 37.25 cm
  27*  py    0.00              $ 21/8 Assembly window Basket pitch 24.5 cm (B-SS
thickness 1cm)
  28   py   61.75              $ 21/8 Assembly window 24.5 * 5/2 + 0.5 = 61.75 cm
c
  29*  p   -1 1 0 0            $ Cross reflective surface of y=x(-1x+1y+0z=0)
c
  40   cz   73.60              $ Cask inner diameter  146 cm
```

```
 41  cz  103.00              $ Cask outer diameter  206 cm
c
c Equidistant 33 nodes in fuel active length
100  pz      0 6             $ bottom of active length
101  pz   12.1875            $
102  pz   24.3750            $
103  pz   36.5625            $
104  pz   48.7500            $
105  pz   60.9375            $
106  pz   73.1250            $
107  pz   85.3125            $
108  pz   97.5000            $
109  pz  109.6875            $
110  pz  121.8750            $
111  pz  134.0625            $
112  pz  146.2500            $
113  pz  158.4375            $
114  pz  170.6250            $
115  pz  182.8125            $
116  pz  195.0000            $
117  pz  207.1875            $
118  pz  219.3750            $
119  pz  231.5625            $
120  pz  243.7500            $
121  pz  255.9375            $
122  pz  268.1250            $
123  pz  280.3125            $
124  pz  292.5000            $
125  pz  304.6875            $
126  pz  316.8750            $
127  pz  329.0625            $
128  pz  341.2500            $
129  pz  353.4375            $
130  pz  365.6250            $
131  pz  377.8125            $
132  pz  390.0               $ top of active length
c
c Lower structure
201  pz   -51.9              $ bottom of cask
202  pz   -51.8              $ bottom of water gap (3cm)
203  pz   -51.8              $ bottom of lower hardware
204  pz   -32.4              $ bottom of fuel full length
c Upper structure
205  pz   407.1              $ top of fuel full length
206  pz   427.1              $ top of upper hardware
207  pz   444.1              $ top of water gap
208  pz   474.1              $ top of cask
c
c
c    Data cards
c
c    materials
m1     $    Isotopic data for case 1 B32C05A222222
       92235.37c          6.068860E-04
       92234.37c          7.304788-06
       92236.37c          1.514048-05
       92237.37c          4.818860-05
       92238.37c          2.16617E-02
       94238.37c          7.944828-07
       94239.37c          4.080258-04
       94240.37c          2.621408-05
       94241.37c          1.041858-05
       94242.37c          1.884458-06
       95241.37c          3.643208-06
       95242.37c          1.647248-07
       42095.37c          2.750868-05
       43099.37c          2.728688-05
       44101.37c          2.963278-05
       45103.37c          1.529878-05
       47109.37c          1.251158-04
       55133.37a          2.870628-06
       60143.37c          2.234328-05
       60145.37c          1.051238-05
       62147.37a          5.934668-06
       62149.37c          1.403738-07
       62150.37c          8.965348-06
       62151.37a          3.758918-07
       62152.37c          2.422728-06
       63153.37c          1.060968-06
       64158.37a          6.060648-06
        8016.37a          4.668608-02
m2     $    Isotopic data for case 1 B32C05A222222
       92235.37c          4.648868-04
       92234.37a          5.788868-06
       92238.37c          8.221918-04
       93237.37c          7.282558-06
       92238.37a          2.157928-02
       94239.37c          7.803448-06
       94258.37c          1.184868-04
       94260.37a          5.401978-06
       94261.37c          1.804418-06
       94242.37c          4.244488-06
       95241.37a          4.775868-06
       95243.37a          8.362788-07
       42095.37c          3.997408-05
       43099.37c          3.553308-05
       44101.37a          3.250918-06
       45103.37c          1.060918-06
       47109.37c          1.594538-05
       55133.37a          2.747408-06
       60143.37a          2.788778-06
       60145.37c          1.148618-06
       62147.37a          7.198238-06
       62149.37c          1.468278-07
       62150.37a          7.937678-06
       62151.37a          4.171308-07
       62152.37a          3.122668-06
       63153.37a          2.668108-06
       64158.37a          8.648308-06
        8016.37a          4.686868-02
m3     $    Isotopic data for case 1 B32C05A222222
       92238.37c          3.46108E-04
       93234.37c          8.33068E-06
       92236.37a          1.05868E-04
       92237.37c          8.128198-06
       92238.37c          2.150168-02
       94238.37c          2.428748-06
       94239.37c          1.240118-04
       94240.37c          4.030038-06
       94241.37c          1.040868-05
       94242.37a          6.506318-06
       95241.37p          6.017298-06
       95243.37a          9.598168-07
       42095.37c          4.198048-05
       43099.37c          4.148058-05
       44101.37a          3.777138-05
       45103.37a          2.288898-06
       47109.37c          2.678868-05
       55133.37a          4.334128-05
       60143.37a          3.118828-05
       60145.37a          2.427468-06
       62147.37c          7.038178-06
       62149.37a          1.488298-07
       62150.37a          9.643218-06
       62151.37c          4.483788-07
       62152.37a          3.532568-06
       63153.37a          3.229278-06
       64156.37c          1.160868-07
        8016.37a          4.586868-02
m4     $    Isotopic data for case 1 B32C05A222222
       92235.37c          2.649038-04
       92234.37a          5.870278-06
       92238.37a          1.084868-04
       93237.37c          1.073508-06
       92238.37a          2.140378-02
       94238.37a          3.528898-06
       94239.37c          1.282448-04
       94240.37a          4.581858-06
       94241.37a          2.251948-06
       94242.37a          8.008868-06
       95241.37c          6.628448-06
       95243.37a          1.558868-06
       42095.37a          4.668868-06
       43099.37c          4.885878-05
       44101.37a          4.258868-05
       45103.37a          2.838438-06
       47109.37c          3.131438-05
       55135.37a          4.838268-06
       60143.37a          3.373648-06
       60145.37a          2.758278-06
       62147.37a          8.463468-06
       62149.37c          1.518538-07
       62150.37a          1.068868-06
       62151.37a          4.758718-07
       62152.37c          3.887138-06
       63153.37a          3.812538-06
       64158.37a          1.457878-07
        8016.37c          4.558088-02
m5     $    Isotopic data for case 1 B32C05A222222
       92235.37a          2.788478-04
       92234.37a          3.881948-06
       92236.37a          1.111938-04
       93237.37a          1.122478-06
       92238.37c          2.141208-02
       94238.37a          3.575718-06
       94239.37a          1.258118-04
       94240.37a          4.887648-06
       94241.37c          2.317468-06
       94242.37a          8.588948-06
       95241.37a          7.038268-06
       95243.37c          1.727808-06
       42095.37a          4.781728-05
       43099.37a          4.788908-06
       44101.37c          4.418658-05
       45103.37a          2.888818-06
       47109.37a          3.228948-06
       55135.37c          4.882628-06
       60143.37a          3.432068-05
       60145.37a          2.828468-06
       62147.37a          8.804788-06
       62149.37a          1.623318-07
       62150.37a          1.133238-06
       62151.37a          4.823838-07
       62152.37a          3.972128-06
       63153.37a          3.862828-06
       64158.37a          1.808478-07
        8016.37a          4.668008-02
m6     $    Isotopic data for case 1 B32C05A222222
       92238.37a          2.98474E-04
       93234.37a          8.048878-06
       92236.37c          1.078868-04
       93237.37a          1.040018-06
       92238.37a          2.144088-02
       94238.37a          3.185258-06
       94239.37a          1.258848-04
       94240.37c          4.483018-06
       94241.37a          2.161148-06
       94242.37a          8.561788-06
       95241.37c          6.638278-06
       95243.37a          1.418418-06
       42095.37a          4.553828-05
       43099.37a          4.867788-06
       44101.37c          4.177898-05
       45103.37a          2.477848-06
       47109.37a          3.088828-06
       55133.37c          4.726348-06
       60143.37a          3.320128-05
       60145.37c          2.698418-06
       62147.37c          8.372898-06
       62149.37c          1.518558-07
       62150.37a          1.068288-06
       62151.37a          4.667718-07
       62152.37c          3.812318-06
       63153.37c          3.668518-06
       64158.37a          1.571048-07
        8016.37c          4.668088-02
m7     $    Isotopic data for case 1 B32C05A222222
       92238.37a          2.738638-04
```

```
      64155.37c          1.39618E-07
       8016.37c          4.56560E-02
m15   $    Isotopic data for case 1 B32C05A222222
      92235.37c          3.08878E-04
      92234.37c          6.11382E-06
      92236.37c          1.06882E-04
      92237.37c          1.01206E-05
      92238.37c          2.14507E-02
      94238.37c          2.94848E-06
      94239.37c          1.26500E-04
      94240.37c          4.36810E-05
      94241.37c          2.14027E-05
      94242.37c          7.89877E-06
      95241.37c          6.47345E-06
      95243.37c          1.30913E-06
      42095.37c          4.45403E-05
      43099.37c          4.44007E-06
      44101.37c          4.68324E-05
      45103.37c          2.40388E-05
      47109.37c          2.90602E-06
      56138.37c          4.63359E-05
      60143.37c          3.27420E-05
      60145.37c          2.64710E-06
      62147.37c          8.22489E-06
      62149.37c          1.61218E-07
      62150.37c          1.03948E-06
      62151.37c          4.64788E-07
      62152.37c          3.74837E-06
      63153.37c          3.67548E-06
      64155.37c          1.32008E-07
       8016.37c          4.56560E-02
m16   $    Isotopic data for case 1 B32C05A222222
      92235.37c          3.13956E-04
      92234.37c          6.95127E-06
      92236.37c          1.08948E-04
      92237.37c          9.94228E-06
      92238.37c          2.14684E-02
      94238.37c          2.86614E-06
      94239.37c          1.28078E-04
      94240.37c          4.30458E-05
      94241.37c          2.11218E-05
      94242.37c          7.65483E-06
      95241.37c          6.38270E-06
      95243.37c          1.29110E-06
      42095.37c          4.41463E-05
      43099.37c          4.41581E-05
      44101.37c          4.63188E-05
      45103.37c          2.40243E-05
      47109.37c          2.84987E-06
      56138.37c          4.58388E-05
      60143.37c          3.24536E-05
      60145.37c          2.61888E-06
      62147.37c          8.23081E-06
      62150.37c          1.02533E-06
      62151.37c          4.60324E-07
      62152.37c          3.71220E-06
      63153.37c          3.51570E-06
      64155.37c          1.39244E-07
       8016.37c          4.56560E-02
m17   $    Isotopic data for case 1 B32C05A222222
      92235.37c          3.25115E-04
      92234.37c          6.72840E-06
      92236.37c          1.04316E-04
      92237.37c          9.59800E-06
      92238.37c          2.14814E-02
      94238.37c          2.68735E-06
      94239.37c          1.24787E-04
      94240.37c          4.18146E-05
      94241.37c          2.05062E-05
      94242.37c          7.14038E-06
      95241.37c          6.18894E-06
      95243.37c          1.13987E-06
      42095.37c          4.30842E-05
      43099.37c          4.30625E-05
      44101.37c          4.52181E-05
      45103.37c          2.33715E-05
      47109.37c          2.73221E-06
      56138.37c          4.47568E-05
      60143.37c          3.19269E-05
      60145.37c          2.55846E-06
      62147.37c          8.02630E-06
      62149.37c          1.60482E-07
      62150.37c          9.84777E-06
      62151.37c          4.56284E-07
      62152.37c          3.63458E-06
      63153.37c          3.38868E-06
      64156.37c          1.23486E-07
       8016.37c          4.56560E-02
m18   $    Isotopic data for case 1 B32C05A222222
      92235.37c          3.78622E-04
      92234.37c          8.80104E-06
      92236.37c          9.52804E-06
      92237.37c          7.89286E-06
      92238.37c          2.16504E-02
      94238.37c          1.90148E-06
      94239.37c          1.21529E-04
      94240.37c          3.85533E-05
      94241.37c          1.78078E-05
      94242.37c          5.08519E-06
      95241.37c          5.23568E-06
      95243.37c          9.80343E-07
      42095.37c          3.92246E-05
      43099.37c          3.81176E-05
      44101.37c          3.47443E-05
      45103.37c          2.10518E-05
      47109.37c          2.21588E-06
      56138.37c          3.97483E-05
      60143.37c          2.92014E-06
      60145.37c          2.27126E-05
      62147.37c          7.50248E-06
      62149.37c          1.48143E-07
      62150.37c          6.58187E-06
      62151.37c          4.29533E-07
      62152.37c          3.27356E-06
      63153.37c          3.02133E-06
      64155.37c          9.87158E-08
       8016.37c          4.56560E-02
m19   $    Isotopic data for case 1 B32C05A222222
      92235.37c          3.84048E-04
      92234.37c          6.85298E-06
      92236.37c          9.48098E-05
      92237.37c          7.73257E-06
      92238.37c          2.14604E-02
      94238.37c          1.78024E-06
      94239.37c          1.26828E-04
      94240.37c          3.96336E-05
      94241.37c          1.84908E-05
      94242.37c          4.75496E-06
      95241.37c          5.06832E-06
      95243.37c          8.36645E-07
      42095.37c          3.74038E-05
      43099.37c          3.72877E-05
      44101.37c          3.34284E-05
      45103.37c          2.06545E-05
      47109.37c          2.13402E-06
      56133.37c          3.89438E-05
      60143.37c          2.87197E-06
      60145.37c          2.22987E-05
      62147.37c          7.35520E-06
      62149.37c          1.43765E-07
      62150.37c          5.33328E-06
      62151.37c          4.25027E-07
      62152.37c          3.21161E-06
      63153.37c          2.72881E-06
      64156.37c          9.48179E-08
       8016.37c          4.56560E-02
m20   $    Isotopic data for case 1 B32C05A222222
      92235.37c          4.83618E-04
      92234.37c          7.13534E-06
      92236.37c          8.28878E-06
      92237.37c          6.64561E-06
      92238.37c          2.18406E-02
      94238.37c          1.13545E-06
      94239.37c          1.25567E-04
      94240.37c          2.85857E-05
      94241.37c          1.27912E-05
      94242.37c          2.74311E-06
      95241.37c          3.74722E-06
      95243.37c          2.86915E-07
      42095.37c          3.10838E-05
      43099.37c          3.04713E-05
      44101.37c          2.72944E-05
      45103.37c          1.72885E-05
      47109.37c          1.54532E-06
      56133.37c          3.24174E-05
      60143.37c          2.07561E-05
      60145.37c          1.86107E-06
      62147.37c          6.48037E-06
      62149.37c          1.42404E-07
      62150.37c          4.07084E-06
      62151.37c          3.60730E-07
      62152.37c          2.71883E-06
      63153.37c          2.04837E-06
      64156.37c          9.67569E-08
       8016.37c          4.56560E-02
m21   $    Isotopic data for case 1 B32C05A222222
      92235.37c          5.54180E-04
      92234.37c          7.85195E-06
      92236.37c          8.74180E-06
      92237.37c          5.92903E-06
      92238.37c          2.17286E-02
      94238.37c          5.26368E-07
      94239.37c          1.01238E-04
      94240.37c          2.02383E-05
      94241.37c          8.19982E-06
      94242.37c          1.23780E-06
      95241.37c          2.37414E-06
      95243.37c          9.36294E-08
      42095.37c          2.40780E-05
      43099.37c          2.34050E-05
      44101.37c          2.08388E-05
      45103.37c          1.33630E-05
      47109.37c          9.93322E-07
      56133.37c          2.61250E-06
      60143.37c          1.98128E-06
      60145.37c          1.44088E-07
      62147.37c          5.31057E-06
      62149.37c          1.37121E-07
      62150.37c          4.53928E-06
      62151.37c          3.84723E-07
      62152.37c          2.73088E-06
      63153.37c          1.94844E-06
      64156.37c          8.85222E-08
       8016.37c          4.56560E-02
m102
      24000.37c          7.58e-05    $ Clad (Zircaloy)
      26000.37c          1.46e-04
      40000.37c          4.29e-02
m103
       1001.37c          5.67e-02    $ H2O
       8016.37c          3.33e-02
mt103 lwtr                           $ S(a,b) light water
m104
      24000.37c          1.74e-02    $ SS
      28000.37c          7.73e-03
      26000.37c          5.63e-02
      28000.37c          7.72e-03
m105
      24000.37c          1.65e-02    $ Borated (1 wt. %) SS
      25055.37c          1.66e-03
      28000.37c          8.73e-03
      28000.37c          7.48e-03
       5010.37c          7.60e-04
       5011.37c          3.10e-03
m106                                 $ Lower and upper fixtures
      24000.37c          5.71e-03    $ 80%,60% SS/water mixture
      25055.37c          5.62e-04
```

```
      20400 37c     2.988e-02
      20000 37c     3.609e-03
       1001 37c     3.331e-02
       9016 37c     1.668e-02
mt106 h2o                        $ SUs b) light water
c
c     tallies
c
c     Hart volume of not symmetric cell because of 1/8 configure
c     should be inputed with vol card for tallying
vol   40) 3 2338372 31r
c
c Averaged flux in each zone 1-32
f4 n    (1 101) (2 102) (3 103) (4 104) (5 105) (6 106) (7 107) (8 108) (9 109)
        (10 110) (11 111) (12 112) (13 113) (14 114) (15 115) (16 116) (17 117)
        (18 118) (19 119) (20 120) (21 121) (22 122) (23 123) (24 124) (25 125)
        (26 126) (27 127) (28 128) (29 129) (30 130) (31 131) (32 132)
fm4 n   (1 101)          $ n8sg fMus^vol in cell 1
fm14    ( 1 -6 7)
sd14      1
f24 n   (2 102)          $ n3sg fMus^vol in cell 2
fm24    ( 1 2 -6 7)
sd24      1
f34 n   (3 103)          $ n3sg fMus^vol in cell 3
fm34    ( 1 3 -6 7)
sd34      1
f44 n   (4 104)          $ n3sg fMus^vol in cell 4
fm44    ( 1 4 -6 7)
sd44      1
f54 n   (5 105)          $ n3sg fMus^vol in cell 5
fm54    ( 1 5 -6 7)
sd54      1
f64 n   (6 106)          $ n3sg fMus^vol in cell 6
fm64    ( 1 5 -6 7)
sd64      1
f74 n   (7 107)          $ n3sg fMus^vol in cell 7
fm74    ( 1 6 -6 7)
sd74      1
f84 n   (8 108)          $ n3sg fMus^vol in cell 8
fm84    ( 1 7 -6 7)
sd84      1
f94 n   (9 109)          $ n3sg fMus^vol in cell 9
fm94    ( 1 7 -6 7)
sd94      1
f104 n (10 110)          $ n3sg fMus^vol  n cell 10
fm104   ( 1 7 -6 7)
sd104     1
f114 n (11 111)          $ n3sg fMus^vol in cell 11
fm114   ( 1 8 -6 7)
sd114     1
f124 n (12 112)          $ n3 g fMus^vol in cell 12
fm124   ( 1 8 -6 7)
sd124     1
f134 n (13 113)          $ n3sg fMus^vol in cell 13
fm134   ( 1 8 -6 7)
sd134     1
f144 n (14 114)          $ n3sg fMus^vol in cell 14
fm144   ( 1 80 -6 7)
sd144     1
f154 n (15 115)          $ n3 g fMus^vol in cell 15
fm154   ( 1 80 -6 7)
sd154     1
f164 n (16 116)          $ n3sg fMus^vol in cell 16
fm164   ( 1 81 -6 7)
sd164     1
f174 n (17 117)          $ n3sg fMus^vol in cell 17
fm174   ( 1 12 -6 7)
sd174     1
f184 n (18 118)          $ n3sg fMus^vol in cell 18
fm184   ( 1 82 -6 7)
sd184     1
f194 n (19 119)          $ n3sg fMus^vol in cell 19
fm194   ( 1 82 -6 7)
sd194     1
f204 n (20 120)          $ n3sg fMus^vol in cell 20
fm204   ( 1 13 -6 7)
sd204     1
f214 n (21 121)          $ n3 g fMus^vol in cell 21
fm214   ( 1 14 -6 7)
sd214     1
f224 n (22 122)          $ n3 g fMus^vol in cell 22
fm224   ( 1 14 -6 7)
sd224     1
f234 n (23 123)          $ n3sg fMus^vol in cell 23
fm234   ( 1 14 -6 7)
sd234     1
f244 n (24 124)          $ n3 g fMus^vol in cell 24
fm244   ( 1 15 -6 7)
sd244     1
f254 n (25 125)          $ n3sg fMus^vol in cell 25
fm254   ( 1 15 -6 7)
sd254     1
f264 n (26 126)          $ n3sg fMus^vol in cell 26
fm264   ( 1 15 -6 7)
sd264     1
f274 n (27 127)          $ n3sg fMus^vol in cell 27
fm274   ( 1 16 -6 7)
sd274     1
f284 n (28 128)          $ n3sg fMus^vol in cell 28
fm284   ( 1 17 -6 7)
sd284     1
f294 n (29 129)          $ n3sg fMus^vol in cell 29
fm294   ( 1 18 -6 7)
sd294     1
f304 n (30 130)          $ n3sg fMus^vol in cell 30
fm304   ( 1 18 -6 7)
sd304     1
f314 n (31 131)          $ n3sg fMus^vol in cell 31
fm314   ( 1 20 -6 7)
sd314     1
f324 n (32 132)          $ n3sg fMus^vol in cell 32
fm324   ( 1 21 -6 7)
sd324     1
c Pu-vessel flux
```

```
c f994 n ( 1  2  3  4  5  6  7  8  9 10 11 12 13 14 15 16
c       17 18 19 20 21 22 23 24 25 26 27 28 29 30 31 32)
c       < 57| 1 20  1 30  2 30  1 40  2 40  3 40  1 50  3 50  4 50
c           1 60  2 60  3 60  4 60  5 60  1 70  2 70  4 70  3 70
c           4 70  1 80  2 80  3 80  4 80  5 80  1 90  2 90  3 90
c           2 90  3 90  4 90  5 90  6 90  7 90  8 90|
c       < 58 < 71|0 0 0| < 72 )
c       [ f101 102 103 104  905  906  907  908  909  110  111  112  113  114  115  116
c         117 118 119 120 121 122 123 124 125 126 127 128 129 130 131 132)
c       < 57|1 1 0  2 2 0  3 3 0  4 5 6  0  7 7 0  8 8 0  9 9 0|
c       < 58 < 71|0 0 0| < 72 )
c
c       f( 1  2  3  4  5  6  7  8  9 10 11 12 13 14 15 16
c         17 18 19 20 21 22 23 24 25 26 27 28 29 30 31 32)
c         < 58| 1 80  2 80  3 80  4 80  5 80  6 80  7 80  8 80
c              9 80  1 70  2 70  3 70  4 70  5 70  6 70  7 70  8 70
c              8 70  9 70  1 60  2 60  4 60  5 60  6 60  7 60  8 60
c              8 60  9 60  1 50  2 50  3 50  4 50  5 50  6 50  7 50
c              8 50  9 50  1 40  3 40  4 40  5 40  6 40  7 40  8 40
c              9 40  1 30  2 30  3 30  5 30  6 30  7 30  8 30  9 30
c              1 20  2 20  3 20  4 20  5 20  6 20  7 20  8 20  9 20
c              1 10  2 10  3 10  4 10  6 10  7 10  8 10  9 10 100 200 300 400 500 600 700
c              800 900 110 210 310 410 510 610 710 810
c              910 120 220 320 420 520 620 720 820
c              920 130 230 330 430 530 630 730 830
c              140 240 340 540 640 740 840 940 150
c              350 450 550 650 750 850 950 160 260
c              360 460 560 760 860 960 170 270 470
c              570 670 770 870 970 180 280 380 480
c              580 680 780 880 980 190 290 390 490
c              590 690 790 890 990|
c         < 59 < 71|0 1 0| < 72 )
c
c       [ 1  2  3  4  5  6  7  8  9 10 11 12 13 14 15 16
c         17 18 19 20 21 22 23 24 25 26 27 28 29 30 31 32)
c         < 57| 1 70  2 60  3 80  4 50  5 70  6 40  7 60  8 30
c              7 40  8 40  9 40  1 30  2 50  3 30  4 30  5 20
c              4 20  6 20  7 20  8 20  9 20  1 10  2 10  3 10
c              7 10  8 10  9 10  1 10  2 10  3 10  4 10  5 10
c              600 500 400 300 200 100 810 710
c              610 510 410 310 210 110 910 820
c              720 620 520 320 220 120 920 820
c              830 730 530 430 330 230 930 830
c              130 230 840 740 640 540 440 240
c              140 940 140 240 340 650 750 850
c              550 450 350 250 050 150 350 450
c              850 750 650 450 350 250 150 050
c              160 260 360 460 560 670 770 870 970
c              470 370 170 070 170 270 470 570 670
c              480 780 680 580 480 380 280 180
c              990 190 290 390 490 590 690 790 890
c              790 890 990 190 290 390 490 590 690
c              690 490 790 890 990|
c         < 58 < 71|1 1 0| < 72 )
c
c       [ 1  2  3  4  5  6  7  8  9 10 11 12 13 14 15 16
c         17 18 19 20 21 22 23 24 25 26 27 28 29 30 31 32)
c         < 57| 1 80  2 80  3 80  4 80  5 80  6 80  7 80  8 80
c              9 80  1 70  2 70  3 70  4 70  5 70  6 70  7 70  8 70
c              8 70  9 70  1 60  2 60  4 60  5 60  6 60  7 60  8 60
c              8 60  9 60  1 50  2 50  3 50  4 50  5 50  6 50  7 50
c              8 50  9 50  1 40  3 40  4 40  5 40  6 40  7 40  8 40
c              9 40  1 30  2 30  3 30  5 30  6 30  7 30  8 30  9 30
c              1 20  2 20  3 20  4 20  5 20  6 20  7 20  8 20  9 20
c              1 10  2 10  3 10  4 10  6 10  7 10  8 10  9 10 100 200 300 400 500 600 700
c              800 900 110 210 310 410 510 610 710 810
c              910 120 220 320 420 520 620 720 820
c              920 130 230 330 430 530 630 730 830
c              140 240 340 540 640 740 840 940 150
c              350 450 550 650 750 850 950 160 260
c              360 460 560 760 860 960 170 270 470
c              570 670 770 870 970 180 280 380 480
c              580 680 780 880 980 190 290 390 490
c              590 690 790 890 990|
c         < 64 < 71|0 2 0| < 72 )
c
c       ( 1  2  3  4  5  6  7  8  9 10 11 12 13 14 15 16
c         17 18 19 20 21 22 23 24 25 26 27 28 29 30 31 32)
c         < 58| 1 90  7 90  8 80  5 80  6 80  4 80  3 80  2 80
c              1 80  9 80  1 80  2 80  3 80  4 80  5 80  6 80  7 80
c              7 80  8 80  9 80  9 70  7 70  8 70  5 70  6 70  4 70
c              4 70  3 70  2 70  1 70  9 70  8 70  7 70  6 70  5 70
c              7 70  8 70  6 70  5 70  7 70  8 70  6 70  5 70  4 70
c              3 70  4 70  5 70  6 70  7 70  8 70  9 70  1 60  2 60
c              3 60  4 60  5 60  6 60  7 60  8 60  9 60  1 50  2 50
c              3 50  4 50  5 50  6 50  7 50  8 50  9 50  1 40  2 40
c              3 40  4 40  5 40  6 40  7 40  8 40  9 40  1 30  2 30
c              3 30  4 30  5 30  6 30  7 30  8 30  9 30  1 20  2 20
c              3 20  4 20  5 20  6 20  7 20  8 20  9 20  1 10  2 10
c              3 10  4 10  6 10  7 10  8 10  9 10 100 200 300 400 500
c              600 700 800 900 110 210 310 410 510 610 710 810
c              910 120 220 320 420 520 620 720 820
c              920 130 230 330 430 530 630 730 830
c              140 240 340 540 640 740 840 940 150
c              350 450 550 650 750 850 950 160 260
c              360 460 560 760 860 960 170 270 470
c              570 670 770 870 970 180 280 380 480
c              580 680 780 880 980 190 290 390 490
c              590 690 790 890 990|
c         < 65 < 71|0 3 0| < 72 )
c
c       ( 1  2  3  4  5  6  7  8  9 10 11 12 13 14 15 16
c         17 18 19 20 21 22 23 24 25 26 27 28 29 30 31 32)
c         < 58| 1 90  7 80  8 80  5 80  6 80  4 80  3 80  2 80
c              1 80  9 80  1 80  2 80  3 80  4 80  5 80  6 80  7 80
c              7 80  8 80  9 80  9 70  7 70  8 70  5 70  6 70  4 70
c              4 70  3 70  2 70  1 70  9 70  8 70  7 70  6 70  5 70
c              7 70  8 70  6 70  5 70  7 70  8 70  6 70  5 70  4 70
c              3 70  4 70  5 70  6 70  7 70  8 70  9 70  1 60  2 60
c              3 60  4 60  5 60  6 60  7 60  8 60  9 60  1 50  2 50
c              3 50  4 50  5 50  6 50  7 50  8 50  9 50  1 40  2 40
c              3 40  4 40  5 40  6 40  7 40  8 40  9 40  1 30  2 30
c              3 30  4 30  5 30  6 30  7 30  8 30  9 30  1 20  2 20
c              3 20  4 20  5 20  6 20  7 20  8 20  9 20  1 10  2 10
c              3 10  4 10  6 10  7 10  8 10  9 10 100 200 300 400 500
c              600 700 800 900 110 210 310 410 510 610 710 810
c              910 120 220 320 420 520 620 720 820
c              920 130 230 330 430 530 630 730 830
c              140 240 340 540 640 740 840 940 150
c              350 450 550 650 750 850 950 160 260
c              360 460 560 760 860 960 170 270 470
c              570 670 770 870 970 180 280 380 480
c              580 680 780 880 980 190 290 390 490
c              590 690 790 890 990|
c         < 66 < 71|0 4 0| < 72 )
```

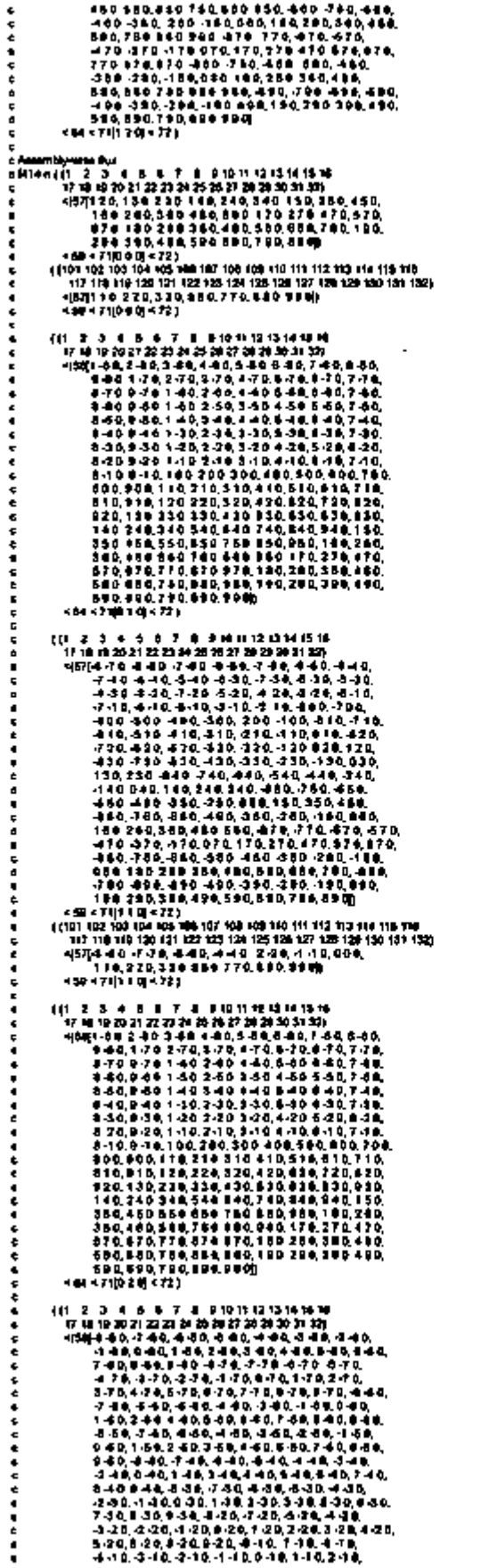

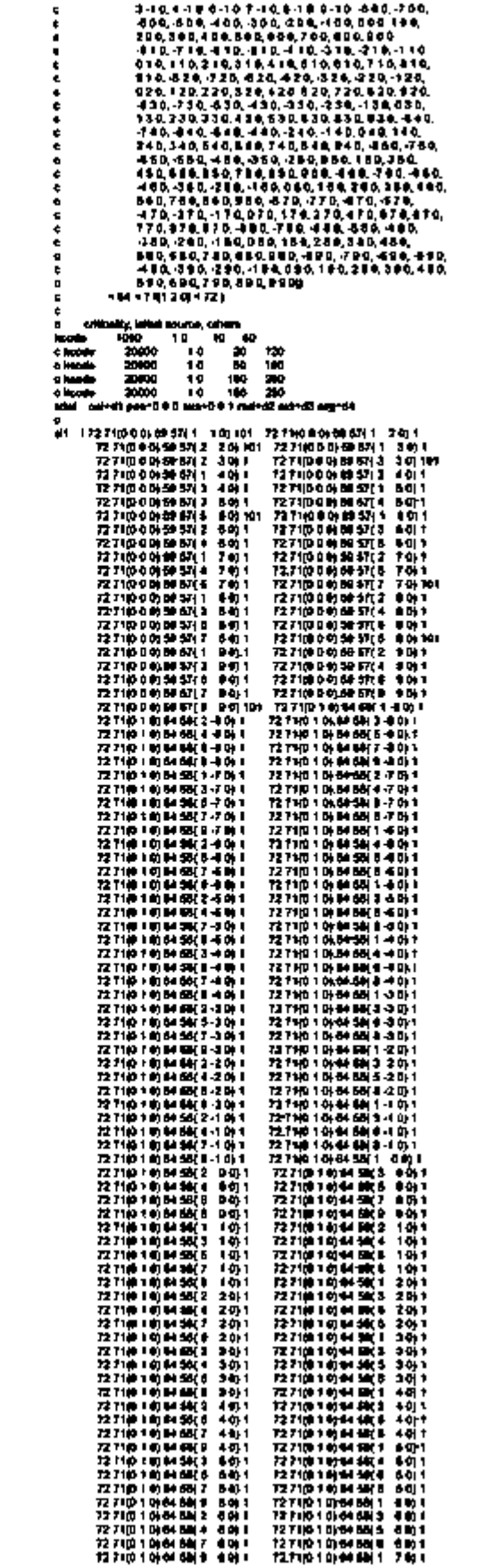

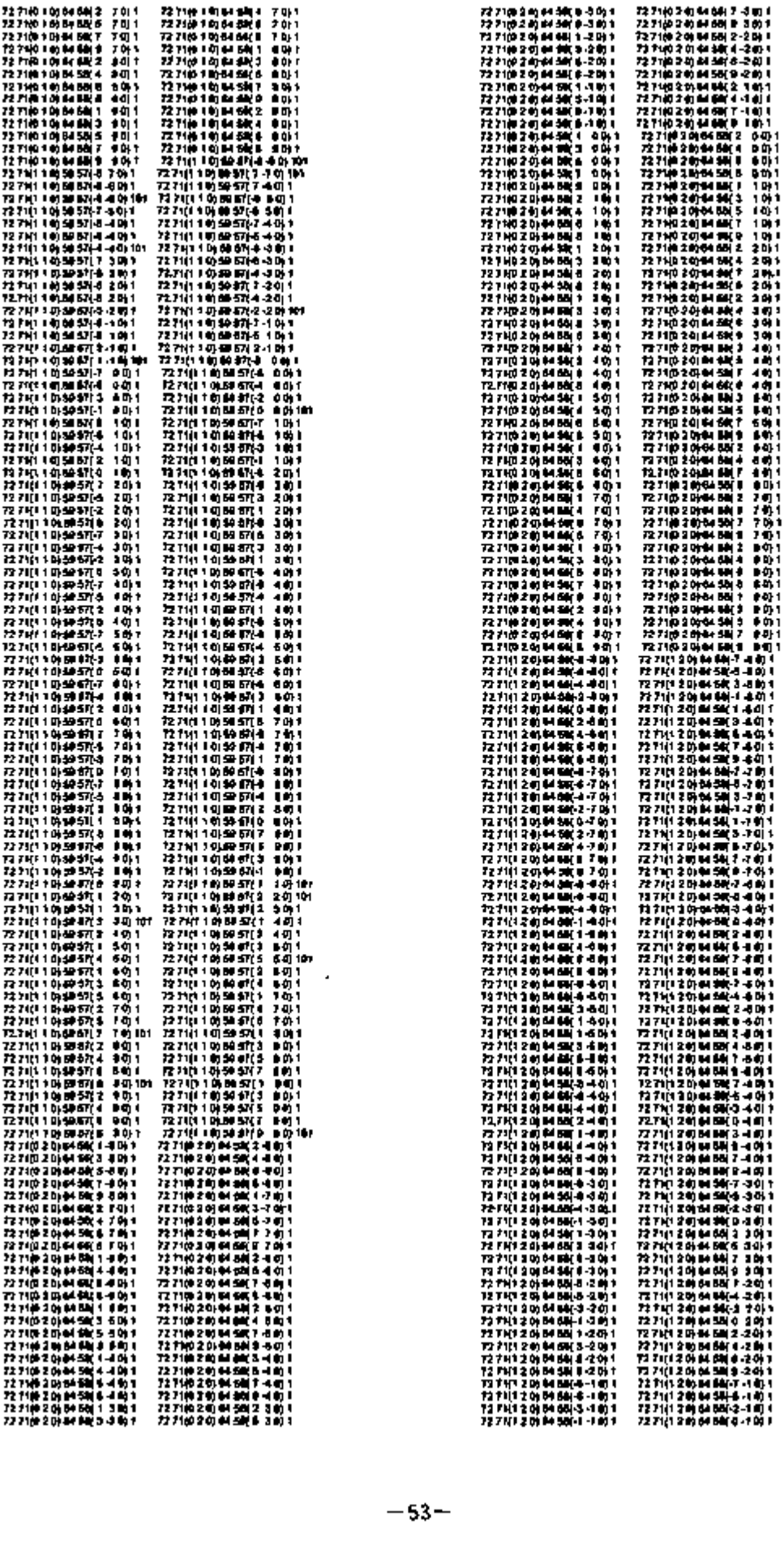

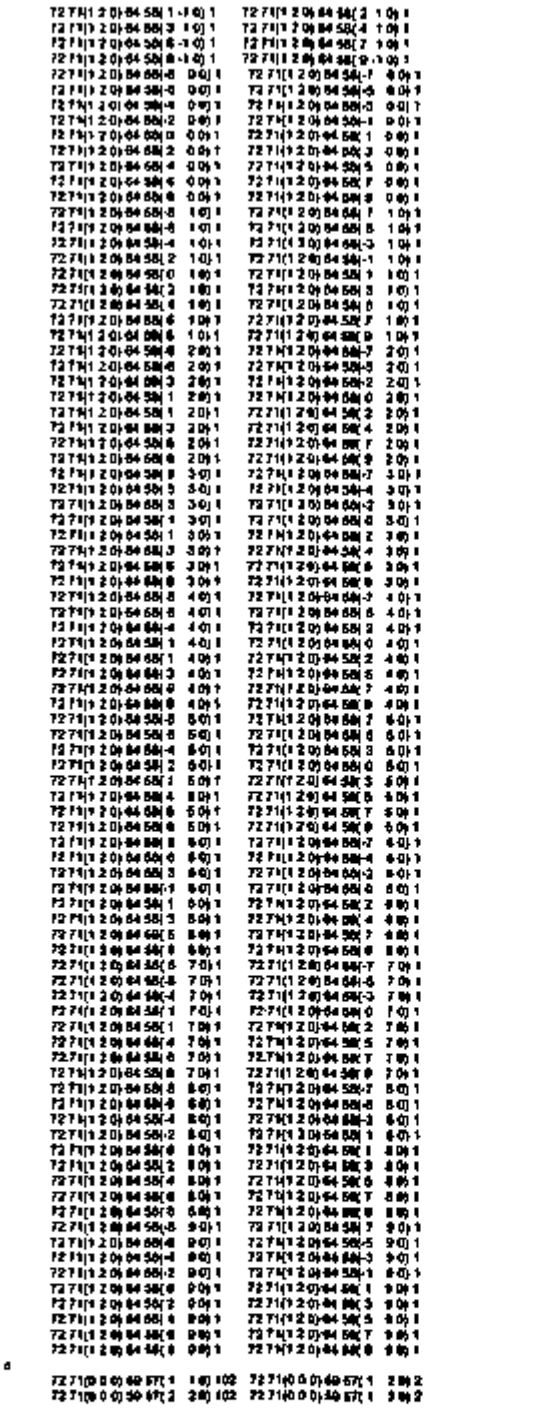

Appendix II

Table of Fission Source Distributions

This is a blank page.

Table A-1 Fission source fraction at 32 MWd/kgU based on AC+FP approach

Axial node	Case – Symmetric	Case – Uniform	Case 01 A222222	Case 02 A111111	Case 03 A111112	Case 04 A111122	Case 05 A111222	Case 06 A112222	Case 07 A122222	Case 08 A222223	Case 09 A222233	Case 10 A223333	Case 11 A233333	Case 12 A333333	Case 13 A122223	Case 14 A112233	Case 15 A322221	Case 16 A332211	Case 17
32	0.03943	0.03854	1.1E-05	0	0	2.8E-06	0	0	7.1E-06	0	4.9E-06	3.6E-06	4E-06	0.00123	0.00079	0	0	0	0
31	0.05304	0.05096	2.8E-05	0	0	4.6E-06	0	0	8.4E-06	0	1.8E-05	0.00011	8E-05	0.00167	0.00104	0	0	0	4.2E-07
30	0.05423	0.01439	2.6E-05	0	0	9.2E-06	0	0	1.6E-05	0	2.6E-05	0.00014	5.7E-05	0.00176	0.00138	3.2E-06	4E-07	5.2E-07	6.1E-07
29	0.05107	0.01965	5.3E-05	0	0	1.3E-05	0	0	1.9E-05	0	4.4E-05	0.00019	4.9E-05	0.00148	0.00167	4.6E-06	1.1E-06	8E-08	9.1E-06
28	0.04515	0.02255	0.0001	9.2E-07	0	4.5E-06	0	1.2E-06	2.3E-05	0	6.4E-06	0.00017	5.6E-06	0.00138	0.00172	1.5E-06	2E-05	9.8E-06	2.3E-05
27	0.03931	0.02605	0.00018	4.1E-07	2E-06	4.1E-06	0	6.4E-06	4.9E-06	0	7.8E-05	0.0002	6.3E-05	0.00124	0.00185	1.1E-06	4.4E-05	3.2E-05	4E-05
26	0.03538	0.02848	0.00025	1.4E-06	3.1E-06	6.7E-06	7.3E-07	8.7E-06	8.7E-05	2.5E-09	9.5E-05	0.00022	0.00011	0.00106	0.00202	4E-05	5.5E-05	4.7E-05	9.5E-05
25	0.03006	0.03271	0.00028	7.4E-06	7.7E-06	1.9E-05	1.1E-06	1.4E-05	7.3E-05	7.7E-06	0.00012	0.00026	0.00011	0.00081	0.00188	9.4E-05	6.1E-05	9.6E-05	0.00016
24	0.02563	0.03578	0.00036	2.2E-05	1.7E-05	7.7E-05	5.1E-06	1.9E-05	0.00011	3E-05	0.00014	0.00036	0.00012	0.00106	0.00184	0.00011	0.00011	0.00019	0.00023
23	0.02163	0.03618	0.00049	2.6E-05	2.6E-05	0.00012	2.4E-05	3.1E-05	0.00016	6.4E-05	0.00023	0.00044	0.00021	0.00118	0.00214	0.00018	0.00011	0.00023	0.00035
22	0.0189	0.04068	0.00068	3.9E-05	4.7E-05	8.4E-05	3E-05	4.5E-05	0.00023	0.00018	0.00033	0.00056	0.0004	0.00125	0.00253	0.00028	0.00014	0.00033	0.00048
21	0.01574	0.04265	0.0008	5.3E-05	0.00012	8.4E-05	9.4E-05	0.00019	0.00033	0.00023	0.00049	0.0007	0.00078	0.00149	0.00337	0.00045	0.00028	0.00048	0.00073
20	0.01345	0.04473	0.00085	0.00018	0.00029	8.7E-05	0.0002	0.00036	0.00048	0.00034	0.00068	0.00087	0.00128	0.00205	0.00415	0.00067	0.0004	0.00068	0.00099
19	0.01113	0.04571	0.00097	0.00029	0.00044	0.00012	0.00029	0.0006	0.0006	0.00062	0.00096	0.00145	0.00179	0.0026	0.00504	0.00093	0.00058	0.00104	0.00161
18	0.01018	0.04613	0.00132	0.00054	0.0006	0.00026	0.00041	0.00075	0.00091	0.00104	0.0011	0.00176	0.00245	0.00372	0.0061	0.00126	0.00104	0.0016	0.00228
17	0.00983	0.04636	0.0018	0.00087	0.0008	0.00053	0.0007	0.00105	0.00154	0.00169	0.00163	0.00236	0.00381	0.00506	0.00737	0.00166	0.00158	0.00233	0.00313
16	0.00976	0.04617	0.00259	0.00133	0.00118	0.00103	0.00116	0.00168	0.00211	0.00247	0.00215	0.00337	0.00487	0.00685	0.00908	0.00224	0.00214	0.00331	0.00459
15	0.00958	0.04749	0.00342	0.00217	0.00196	0.00183	0.00196	0.00266	0.00312	0.0031	0.00322	0.00436	0.00709	0.00936	0.01143	0.00325	0.00307	0.00464	0.00667
14	0.01089	0.04639	0.005	0.00353	0.00263	0.00294	0.00307	0.00452	0.00488	0.00546	0.0052	0.00825	0.0103	0.01234	0.01528	0.00463	0.00463	0.00647	0.00928
13	0.01226	0.04516	0.00721	0.0056	0.0043	0.00458	0.00502	0.00683	0.00744	0.00804	0.00776	0.00823	0.01445	0.0165	0.02062	0.0074	0.00668	0.00927	0.01289
12	0.01466	0.04306	0.00975	0.00807	0.0065	0.00641	0.00727	0.00915	0.01016	0.01117	0.01127	0.01211	0.01813	0.02006	0.02524	0.01008	0.00916	0.01284	0.0164
11	0.01779	0.04035	0.01429	0.0119	0.00958	0.00982	0.01072	0.01271	0.01375	0.01564	0.01583	0.01661	0.02309	0.02617	0.03148	0.01423	0.01302	0.01691	0.02237
10	0.02187	0.03767	0.02109	0.01783	0.01461	0.01545	0.01628	0.01783	0.01964	0.02315	0.02352	0.02289	0.02926	0.03408	0.0395	0.02151	0.01786	0.02729	0.03057
9	0.02664	0.03477	0.03123	0.02666	0.02262	0.02485	0.02444	0.02581	0.02878	0.03356	0.03239	0.03299	0.03787	0.04416	0.04974	0.0316	0.02582	0.0387	0.0416
8	0.0319	0.03172	0.04414	0.03884	0.03497	0.03621	0.03547	0.03888	0.04062	0.04578	0.04377	0.04455	0.04905	0.05439	0.05928	0.04301	0.03606	0.0524	0.05583
7	0.0389	0.0284	0.06111	0.05552	0.0525	0.05202	0.05109	0.05426	0.0566	0.06008	0.05815	0.06553	0.06115	0.06659	0.07014	0.06806	0.04889	0.06515	0.07221
6	0.04511	0.02469	0.08297	0.08084	0.07961	0.07566	0.07364	0.07891	0.07893	0.07967	0.07735	0.07643	0.07689	0.07946	0.08315	0.07896	0.0674	0.08268	0.08456
5	0.0527	0.02147	0.11158	0.11276	0.11259	0.10776	0.10721	0.1065	0.10818	0.10913	0.10522	0.10324	0.09931	0.09731	0.08993	0.10725	0.09695	0.11424	0.11659
4	0.06084	0.01777	0.14707	0.15169	0.15462	0.15286	0.14981	0.14479	0.14617	0.14548	0.14623	0.13774	0.12877	0.1213	0.11739	0.14449	0.14325	0.14354	0.13959
3	0.06547	0.01576	0.16513	0.17296	0.18061	0.1819	0.18217	0.17127	0.1685	0.16476	0.16624	0.16542	0.15025	0.13612	0.12402	0.16506	0.17768	0.15587	0.14585
2	0.06259	0.00936	0.18404	0.17713	0.16398	0.16561	0.16539	0.1656	0.17306	0.16514	0.16617	0.17037	0.15812	0.13605	0.11746	0.17146	0.19369	0.14794	0.1254
1	0.04486	0.00511	0.12127	0.11313	0.10562	0.13906	0.14063	0.14062	0.13344	0.12281	0.12489	0.12681	0.11826	0.10795	0.09288	0.1319	0.14914	0.09949	0.09692

Table A-2 Fission source fraction at 50 MWd/kgU based on AC+FP approach

Axial node	Case – Symmetric	Case – Uniform	Case 18 A222222	Case 19 A111111	Case 20 A111112	Case 21 A111122	Case 22 A112222	Case 23 A122222	Case 24 A222223	Case 25 A222233	Case 26 A222333	Case 27 A223333	Case 28 A233333	Case 29 A333333	Case 30 A122225	Case 31 A112233	Case 32 A322221	Case 33 A332211	Case 34
32	0.0893	0.00558	0	0	0	0	0	0	0	0	5.6E-09	0	0	0	0	0	0	0	6E-08
31	0.10374	0.01022	0	0	0	0	0	0	0	0	1.7E-06	0	0	0	0	0	0	0	1.2E-05
30	0.09856	0.01491	0	0	0	0	0	0	0	0	9.2E-07	0	0	0	0	0	0	0	9.7E-06
29	0.09847	0.01947	0	0	0	0	0	0	0	0	5E-08	0	0	0	0	0	0	0	1.6E-05
28	0.04677	0.02383	0	0	2.6E-07	0	0	0	0	0	1.6E-05	0	0	0	0	0	0	0	4.3E-05
27	0.03232	0.02779	0	0	1.6E-06	0	0	0	0	0	2.4E-05	0	0	0	1.8E-07	0	0	0	4.2E-05
26	0.02276	0.03125	0	0	6.6E-06	0	0	0	0	0	6.6E-05	0	0	0	4.9E-06	0	0	0	1.8E-05
25	0.01521	0.03429	0	0	2E-05	0	0	0	0	0	3.9E-05	0	0	4.6E-09	1.5E-05	6.7E-08	0	0	1.3E-05
24	0.01011	0.03696	0	0	1.2E-05	0	0	0	1.7E-08	9E-08	3.1E-05	0	0	7.4E-08	1.2E-05	4.6E-08	1.2E-08	0	2.2E-05
23	0.00655	0.03831	1.1E-06	0	7.6E-06	0	0	0	4.7E-08	1.3E-08	1.8E-05	0	0	1.7E-06	1.8E-05	7.6E-08	2.2E-08	0	2E-05
22	0.00447	0.04162	1.3E-05	0	3.9E-06	0	0	0	2.1E-05	3.6E-08	2.2E-05	2.5E-07	0	5E-08	2.4E-05	9.6E-08	2.2E-07	2.9E-07	8.6E-06
21	0.00288	0.04382	9.6E-06	2.6E-05	1E-05	0	0	2.5E-06	4.9E-05	5.1E-08	1.4E-05	2.7E-05	2.3E-06	1.5E-05	3.1E-05	8.3E-08	1.9E-08	1.3E-05	1.6E-05
20	0.00204	0.04573	2.4E-05	2.5E-07	1.4E-06	1.5E-06	5.2E-07	1E-06	8.9E-05	2.8E-08	4.2E-06	9.6E-06	4.9E-06	4.1E-06	7E-05	4E-06	4.2E-08	1.2E-06	4.3E-05
19	0.00135	0.04704	4.4E-05	1E-05	3.1E-06	6.5E-06	3.2E-06	7.5E-06	0.00016	1.7E-05	7.9E-05	2E-05	1.9E-05	8.9E-05	0.00016	1.6E-05	1.7E-06	5.2E-05	9.5E-05
18	0.00114	0.04745	7.7E-05	3.1E-05	5.6E-06	1E-05	7.6E-06	2.3E-05	0.00012	4.6E-05	0.00011	3.3E-05	5.6E-05	0.00019	0.0003	4.1E-05	1.7E-05	5.9E-05	0.00019
17	0.00098	0.04748	0.00017	5.7E-05	0.00013	3.3E-05	3.1E-05	4.5E-05	0.00018	0.0001	0.00014	8.3E-05	0.00016	0.00042	0.00067	8.3E-05	4.9E-05	9.7E-05	0.00038
16	0.00097	0.04852	0.00028	0.00014	0.0002	5.6E-06	5.8E-06	0.00016	0.00027	0.00021	0.00023	0.00023	0.00026	0.00069	0.00106	0.00014	0.00016	0.00021	0.0006
15	0.00107	0.04598	0.00056	0.00028	0.0004	0.00014	0.00022	0.00028	0.00038	0.00032	0.00048	0.00045	0.00046	0.00117	0.00144	0.00029	0.00034	0.00042	0.00103
14	0.00142	0.04462	0.00091	0.00052	0.00068	0.00031	0.00047	0.00052	0.00068	0.00056	0.00065	0.00079	0.00086	0.00187	0.0023	0.0008	0.00052	0.00063	0.00175
13	0.00199	0.043	0.0015	0.001	0.00112	0.00078	0.00105	0.00112	0.00132	0.00116	0.00145	0.00154	0.00162	0.00317	0.00382	0.00133	0.00101	0.00169	0.00288
12	0.00285	0.04112	0.00259	0.00176	0.0019	0.00131	0.00179	0.00189	0.00216	0.00201	0.00242	0.00243	0.00321	0.00427	0.00606	0.00215	0.00176	0.00276	0.00485
11	0.00431	0.03907	0.00404	0.00313	0.00366	0.00263	0.00304	0.00331	0.00361	0.00348	0.00417	0.00421	0.00508	0.00643	0.00928	0.00368	0.00292	0.00483	0.00744
10	0.00653	0.03664	0.00674	0.00564	0.00606	0.00504	0.00543	0.00619	0.00655	0.00639	0.00752	0.00707	0.00815	0.00983	0.0144	0.00603	0.00501	0.00807	0.01184
9	0.01027	0.03418	0.01189	0.01005	0.01048	0.00969	0.00977	0.0105	0.01149	0.01163	0.01249	0.01202	0.01323	0.0162	0.02169	0.01026	0.00896	0.01376	0.01929
8	0.0162	0.0313	0.02	0.01758	0.01802	0.01683	0.01739	0.01784	0.01944	0.01979	0.02029	0.01947	0.02085	0.02502	0.03253	0.01815	0.01562	0.02289	0.03061
7	0.02412	0.02841	0.03261	0.031	0.03094	0.02935	0.02955	0.03062	0.03276	0.03261	0.03229	0.03114	0.03309	0.03817	0.04674	0.03098	0.02723	0.03664	0.04669
6	0.03303	0.02521	0.05432	0.05411	0.05236	0.05137	0.05065	0.05185	0.05347	0.0534	0.05061	0.05002	0.05162	0.05732	0.06533	0.05135	0.04549	0.0604	0.07185
5	0.04723	0.02135	0.09068	0.09067	0.08787	0.08632	0.08639	0.0866	0.08769	0.08728	0.08512	0.08155	0.08273	0.0875	0.09569	0.08785	0.08136	0.09707	0.10798
4	0.06799	0.01758	0.14652	0.14619	0.1483	0.14651	0.14611	0.14321	0.14386	0.14533	0.14516	0.13579	0.1319	0.13669	0.14197	0.14474	0.14361	0.15477	0.15597
3	0.08847	0.01351	0.19828	0.19825	0.19652	0.20084	0.20143	0.19697	0.1935	0.19845	0.19756	0.19884	0.18282	0.18144	0.17935	0.197	0.20106	0.19872	0.18782
2	0.1051	0.00916	0.23386	0.23795	0.23772	0.23987	0.24195	0.24158	0.23706	0.23438	0.23686	0.24558	0.24812	0.22371	0.20706	0.23843	0.24925	0.22542	0.19496
1	0.09178	0.00504	0.19701	0.20145	0.20264	0.20491	0.20575	0.20702	0.20521	0.1958	0.20143	0.20873	0.21731	0.20658	0.17175	0.20694	0.21414	0.17128	0.15395

Table A-3 Fission source fraction at 32 MWd/kgU based on AC-only approach

Axial node	Case – Symmetric	Case – Uniform	Case 01 A222222	Case 02 A111111	Case 03 A111112	Case 04 A111122	Case 05 A111222	Case 06 A112222	Case 07 A122222	Case 08 A222223	Case 09 A222233	Case 10 A222333	Case 11 A233333	Case 12 A333333	Case 13 A122223	Case 14 A112233	Case 15 A112221	Case 16 A332221	Case 17 A332211
32	0.02726	0.06569	0.00011	1E-06	0	0	0.00023	1.3E-06	8E-06	0.00019	0.0002	0.00041	0.00166	0.00156	0.00404	0.0002	2.9E-05	4.7E-05	0.00027
31	0.04017	0.06929	0.00024	3E-07	0	2.8E-07	0.00029	5.8E-06	8.7E-06	0.00028	0.00026	0.00022	0.00208	0.00254	0.00595	0.00026	3.4E-05	4.5E-05	0.00041
30	0.04651	0.01349	0.00036	6.4E-06	0	3.2E-06	0.00042	1.2E-06	9.5E-06	0.00017	0.00036	0.00037	0.00213	0.00312	0.00676	0.00035	6.3E-05	4.6E-05	0.00044
29	0.04876	0.0174	0.00056	2.9E-05	1.6E-07	1.1E-05	0.00042	6.5E-06	0.00017	0.0002	0.00042	0.00052	0.00217	0.00345	0.00699	0.00027	0.0001	5.7E-05	0.00045
28	0.0486	0.02123	0.00067	3.7E-05	1.4E-06	1.7E-05	0.00043	2.1E-05	0.00026	0.00021	0.00059	0.00077	0.00225	0.00401	0.00704	0.00031	0.00012	0.00014	0.0005
27	0.04823	0.02491	0.00078	2.6E-05	1.1E-06	1.4E-05	0.00047	5.7E-06	0.00039	0.00028	0.0006	0.00086	0.00244	0.00431	0.0068	0.00039	0.00023	0.00026	0.00056
26	0.04661	0.02868	0.00103	2.8E-05	1.3E-06	5.7E-06	0.00047	8.5E-05	0.00061	0.00055	0.00063	0.00113	0.00258	0.00477	0.00668	0.00055	0.00031	0.00037	0.00067
25	0.04396	0.03212	0.00121	2.5E-05	5.2E-05	0.00013	0.00047	0.00014	0.00088	0.00069	0.00112	0.0013	0.00294	0.00541	0.00629	0.0008	0.0005	0.00052	0.00066
24	0.04156	0.03526	0.00144	3.9E-05	7.5E-05	0.00018	0.00071	0.00032	0.00077	0.00084	0.00106	0.00151	0.00345	0.00624	0.00606	0.00103	0.00061	0.0007	0.00078
23	0.03971	0.03812	0.00163	0.00013	0.00013	0.00029	0.00092	0.00062	0.00088	0.0012	0.00121	0.00165	0.00429	0.00719	0.00596	0.00127	0.00119	0.00095	0.00102
22	0.03846	0.04054	0.00244	0.00024	0.00024	0.0004	0.00108	0.00101	0.00115	0.00172	0.00153	0.00206	0.00516	0.00825	0.00704	0.00164	0.00154	0.00127	0.00143
21	0.03383	0.04244	0.00306	0.00032	0.00064	0.00054	0.00134	0.0015	0.00139	0.00225	0.00191	0.00247	0.00554	0.0089	0.00859	0.00217	0.00184	0.00163	0.00203
20	0.03087	0.04438	0.00402	0.00065	0.00106	0.00083	0.00173	0.00192	0.00185	0.00297	0.00262	0.00354	0.00677	0.00995	0.01039	0.00301	0.00222	0.00202	0.00316
19	0.02884	0.04578	0.00509	0.00111	0.00145	0.00122	0.00223	0.00257	0.00277	0.00387	0.00341	0.00476	0.00809	0.01141	0.01226	0.00417	0.00285	0.00248	0.00445
18	0.02643	0.04722	0.00688	0.00173	0.00218	0.00181	0.00293	0.00351	0.00383	0.00535	0.00482	0.006	0.01023	0.01322	0.01453	0.00549	0.00366	0.00458	0.00606
17	0.02426	0.04783	0.00887	0.00282	0.00328	0.00267	0.00408	0.00484	0.00517	0.00748	0.00673	0.00754	0.0126	0.01587	0.01703	0.00712	0.00484	0.00621	0.00808
16	0.02372	0.04782	0.01072	0.00411	0.0045	0.00408	0.00552	0.00678	0.00694	0.00969	0.00921	0.00943	0.01557	0.01845	0.01851	0.00911	0.00645	0.00819	0.01085
15	0.02295	0.04757	0.0137	0.00568	0.00602	0.0057	0.00749	0.00957	0.00931	0.01238	0.01231	0.01203	0.0189	0.02286	0.02211	0.01136	0.00852	0.01103	0.01406
14	0.02242	0.0488	0.01738	0.00691	0.00671	0.00618	0.01043	0.0128	0.01227	0.01611	0.01654	0.01589	0.02296	0.02783	0.0268	0.01502	0.01161	0.01506	0.01792
13	0.02226	0.04532	0.0226	0.01271	0.01253	0.01191	0.01425	0.01775	0.01689	0.02036	0.02024	0.02129	0.02884	0.03395	0.03241	0.01894	0.0158	0.02083	0.02313
12	0.02204	0.04331	0.02682	0.01718	0.01686	0.01601	0.01765	0.02247	0.02083	0.0239	0.02537	0.02618	0.03369	0.0386	0.0373	0.02382	0.01977	0.02625	0.02885
11	0.02247	0.04124	0.03253	0.023	0.02238	0.02162	0.02369	0.02854	0.02716	0.02864	0.0317	0.03272	0.04	0.04456	0.04374	0.03038	0.02504	0.03291	0.03679
10	0.02315	0.03872	0.04091	0.03007	0.02978	0.02787	0.03081	0.03648	0.03539	0.03514	0.03937	0.04082	0.0487	0.05147	0.05187	0.03792	0.03166	0.04267	0.04583
9	0.02412	0.03617	0.05088	0.04009	0.03926	0.03817	0.04081	0.04439	0.04529	0.04458	0.04822	0.05145	0.05488	0.0588	0.06068	0.04864	0.04205	0.05371	0.05647
8	0.02564	0.03332	0.06084	0.05344	0.05111	0.05103	0.05291	0.05474	0.05918	0.05529	0.0588	0.06094	0.06185	0.06383	0.06879	0.06071	0.05332	0.06483	0.0678
7	0.02714	0.02969	0.07243	0.07036	0.06856	0.06713	0.06758	0.06789	0.07425	0.06765	0.07041	0.07128	0.0691	0.06873	0.07117	0.07337	0.06712	0.07661	0.08062
6	0.02718	0.02625	0.08498	0.0833	0.08666	0.08674	0.0854	0.08444	0.09065	0.08283	0.08165	0.08193	0.07566	0.0734	0.07345	0.08549	0.08319	0.09501	0.09524
5	0.02817	0.02234	0.09665	0.11663	0.11302	0.11034	0.10728	0.10416	0.10829	0.10433	0.09832	0.09762	0.08553	0.07938	0.07812	0.10518	0.10429	0.10753	0.1093
4	0.03028	0.01839	0.11725	0.14066	0.13696	0.13992	0.13248	0.12761	0.12796	0.12642	0.12227	0.11606	0.096	0.08714	0.08411	0.12236	0.13168	0.12022	0.11627
3	0.03032	0.01419	0.12073	0.14847	0.15123	0.15332	0.14656	0.13782	0.1324	0.13296	0.13102	0.12605	0.10253	0.09691	0.09187	0.12678	0.14202	0.12174	0.11242
2	0.02721	0.0097	0.11228	0.13458	0.143	0.14723	0.14109	0.13381	0.12336	0.12483	0.12235	0.11891	0.10002	0.07791	0.07161	0.11683	0.13679	0.10911	0.09291
1	0.01834	0.00531	0.07794	0.09267	0.09832	0.10261	0.09921	0.09654	0.08765	0.08464	0.08565	0.08267	0.07097	0.06619	0.0472	0.0839	0.0963	0.08928	0.05969

Table A-4 Fission source fraction at 50 MWd/kgU based on AC-only approach

Axial node	Case – Symmetric	Case – Uniform	Case 18 A222222	Case 19 A111111	Case 20 A111112	Case 21 A111122	Case 22 A111222	Case 23 A112222	Case 24 A122222	Case 25 A222223	Case 26 A222233	Case 27 A222333	Case 28 A223333	Case 29 A233333	Case 30 A333333	Case 31 A122223	Case 32 A112233	Case 33 A332221	Case 34 A332211
32	0.06117	0.00464	0	0	0	0	0	0	0	0	0	0	0	4.3E-07	0.00062	0	0	0	1.7E-05
31	0.06862	0.00861	0	0	0	0	0	0	0	0	0	4.1E-06	0	8.5E-06	0.00073	0	0	6.3E-07	2.2E-05
30	0.06368	0.01268	0	0	0	0	0	0	0	0	0	7.9E-06	0	1.9E-05	0.00085	0	0	5.7E-06	1.5E-05
29	0.0548	0.01684	0	0	0	0	0	0	0	6.9E-07	0	4E-06	0	3.4E-05	0.00091	0	0	1.5E-05	2E-05
28	0.0431	0.02074	0	0	0	0	5.9E-09	0	0	1.6E-06	0	1.2E-05	0	8.2E-05	0.00089	0	1.8E-06	8.6E-06	2.6E-05
27	0.03538	0.02456	0	3.5E-06	7.6E-10	0	1.9E-06	0	0	5.1E-06	3.2E-06	1.3E-05	0	0.00014	0.00082	0	1.8E-05	7.6E-06	2.7E-05
26	0.02926	0.02829	0	5.7E-06	4.4E-06	0	9.6E-06	0	0	1.5E-05	8.5E-06	1E-05	8.5E-07	0.00016	0.00068	5.5E-06	1.5E-05	1.2E-05	4E-05
25	0.02271	0.03157	8.1E-07	6.7E-06	1.6E-05	1.4E-06	1.3E-05	0	9.6E-07	3.7E-05	6.9E-05	1.9E-05	1.1E-06	0.00022	0.00061	5E-06	2E-05	1.6E-05	5.1E-05
24	0.01764	0.03424	4E-06	9.3E-06	3.5E-05	3.3E-06	3E-05	9.6E-07	7.9E-06	7.4E-05	0.0001	4.7E-05	4.5E-06	0.00035	0.00052	3.8E-06	2.3E-05	3E-06	8.1E-05
23	0.01324	0.03661	1.1E-05	2.9E-05	5.1E-05	1.2E-05	5.4E-05	2.2E-06	1.7E-05	0.00014	0.00014	8.6E-05	1.3E-05	0.00053	0.00048	5.4E-06	4.5E-06	0.00012	0.0001
22	0.01022	0.03879	4E-05	4.5E-05	6.6E-06	2.6E-05	9.3E-06	1.3E-05	3.4E-05	0.0002	0.00017	0.00015	6.3E-05	0.00063	0.00058	2.1E-05	7.1E-05	0.00015	0.00012
21	0.00787	0.04115	7.5E-05	6.2E-05	0.0001	5.2E-05	0.00013	3.6E-05	5.7E-05	0.00023	0.00026	0.0002	0.00015	0.00084	0.00067	3.7E-05	0.00017	0.00021	0.00021
20	0.0061	0.04303	0.00017	0.00016	0.00018	0.00013	0.0002	5.6E-05	0.00013	0.00029	0.00039	0.00028	0.00028	0.00069	0.0006	7.6E-05	0.00027	0.00026	0.00034
19	0.00513	0.04423	0.00033	0.0002	0.00019	0.00027	0.0003	0.00018	0.00022	0.00048	0.00058	0.00038	0.00047	0.00111	0.0013	0.00012	0.00037	0.00038	0.00058
18	0.00469	0.0452	0.0006	0.00038	0.00027	0.00041	0.00048	0.00023	0.00041	0.00076	0.0008	0.0006	0.00076	0.00149	0.00188	0.0003	0.00051	0.0006	0.00097
17	0.00447	0.04617	0.0008	0.00058	0.00044	0.00063	0.00072	0.00043	0.00078	0.00109	0.00119	0.00078	0.00129	0.00225	0.00271	0.00051	0.00081	0.00089	0.0015
16	0.00445	0.0468	0.00108	0.001	0.0008	0.00112	0.00109	0.00081	0.0014	0.00154	0.00142	0.00131	0.00189	0.00305	0.0038	0.00085	0.00116	0.00152	0.00226
15	0.00463	0.04732	0.00158	0.00168	0.0013	0.00164	0.00162	0.00138	0.00208	0.00208	0.0019	0.0021	0.00267	0.00457	0.00553	0.00148	0.00158	0.00241	0.00347
14	0.00553	0.04727	0.00237	0.00233	0.00214	0.00254	0.00223	0.00233	0.00285	0.00316	0.00278	0.00318	0.00373	0.00582	0.00706	0.00237	0.0023	0.0037	0.00519
13	0.00743	0.04647	0.00383	0.00403	0.00375	0.00368	0.00354	0.00382	0.00437	0.00467	0.00436	0.00514	0.00571	0.01037	0.01087	0.00407	0.00364	0.0059	0.00832
12	0.01008	0.04532	0.00681	0.00596	0.00577	0.00563	0.0055	0.00588	0.00821	0.00679	0.00599	0.00725	0.00788	0.01363	0.01386	0.00592	0.00537	0.00814	0.01131
11	0.01313	0.04351	0.00971	0.00824	0.00894	0.00828	0.00868	0.00892	0.00938	0.0097	0.0088	0.01003	0.01148	0.01841	0.01873	0.00837	0.00798	0.01212	0.01569
10	0.01702	0.04119	0.0142	0.0137	0.01347	0.01288	0.01328	0.01398	0.01538	0.01483	0.01308	0.01505	0.01748	0.02411	0.02522	0.0144	0.01205	0.01791	0.02201
9	0.02214	0.03847	0.02198	0.0208	0.02171	0.02053	0.02068	0.02193	0.02451	0.0217	0.02004	0.02313	0.02577	0.03334	0.03456	0.02238	0.01911	0.02693	0.03176
8	0.02768	0.03522	0.03378	0.0307	0.03252	0.0308	0.03226	0.03247	0.03623	0.03229	0.03059	0.03283	0.03703	0.04414	0.04581	0.03358	0.02834	0.03882	0.04383
7	0.0354	0.03166	0.0495	0.04594	0.04798	0.04752	0.0488	0.04812	0.05182	0.04723	0.04529	0.04737	0.05189	0.0577	0.06145	0.04861	0.04392	0.05429	0.06037
6	0.04459	0.02773	0.07235	0.07003	0.07088	0.07008	0.06838	0.07138	0.07508	0.06979	0.06695	0.06783	0.07131	0.07574	0.07906	0.07064	0.06533	0.0786	0.08351
5	0.0578	0.02345	0.10414	0.10497	0.10469	0.1036	0.10201	0.10338	0.10514	0.10421	0.09949	0.09846	0.09978	0.10349	0.1042	0.09814	0.10977	0.11336	
4	0.07291	0.01906	0.14826	0.15174	0.15105	0.15199	0.14827	0.14902	0.14758	0.15062	0.15171	0.14317	0.13894	0.13408	0.13901	0.1465	0.149	0.15086	0.14841
3	0.08416	0.01421	0.18192	0.18413	0.18404	0.18369	0.18495	0.18098	0.17709	0.18269	0.18648	0.18222	0.18691	0.18527	0.18495	0.17868	0.18704	0.17528	0.16775
2	0.0883	0.00964	0.19588	0.19768	0.19712	0.19841	0.20075	0.19967	0.19018	0.19499	0.20181	0.20212	0.19832	0.18962	0.18059	0.1982	0.20705	0.18144	0.18064
1	0.06826	0.00624	0.15158	0.15441	0.15253	0.1567	0.15702	0.15696	0.14917	0.15034	0.15583	0.15638	0.15634	0.13958	0.12171	0.15828	0.16478	0.1296	0.11722

国際単位系 (SI) と換算表

表1　SI基本単位および補助単位

量	名称	記号
長さ	メートル	m
質量	キログラム	kg
時間	秒	s
電流	アンペア	A
熱力学温度	ケルビン	K
物質量	モル	mol
光度	カンデラ	cd
平面角	ラジアン	rad
立体角	ステラジアン	sr

表2　SIと併用される単位

名称	記号
分，時，日	min，h，d
度，分，秒	°，′，″
リットル	l，L
トン	t
電子ボルト	eV
原子質量単位	u

1 eV = 1.60218 × 10⁻¹⁹ J

1 u = 1.66054 × 10⁻²⁷ kg

表3　固有の名称をもつSI組立単位

量	名称	記号	他のSI単位による表現
周波数	ヘルツ	Hz	s⁻¹
力	ニュートン	N	m kg/s²
圧力，応力	パスカル	Pa	N/m²
エネルギー，仕事，熱量	ジュール	J	N m
工率，放射束	ワット	W	J/s
電気量，電荷	クーロン	C	A s
電位，電圧，起電力	ボルト	V	W/A
静電容量	ファラド	F	C/V
電気抵抗	オーム	Ω	V/A
コンダクタンス	ジーメンス	S	A/V
磁束	ウェーバ	Wb	V s
磁束密度	テスラ	T	Wb/m²
インダクタンス	ヘンリー	H	Wb/A
セルシウス温度	セルシウス度	℃	
光束	ルーメン	lm	cd sr
照度	ルクス	lx	lm/m²
放射能	ベクレル	Bq	s⁻¹
吸収線量	グレイ	Gy	J/kg
線量当量	シーベルト	Sv	J/kg

表4　SIと共に暫定的に維持される単位

名称	記号
オングストローム	Å
バーン	b
バール	bar
ガル	Gal
キュリー	Ci
レントゲン	R
ラド	rad
レム	rem

1 Å = 0.1 nm = 10⁻¹⁰ m

1 b = 100 fm² = 10⁻²⁸ m²

1 bar = 0.1 MPa = 10⁵ Pa

1 Gal = 1 cm/s² = 10⁻² m/s²

1 Ci = 3.7 × 10¹⁰ Bq

1 R = 2.58 × 10⁻⁴ C/kg

1 rad = 1 cGy = 10⁻² Gy

1 rem = 1 cSv = 10⁻² Sv

表5　SI接頭語

倍数	接頭語	記号
10¹⁸	エクサ	E
10¹⁵	ペタ	P
10¹²	テラ	T
10⁹	ギガ	G
10⁶	メガ	M
10³	キロ	k
10²	ヘクト	h
10¹	デカ	da
10⁻¹	デシ	d
10⁻²	センチ	c
10⁻³	ミリ	m
10⁻⁶	マイクロ	μ
10⁻⁹	ナノ	n
10⁻¹²	ピコ	p
10⁻¹⁵	フェムト	f
10⁻¹⁸	アト	a

（注）

1　表1～5は「国際単位系」第5版，国際度量衡局 1985年刊行による。ただし，1 eVおよび1 uの値はCODATAの1986年推奨値によった。

2　表4には海里，ノット，アール，ヘクタールも含まれているが日常の単位なのでここでは省略した。

3　barは，JISでは液体の圧力を表わす場合に限り表2のカテゴリーに分類されている。

4　EC閣僚理事会指令ではbar，barnおよび「血圧の単位」mmHgを表2のカテゴリーに入れている。

換　算　表

力	N (= 10⁵ dyn)	kgf	lbf
	1	0.101972	0.224809
	9.80665	1	2.20462
	4.44822	0.453592	1

粘度　1 Pa s (= 1 N s/m²) = 10 P (ポアズ) (g/(cm s))

動粘度　1 m²/s = 10⁴ St (ストークス) (cm²/s)

圧力	MPa (= 10 bar)	kgf/cm²	atm	mmHg (Torr)	lbf/in² (psi)
	1	10.1972	9.86923	7.50062 × 10³	145.038
	0.0980665	1	0.967841	735.559	14.2233
	0.101325	1.03323	1	760	14.6959
	1.33322 × 10⁻⁴	1.35951 × 10⁻³	1.31579 × 10⁻³	1	1.93368 × 10⁻²
	6.89476 × 10⁻³	7.03070 × 10⁻²	6.80460 × 10⁻²	51.7149	1

エネルギー・仕事・熱量	J (= 10⁷ erg)	kgf·m	kW·h	cal (計量法)	Btu	ft·lbf	eV
	1	0.101972	2.77778 × 10⁻⁷	0.238889	9.47813 × 10⁻⁴	0.737562	6.24150 × 10¹⁸
	9.80665	1	2.72407 × 10⁻⁶	2.34270	9.29487 × 10⁻³	7.23301	6.12082 × 10¹⁹
	3.6 × 10⁶	3.67098 × 10⁵	1	8.59999 × 10⁵	3412.13	2.65522 × 10⁶	2.24694 × 10²⁵
	4.18605	0.426858	1.16279 × 10⁻⁶	1	3.96759 × 10⁻³	3.08747	2.61272 × 10¹⁹
	1055.06	107.586	2.93072 × 10⁻⁴	252.042	1	778.172	6.58515 × 10²¹
	1.35582	0.138255	3.76616 × 10⁻⁷	0.323890	1.28506 × 10⁻³	1	8.46233 × 10¹⁸
	1.60218 × 10⁻¹²	1.63377 × 10⁻²⁰	4.45050 × 10⁻²⁶	3.82743 × 10⁻²⁰	1.51857 × 10⁻²²	1.18171 × 10⁻¹⁹	1

1 cal = 4.18605 J (計量法)
= 4.184 J　(熱化学)
= 4.1855 J　(15 °C)
= 4.1868 J (国際蒸気表)

仕事率　1 PS (仏馬力)
= 75 kgf m/s
= 735.499 W

放射能	Bq	Ci
	1	2.70270 × 10⁻¹¹
	3.7 × 10¹⁰	1

吸収線量	Gy	rad
	1	100
	0.01	1

照射線量	C/kg	R
	1	3876
	2.58 × 10⁻⁴	1

線量当量	Sv	rem
	1	100
	0.01	1

(86年12月26日現在)

[redacted]